Excitations of interacting fermions in reduced dimensions

Dissertation
zur Erlangung des Doktorgrades
der Naturwissenschaften

vorgelegt beim Fachbereich Physik
der Johann Wolfgang Goethe-Universität
in Frankfurt am Main

von
Peyman Pirooznia
aus Shemiran

Frankfurt (2010)
(D 30)

vom Fachbereich Physik der
Johann Wolfgang Goethe-Universität als Dissertation angenommen.

Dekan: Prof. Dr. Dirk-Hermann Rischke

Gutachter: Prof. Dr. Peter Kopietz
                           Prof. Dr. Walter Hofstetter

Datum der Disputation:

Contents

Chapter 1

Foreword

In this thesis, we study the properties of excitations in the systems of interacting fermions. These excitations can be bosonic such as collective modes which we handle in the first part of this thesis or fermionic like quasi particles and quasi holes [1,2]. One of the important points, to investigate the excitations is their damping which corresponds to their life-time in the system. This thesis consists of two parts, where in both parts, we use the field-theoretical methods to examine the problem.

The first part of this thesis is dedicated to spinless fermions in one dimension. Here, we are interested in the behavior of a bosonic collective excitation which is called zero sound and is associated with density fluctuations. To this end, we calculate the dynamic structure factor $S(\omega, q)$ with the quadratic energy dispersion and long range density-density interaction. We assume that the Fourier transform f_q of the long range interaction is dominated by small momentum-transfers $q \ll q_0 \ll k_F$, where q_0 is the momentum-transfer cutoff and k_F is the Fermi momentum. If the energy dispersion is linearized, the collective zero sound mode is undamped. Other works have shown that the damping of zero sound is proportional to q^2/m for $q \to 0$ [3,4].

In this thesis, we develop a perturbative approach within functional bosonization. In contrast to perturbation theory based on conventional bosonization, our functional bosonization approach is not plagued by unphysical singularities, which implement that close to a mass-shell the perturbation theory breaks down [5,6]. For interactions which can be expanded as $f_q = f_0 + f_0'' q^2/2 + O(q^4)$ with $f_0'' < 0$ we show that the momentum scale $q_c = 1/|m f_0''|$ separates two regimes characterized by a different q-dependence of the width γ_q of the collective zero sound mode and other features of $S(\omega, q)$. For $q_c \ll q \ll k_F$ all integrations in our functional bosonization result for $S(\omega, q)$ can be evaluated analytically; we find that the line shape in this regime is non-Lorentzian with an overall width $\gamma_q \propto q^3/(mq_c)$ and a threshold singularity $[(\omega - \omega_q^-) \ln^2(\omega - \omega_q^-)]^{-1}$ at the lower edge $\omega \to \omega_q^- = vq - 4\gamma_q/3$, where v is the velocity of the zero sound mode. Assuming that higher orders in perturbation theory transform the logarithmic singularity into an algebraic one, we find for the corresponding threshold exponent $\mu_q = 1 - 2\eta_q$ with $\eta_q \propto q_c^2/q^2$. Although for $q \lesssim q_c$ we have not succeeded to explicitly evaluate our functional bosonization result for $S(\omega, q)$, we argue that for any one-dimensional model belonging to the Luttinger

liquid universality class the width of the zero sound mode scales as q^2/m for $q \to 0$.

In the second part of this thesis we investigate the spectral function of impurity d-electrons in the Anderson impurity model. In the Fermi liquid regime we obtain the behavior of the Kondo peak which corresponds to the elementary quasi particle excitation. Since Anderson impurity model exhibits a single correlated impurity, the system is here zero-dimensional. In this part, we use the functional renormalization group approach to study one-particle excitation in Fermi liquid regime. We use here a strategy which is developed in Ref. [7], introducing bosonic Hubbard-Stratonovich fields to work out the problem in a mixed Bose-Fermi system. In our renormalization group scheme we impose a cutoff in the fermionic propagator and find a reliable truncation to handle the problem. We also use Dyson-Schwinger equations to express the irreducible bosonic vertices in terms of the fermionic ones. We show that within the transverse spin-singlet particle-hole channel the unphysical singularities are removed and for $U \lesssim 2\pi\Delta$, our results are consistent with the accurate results obtained via the numerical renormalization group. Here U is the one site Coulomb repulsion and Δ is the hybridization in the wide band limit. However, we are not able to reproduce the exponential suppression of the Kondo scale for $U \gg \Delta$. We argue how this important feature can be obtained if we use a more complicated approach.

Part I

Dynamic structure factor of Luttinger liquids

Chapter 2

Introduction

One-dimensional systems of interacting electrons have fascinated theorist and experimental physicist in the last fifty years [8–10]. Correlated fermions in one dimension are characterized by several exotic properties, stating the deviation from the Fermi liquid behavior (which is described by the Landau theory [2]). In 1981, analogue to the three dimensional electron gases, Haldane [10] introduced the term *Luttinger liquid* for fermions in one dimension with the following features: the absence of a discontinuity in the momentum distribution function at the Fermi surface, vanishing density of states at the Fermi energy and unusual one particle spectral line shape at low energies involving the separation between charge and spin excitations. The last point implies that one particle excitations are prohibited in Luttinger liquids and therefore only the collective excitations occur. Some of these non-Fermi liquids feature are observed experimentally, in particular in Refs. [11–14] which are based on photoemission spectroscopy.

For the examination of the Luttinger liquids behavior, a couple of exactly solvable models have been found which describe the underlying physics of correlated fermions in one dimension. According to Haldane all of these models are equivalent at low energies [8, 10]. One of the most important representative models is *the Tomonaga Luttinger model* (TLM) introduced by Tomonaga [15] and Luttinger [16] in the 1950s and 1960s. The exact solution of the TLM can be obtained through *the bosonization technique*. Luttinger discovered also that there is no sharp step in the momentum distribution at the Fermi surface. A bosonization formalism was used by Mattis and Lieb [17], who confirmed the important result of Luttinger. The one particle spectral line shape of Luttinger liquids was obtained by Luther and Peschel in 1974 [18], who extended the bosonization theory. Finally the elegant approach for *constructive bosonization* was presented by Haldane [8, 10].

Let us start with the Hamiltonian of spinless fermions in one dimension,

$$
\begin{align}
\hat{H} &= \hat{H}_0 + \hat{H}_{\text{int}}\,, \tag{2.1a}\\
\hat{H}_0 &= \sum_k \epsilon_k \hat{c}_k^\dagger \hat{c}_k\,, \tag{2.1b}\\
\hat{H}_{\text{int}} &= \frac{1}{2V} \sum_{k_1,k_2,k_3} U(k_3) \hat{c}_{k_1+k_3}^\dagger \hat{c}_{k_2-k_3}^\dagger \hat{c}_{k_2} \hat{c}_{k_1}\,, \tag{2.1c}
\end{align}
$$
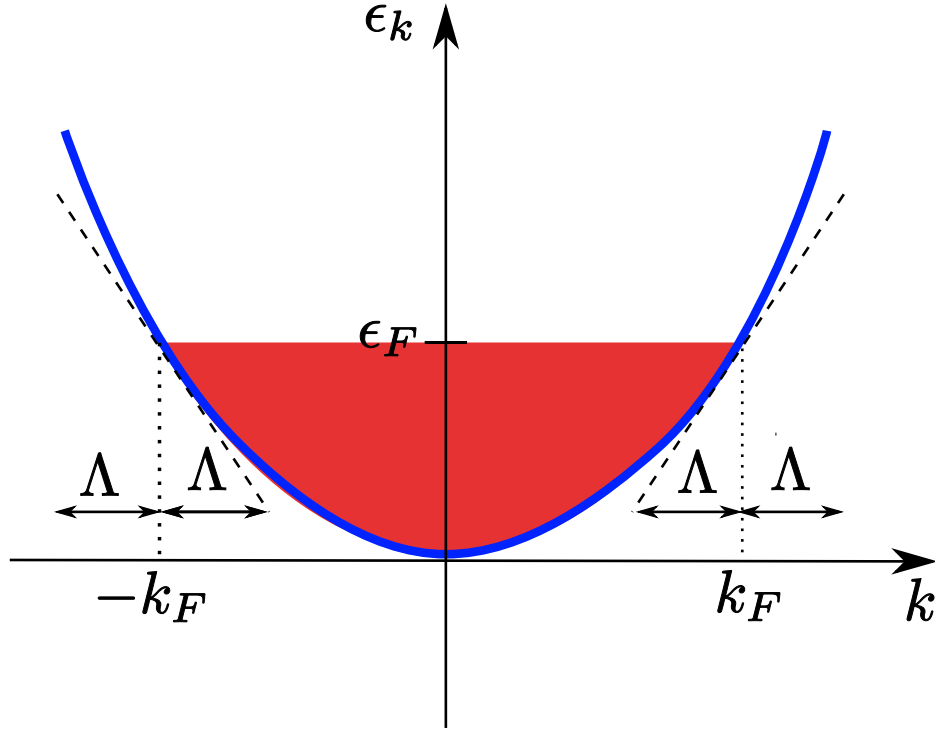
Figure 2.1: Linearizion of the energy dispersion around the Fermi points in one dimensional fermionic system according to the TLM, where Λ denotes the bandwidth cutoff.

where V is the volume of the one dimensional system. The crucial point is that the Fermi surface consists of only two points k_F and $-k_F$, where k_F is the the Fermi momentum and

$$\epsilon_F = \frac{k_F^2}{2m}\,, \tag{2.2}$$

represents the Fermi energy. Tomonaga assumed that one can linearize the energy dispersion ϵ_k around these two Fermi points as follows,

$$\epsilon_k \approx \epsilon_F + \alpha v_F q\,, \qquad\qquad \alpha = \pm\,, \tag{2.3}$$

with

$$q = k - \alpha k_F\,, \qquad\qquad v_F = \frac{k_F}{m}\,, \tag{2.4}$$

where $v_F = k_F/m$ is called the Fermi velocity and the fermions are categorized into the two classes *right movers* for $\alpha = +$ and *left movers* for $\alpha = -$. Fig. 2.1 shows schematically Tomonaga's linearization. Note that this approximation is valid for $|q_\alpha| < \Lambda$ with a given bandwidth cutoff Λ. A finite value for Λ is necessary to avoid unphysical singularities [19]. In order to make the calculations simpler we take the
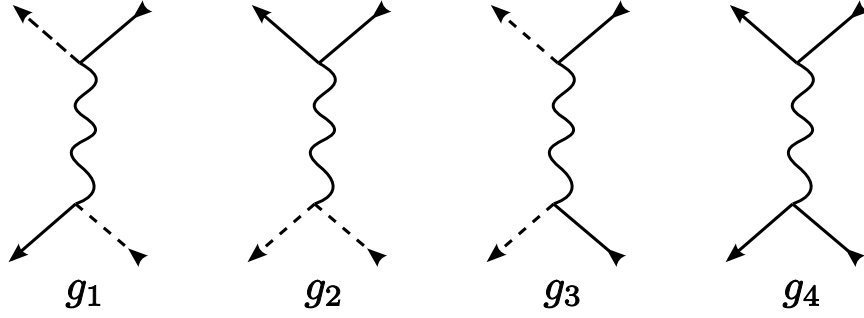
Figure 2.2: Different scattering processes in the TLM which are denoted by the wavy lines. The solid lines represent the right mover electrons while the dashed lines represent the left mover electrons.

limit $\Lambda \to \infty$, which is reliable for sufficiently weak interactions. We obtain for the kinetic energy part of the Hamiltonian

$$\hat{H}_0 = \sum_{\alpha=\pm} \sum_q (\epsilon_F + \alpha v_F q)\, \hat{c}_{q\alpha}^\dagger \hat{c}_{q\alpha}\,, \qquad (2.5)$$

where $\hat{c}_{q\alpha}^\dagger$ and $\hat{c}_{q\alpha}$ are creation and annihilation operators of fermions with momentum $k = \alpha k_F + q$. For noninteracting fermions, the chemical potential is given by $\mu = \epsilon_F$. We obtain thus for the noninteracting Green functions of left and right moving electrons in the TLM

$$G_0^\alpha(i\omega, k) = \frac{1}{i\omega + \mu - \epsilon_k} = \frac{1}{i\omega - \alpha v_F q}\,. \qquad (2.6)$$

By this construction the interaction (2.1c) can be expressed in terms of four coefficients g_1, g_2, g_3 and g_4, identified in *g-ology classification* and represented in Fig. 2.2. In *g*-ology classification g_1 represents the backward scattering, g_2 and g_4 together describe the forward scattering and g_3 is the umklapp scattering. Note that for spinless fermions g_1- and g_2-processes are the same but if we take the spin into account these two scattering processes become different. The umklapp process g_3 is only relevant for half filled bands which give rise to isolators. In addition one can show that in the TLM the backward scattering g_1 becomes irrelevant in the renormalization group (RG) sense [19]. The interaction part of the TLM can therefore be written as

$$\hat{H}_{\text{int}} = \frac{1}{2} \sum_q f_q^{\alpha\alpha'} \hat{\rho}_{-q\alpha} \hat{\rho}_{q\alpha'}\,. \qquad (2.7)$$

where

$$\hat{\rho}_{q\alpha} = \sum_{\alpha=\pm} \sum_k c_{k\alpha}^\dagger c_{k+q\alpha} \qquad (2.8)$$

is the density operator of the right moving (for $\alpha = +$) and the left moving (for $\alpha = -$) electrons in momentum space. We have defined the following matrix to describe the interaction between the electrons with the indices $\alpha = (+, -)$,

$$f_q^{\alpha\alpha'} = \begin{pmatrix} g_4 & g_2 \\ g_2 & g_4 \end{pmatrix}. \tag{2.9}$$

For more simplification we demand that

$$g_2 = g_4 = f_q, \qquad \Leftrightarrow \qquad f_q^{\alpha\alpha'} = f_q \quad \forall\, \alpha, \alpha' \in \{+, -\}. \tag{2.10}$$

In Sec. 2.2 we introduce a new model called *forward scattering model* which only includes g_2 and g_4 and in comparison with the TLM the difference is that the energy dispersion is not linearized.

2.1   Dynamic structure factor

We have pointed out that only collective excitations are well defined in Luttinger liquids. In this section we show how density fluctuations generate a bosonic collective excitation which is called zero sound [2, 20]. Mathematically, the dynamic structure factor $S(\omega, q)$ is defined as the spectral density of the density-density correlation function,

$$S(\omega, q) = \frac{1}{\pi} \mathrm{Im}\Pi(i\bar{\omega} \to \omega + i0, q), \qquad \bar{\omega} > 0. \tag{2.11}$$

$$\Pi(\tau) = -\frac{1}{V}\left\langle \hat{T}[\hat{\rho}_q(\tau)\hat{\rho}_{-q}(0)] \right\rangle \tag{2.12}$$

where τ denotes the imaginary time while $\hat{T}$ is the time ordering operator and

$$\hat{\rho}_q(\tau) = \sum_k \hat{c}_k^\dagger(\tau)\hat{c}_{k+q}(\tau) \tag{2.13}$$

is the density operator. The condition $\bar{\omega} > 0$ ensures that we consider inelastic scatterings.

Alternatively the one particle Green function obtained by means of the field-theoretical bosonization, can be derived through the Ward identity, associated with the conservation law at each Fermi point [21, 22]. Within the Ward identity approach one can show that the loop diagrams, involving more than two fermionic external legs do not contribute to the density response function so that the *random-phase approximation* (RPA) for the polarization

$$\Pi_{\mathrm{RPA}}(i\bar{\omega}, q) = \frac{\Pi_0(i\bar{\omega}, q)}{1 + f_q\Pi_0(i\bar{\omega}, q)} \tag{2.14}$$

becomes exact. Here $\Pi_0(i\bar{\omega}, q)$ represents the noninteracting polarization,

$$\Pi_0(i\bar{\omega}, q) = -\frac{1}{\beta V} \sum_{\alpha=\pm} \sum_{k, i\omega} G_0^\alpha(i\omega, k) G_0^\alpha(i\omega + i\bar{\omega}, k+q), \tag{2.15}$$
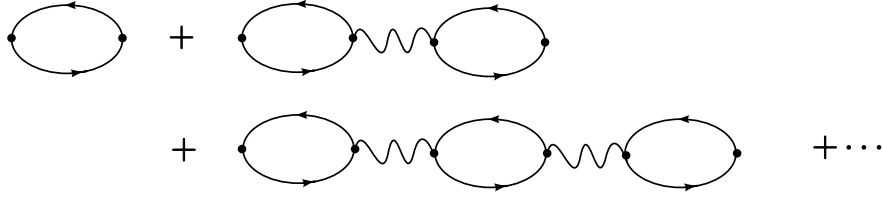
Figure 2.3: Diagrams contributing to the density response function in RPA approximation where the first diagram denotes the noninteracting polarization $\Pi_0(i\bar{\omega}, q)$. The thin wavy line denotes the bare interaction and the solid arrows represent noninteracting fermionic single-particle Green functions.

where β is the inverse temperature. This statement is known as *the closed loop theorem*, which we treat in the context of the functional bosonization in Chap. 3. In the limit $T \to 0$ and $V \to \infty$ the sums are replaced by integrals,

$$\Pi_0(i\bar{\omega}, q) = -\sum_{\alpha=\pm} \int_{-\infty}^{\infty} \frac{dk}{(2\pi)^2} \int_{-\infty}^{\infty} \frac{d\omega}{[i\omega - \alpha v_F k][i\omega + i\bar{\omega} - \alpha v_F (k+q)]} . \quad (2.16)$$

Here the integration over the frequency can be carried out via the residue theorem,

$$\begin{aligned} \Pi_0(i\bar{\omega}, q) &= \sum_{\alpha=\pm} \int_{-\infty}^{\infty} \frac{dk}{2\pi} \frac{\Theta(-\alpha v_F k) - \Theta(-\alpha v_F (k+q))}{i\bar{\omega} - \alpha v_F q} \\ &= -\sum_{\alpha=\pm} \frac{1}{2\pi} \frac{\alpha q}{i\bar{\omega} - \alpha v_F q} = \frac{1}{\pi v_F} \frac{(v_F q)^2}{(v_F q)^2 + \bar{\omega}^2} . \end{aligned} \quad (2.17)$$

Note that this exact result can be obtained using bosonization which generates from (2.5) and (2.7) a Hamiltonian that is noninteracting in bosonic language [8,10,19,23–25]. A graphical representation of RPA is shown in Fig. 2.3. As a consequence, the dynamic structure factor of the TLM has only a single δ-function peak corresponding to a collective zero sound (ZS) mode with infinite lifetime[1]. For spinless fermions with long-range density-density interaction f_q one obtains with small q,

$$S_{\text{TLM}}(\omega, q) = \frac{1}{\pi} \text{Im}\Pi_{\text{RPA}}(i\bar{\omega} \to \omega + i0, q) = Z_q \delta(\omega - v_0|q|), \quad (2.18)$$

where the velocity v_0 and the weight Z_q of the collective ZS mode can be written as

$$v_0/v_F = \sqrt{1 + g_0} , \quad (2.19)$$

$$Z_q = \frac{v_F q^2}{2\pi v_0 |q|} = \frac{|q|}{2\pi\sqrt{1 + g_0}} . \quad (2.20)$$

For later convenience we have introduced the relevant dimensionless interaction at vanishing momentum-transfer,

$$g_0 = \nu_0 f_0 , \quad (2.21)$$

---

[1] We consider the neutral spinless fermions in this work. In charged Fermi systems the collective excitation is called plasmon instead of ZS [2].

where ν_0 is the noninteracting density of states at the Fermi energy,

$$
\nu_0 = \frac{1}{V} \sum_k \delta\left(\frac{k^2}{2m} - \frac{k_F^2}{2m}\right) = \int_{-\infty}^{\infty} \frac{dk}{2\pi} \, \delta\left(\frac{k^2}{2m} - \frac{k_F^2}{2m}\right) = \frac{1}{\pi v_F} \, . \tag{2.22}
$$

The question is now how the line shape of $S(\omega, q)$ changes if we do not linearize the energy dispersion.

2.2   Forward scattering model

Despite the exact solution of the TLM, it is not sufficient to understand quantitatively the dynamic structure factor in Luttinger liquids. The spectral line shape is expected to depend on nonuniversal parameters of the model under consideration, such as the nonlinear terms in the expansion of the energy dispersion ϵ_k around the Fermi momentum k_F, or the coefficients in the expansion of the Fourier transform f_q of the interaction for small momentum-transfers q. Because these parameters correspond to the couplings which are irrelevant (in the RG sense) at the Luttinger liquid fixed point, the line shape of $S(\omega, q)$ is hard to obtain using standard field-theoretical methods, such as field-theoretical bosonization, which has otherwise been very successful to obtain the infrared properties of Luttinger liquids [8,10,19,23–25].

   In this section we use a functional integral formalism to analyze a model beyond the TLM *including quadratic energy dispersion*. We consider nonrelativistic spinless fermions interacting with long-range density-density forces in one spatial dimension. The Hamiltonian of the system is of the same form as Eq. (2.1). The first part of the Hamiltonian can be written as

$$
\hat{H}_0 = \sum_k \epsilon_k \hat{c}_k^\dagger \hat{c}_k \, , \tag{2.23}
$$

with

$$
\epsilon_k = \frac{k^2}{2m} \, . \tag{2.24}
$$

Since according to the definition (2.4) we obtain

$$
\epsilon_k = \epsilon_F + \alpha v_F q + \frac{q^2}{2m} \, , \tag{2.25}
$$

the TLM is equivalent to the limit $1/m \to 0$. On the other hand, because of the quadratic energy dispersion, all states on the right and left sides of the band structure are included with $k \in (-\infty, +\infty)$. The splitting of the fermions into the right and left movers is therefore unnecessary. According to Eqs. (2.7, 2.10), the interaction reduces to

$$
\hat{H}_{\text{int}} = \frac{1}{2} \sum_q f_q \hat{\rho}_{-q} \hat{\rho}_q \, , \tag{2.26}
$$

where $\hat{\rho}_q$ is the total density operator which is defined in (2.13). Note that, in contrast to the TLM, the forward scattering model does not require ultraviolet regularization because the quadratic energy dispersion in one dimension renders all loop integrations ultraviolet convergent. Hence the usual problems associated with the removal of ultraviolet cutoffs and the associated anomalies [26,27] simply do not arise in the forward scattering model.

Using path-integral formulation presented in [28] the ratio of the grand canonical partition functions with and without interaction can be written as

$$\frac{\mathcal{Z}}{\mathcal{Z}_0} = \frac{\int \mathcal{D}[\bar{c}, c] \, e^{-S_{\mathrm{E}}[\bar{c}, c]}}{\int \mathcal{D}[\bar{c}, c] \, e^{-S_0[c, \bar{c}]}} \,, \tag{2.27}$$

where

$$\mathcal{D}[c, \bar{c}] = \prod_{k, i\omega} d\bar{c}_K \, dc_K \tag{2.28}$$

and the Grassmann-fields $\{c_K, \bar{c}_K\}$ are associated with the fermionic annihilation and creation operators $\{\hat{c}_k(\tau), \hat{c}_k^\dagger(\tau)\}$. The Euclidean action $S_{\mathrm{E}}[\bar{c}, c]$ is given by

$$S_{\mathrm{E}}[\bar{c}, c] = S_0[\bar{c}, c] + S_{\mathrm{int}}[\bar{c}, c] \,, \tag{2.29}$$

with

$$S_0[\bar{c}, c] = -\int_K (i\omega - \epsilon_k + \mu)\bar{c}_K c_K \,, \tag{2.30}$$

$$S_{\mathrm{int}}[\bar{c}, c] = \frac{1}{2} \int_Q f_q \rho_{-Q} \rho_Q \,, \tag{2.31}$$

$$\rho_Q = \int_K \bar{c}_K c_{K+Q} \,. \tag{2.32}$$

The collective label $K = (i\omega, k)$ denotes fermionic Matsubara frequencies $i\omega$ and wave-vectors k, while $Q = (i\bar{\omega}, q)$ depends on bosonic Matsubara frequencies $i\bar{\omega}$. The corresponding integration symbols are

$$\int_K = \frac{1}{\beta V} \sum_{\omega, k} \,, \qquad\qquad \int_Q = \frac{1}{\beta V} \sum_{\bar{\omega}, q} \,. \tag{2.33}$$

Eventually, we shall take the limit of infinite volume $V \to \infty$ and zero temperature $\beta \to \infty$, where

$$\int_K = \int \frac{d\omega dk}{(2\pi)^2} \,, \qquad\qquad \int_Q = \int \frac{d\bar{\omega} dq}{(2\pi)^2} \,. \tag{2.34}$$

We assume that the Fourier transform f_q of the interaction is suppressed for momentum transfers q exceeding a certain cutoff $q_0 \ll k_F$. For explicit calculations it is sometimes convenient to use a sharp cutoff [29],

$$f_q = f_0 \Theta(q_0 - |q|) \,. \tag{2.35}$$

However, as will be discussed in detail in Chap. 8, the vanishing of all derivatives of f_q at $q = 0$ eliminates an important damping mechanism, so that it is better to work with a more realistic smooth cutoff, such as a Lorentzian,

$$f_q = \frac{f_0}{1 + q^2/q_0^2} \,. \tag{2.36}$$

Throughout this work we assume that the momentum-transfer cutoff q_0 (which for Lorentzian interaction can be identified with the Thomas-Fermi screening wave-vector) satisfies

$$p_0 \equiv \frac{q_0}{2k_F} \ll 1 \,. \tag{2.37}$$

The precise form of f_q is not important for our purpose, as long as for small q we may expand

$$f_q = f_0 + \frac{1}{2} f_0'' q^2 + \mathcal{O}(q^4) \,, \qquad \text{with } f_0'' \neq 0 \,. \tag{2.38}$$

By dimensional analysis, we may use the second derivative f_0'' of the Fourier transform of the interaction to construct a new momentum scale

$$q_c = \frac{1}{m|f_0''|} \,, \tag{2.39}$$

which will play an important role in this work. Note that for Lorentzian cutoff $f_0'' = -2f_0/q_0^2 < 0$ and $q_c = q_0^2/(2mf_0)$, but in general the momentum scale q_c is independent of the momentum transfer cutoff q_0. We assume that

$$q_c \ll q_0 \ll k_F \,. \tag{2.40}$$

For simplicity, we shall refer to the forward scattering model defined above as the FSM. The noninteracting Green function in the FSM is given by

$$G_0(K) = \frac{1}{i\omega - \xi_k} \,, \qquad \xi_k = \frac{k^2}{2m} - \frac{k_F^2}{2m} \,. \tag{2.41}$$

In addition for the Fourier transform of the polarization defined by Eq. (2.12), we get

$$\Pi(Q) = \frac{\int \mathcal{D}[\bar{c}, c] \, e^{-S_{\mathrm{E}}[\bar{c}, c]} \, \rho_Q \rho_{-Q}}{\int \mathcal{D}[\bar{c}, c] \, e^{-S_{\mathrm{E}}[c, \bar{c}]}} \,, \tag{2.42}$$

where for $f_q \to 0$ we obtain

$$\begin{aligned}
\Pi_0(Q) &= -\int_K G_0(K) G_0(K + Q) = \int \frac{\Theta(-\xi_{k+q}) - \Theta(-\xi_k)}{i\bar{\omega} - \xi_{k+q} + \xi_k} \, dk \\
&= \frac{m}{2\pi q} \ln \left[\frac{\bar{\omega}^2 + \left(v_F q + \frac{q^2}{2m} \right)^2}{\bar{\omega}^2 + \left(v_F q - \frac{q^2}{2m} \right)^2} \right] \,.
\end{aligned} \tag{2.43}$$
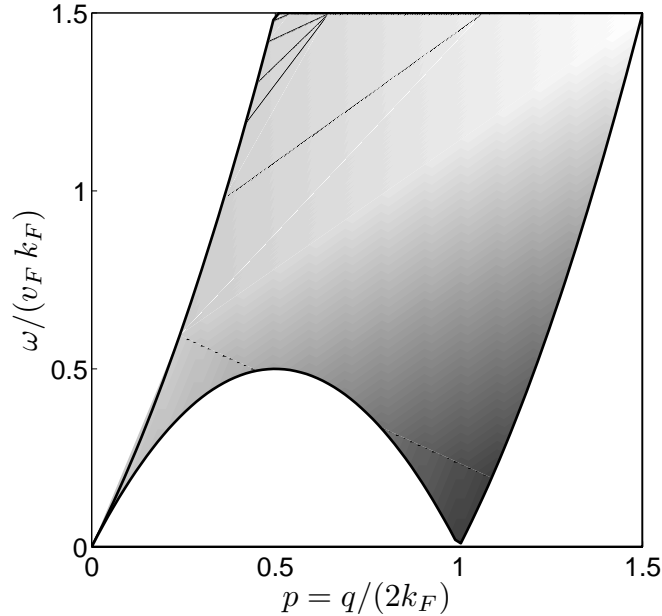
Figure 2.4: Schematical representation of single particle-hole excitations arising in one dimensional fermion systems. The shaded region corresponds to the excitation energy spectrum as a function of q, where $S_0(\omega, q)$ is finite.

Thus, the dynamic structure factor of the noninteracting fermion gases with quadratic energy dispersion is characterized by a step function as follows,

$$S_0(\omega, q) = \frac{1}{\pi} \operatorname{Im}\Pi_0(\omega, q) = \frac{m}{2\pi |q|} \Theta \left(\frac{q^2}{2m} - \left| \omega - v_F |q| \right| \right) . \qquad (2.44)$$

The region $v_F|q| - \frac{q^2}{2m} < \omega < v_F|q| + \frac{q^2}{2m}$ shown in Fig. 2.4 describes the allowed excitation energies of particle-hole pairs. Note that in the limit $1/m \to 0$, $\Pi_0(Q)$ reduces to Eq. (2.17).

Recently there have been many attempts to calculate the dynamic structure factor of interacting fermions with nonlinear energy dispersion in Luttinger liquids [3–6, 29–40]. Most successful works were done by Pustilnik *et al.* [3, 32] and Pereira *et al.* [4, 35, 36], who showed independently that the width of the ZS mode scales as q^2/m. Pustilnik *et al.* expanded the full polarization $\Pi(\omega, q)$ in powers of the bare interaction and found already at the first order in the bare interaction that the correction to $S(\omega, q)$ diverges logarithmically if ω approaches a certain threshold edge ω_q^- from above. They argued that via a resummation procedure analogue to the X-ray problem [41] one can transform the logarithmic singularity into an algebraic one. These authors did not keep track of the finite zero sound velocity which will be discussed in the context of this thesis. Pereira *et al.* [35, 36] have focused on an exactly solvable model belonging to the Luttinger liquid universality class. They have confirmed numerically the existence of the algebraic singularities at lower edge

using Bethe ansatz. But this model obtained from the XXZ-chain [4, 35, 36] is different from the FSM since it includes also backward scattering as well as momentum transfers of the order of k_F.

Let us now give a brief outline of the rest of the first part of this thesis. In Chap. 3 we introduce the functional bosonization approach to the FSM, introducing the irreducible polarization $\Pi_*(\omega, q)$ which consists of the free polarization $\Pi_0(\omega, q)$ and its corrections because of the band curvature. This approach will be then used in Chap. 7 to derive a self-consistency equation for $\Pi_*^{-1}(\omega, q)$ which does not exhibit any mass-shell singularities. In Chap. 4 we outline briefly the theory of functional renormalization group (FRG) and present furthermore a nonperturbative functional renormalization group flow equation for the irreducible polarization of the FSM. However, in this work we shall not attempt to further analyze this rather complicated integro-differential equation. In Chap. 5 we will discuss the dynamic structure factor of the FSM within the RPA and show that in this approximation the ZS mode is not damped. But it is still instructive to start from the RPA because it allows us to understand the origin of the mass-shell singularities encountered in conventional bosonization. In Chap. 6, we derive explicit expressions for the symmetrized closed fermion loops of the FSM which are associated with the interaction in the bosonized model. In addition we show that for linearized energy dispersion (corresponding to the TLM) the RPA becomes exact.

A perturbative expansion in powers of symmetrized fermion loops, in the context of the functional bosonization approach from Chap. 3, is described in Chap. 7. We introduce a reliable approximation and show that within this approximation the mass-shell singularities at $\omega = v_F q$ cancel each other out. In Chap. 8 we present an evaluation of the irreducible polarization for sharp momentum-transfer cutoff (2.35), using the approximation from Chap. 7. We show that for sharp momentum-transfer cutoff our calculation suffer from a mass-shell singularity at $\omega = v_0 q$. Finally, in Chap. 9 we consider a general interaction f_q of the type (2.38) and show that for our forward scattering model there is a large intermediate regime $q_c \lesssim q \ll k_F$ where indeed the damping of ZS behaves as $\gamma_q \propto q^3/(m q_c)$. We also present explicit results for the spectral line shape of $S(\omega, q)$. Due to the complexity of the integrations, in the regime $q \ll q_c$ we cannot evaluate our functional bosonization result for $S(\omega, q)$. However, at $q \approx q_c$ our expression for ZS damping γ_q matches the result $\gamma_q \propto q^2/m$ obtained by several other authors for different model systems for Luttinger liquids [3–5, 31]. In Chap. 10 we summarize our main results and present an outline for further treatments.

Most of the results of this part of the thesis have been published in Ref. [42].

Chapter 3

Functional bosonization

For the treatment of the FSM we use a theoretical approach reproducing the exact solution of the TLM by linearizing the energy dispersion. In the context of the TLM, the functional bosonization idea has been introduced by Fogedby [43] as well as Lee and Chen [44]. Later this technique has been used to bosonize interacting fermions with dominant forward scattering in arbitrary dimensions [45, 46] and to estimate the effect of the nonlinear energy dispersion on the single-particle Green function [47, 48]. For a review of this approach see Ref. [49].

In this chapter we describe briefly the functional bosonization approach to the FSM. Performing the *Hubbard-Stratonovich transformation*, we obtain an effective bosonized action $S_{\text{eff}}[\Delta\phi]$ which depends on bosonic fields $\Delta\phi_Q$. In Sec. 3.2 we construct a systematic expansion of irreducible polarization $\Pi_*(\omega, q)$ in powers of bosonic loops which will be explained in Chap. 7. According to the closed loop theorem we show that the density-density correlation function for the TLM is given by the RPA-polarization. Here we keep track of Hartree corrections to the fermionic self-energy, because these corrections contribute to the renormalization of the ZS velocity.

3.1 Effective bosonized action

In this section we review the functional bosonization approach [45–47, 49] which we will use in Sec. 3.2 in order to calculate the dynamic structure factor. The Hubbard-Stratonovich transformation [50, 51] which is the central concept of our functional bosonization is based on the multidimensional Gaussian integral, i.e.,

$$\int \prod_{i=1}^{n} \frac{dz_i^* \, dz_i}{2\pi i} \, e^{-\sum_{i,j=1}^{n} z_i^* A_{ij} z_j + \sum_{i=1}^{n}(J_i^* z_i + J_i z_i^*)} = [\det A]^{-1} e^{\sum_{i,j=1}^{n} J_i^* A_{ij}^{-1} J_j} , \qquad (3.1)$$

where A is an arbitrary $(n \times n)$ matrix whose Hermitian part (i.e., $(A + A^\dagger)/2$) has only positive eigenvalues.

Using the Gaussian integral (3.1) we can decouple the density-density interac-

tion (2.31), by means of a real Hubbard-Stratonovich field ϕ_Q ($\phi_Q^* = \phi_{-Q}$)[1]

$$e^{-S_{\text{int}}[\bar{c},c]} = e^{-\frac{1}{2}\int_Q f_q \rho_{-Q}\rho_Q} = \frac{\int \mathcal{D}[\phi]\, e^{-S_0[\phi]-S_1[\bar{c},c,\phi]}}{\int \mathcal{D}[\phi]\, e^{-S_0[\phi]}} \ , \tag{3.2}$$

where

$$\int \mathcal{D}[\phi] = \prod_{q>0,i\bar{\omega}} \int \frac{d\phi_Q^*\, d\phi_Q}{2i\pi} \ . \tag{3.3}$$

Here the free fermionic action $S_0[\bar{c},c]$ is given in Eq. (2.30), the free bosonic part is

$$S_0[\phi] = \frac{1}{2}\int_Q f_q^{-1}\phi_{-Q}\phi_Q \ , \tag{3.4}$$

and the Bose-Fermi interaction is

$$S_1[\bar{c},c,\phi] = i\int_Q \rho_{-Q}\phi_Q = i\int_Q \int_K \bar{c}_{K+Q}c_K\phi_Q \ . \tag{3.5}$$

According to (2.27), the ratio of the partition functions can be expressed in the following form

$$\frac{\mathcal{Z}}{\mathcal{Z}_0} = \frac{\int \mathcal{D}[\bar{c},c]\int \mathcal{D}[\phi]\, e^{-S_0[\bar{c},c]-S_0[\phi]-S_1[\bar{c},c,\phi]}}{\int \mathcal{D}[\bar{c},c]\int \mathcal{D}[\phi]\, e^{-S_0[\bar{c},c]-S_0[\phi]}} \ . \tag{3.6}$$

The fermionic part of the action in the numerator of Eq. (3.6) can be written as

$$S_0[\bar{c},c] + S_1[\bar{c},c,\phi] = -\int_K \int_{K'} \bar{c}_K [\mathbf{G}^{-1}]_{KK'} c_{K'} \ , \tag{3.7}$$

where the infinite matrix $\mathbf{G}^{-1}$ is defined by

$$[\mathbf{G}^{-1}]_{KK'} = \delta_{K,K'}[i\omega - \epsilon_k + \mu] - i\phi_{K-K'} \ . \tag{3.8}$$

At finite density, the field ϕ_Q has a nonzero expectation value,

$$\phi_Q = -i\delta_{Q,0}\bar{\phi} + \Delta\phi_Q \ , \tag{3.9}$$

where the δ-symbol is given by $\delta_{Q,0} = \beta V \delta_{\bar{\omega},0}\delta_{q,0}$ which reduces to $(2\pi)^2\delta(\bar{\omega})\delta(q)$ for $\beta \to \infty$ and $V \to \infty$. We fix the real constant $\bar{\phi}$ from the requirement that the effective action $S_{\text{eff}}[\phi]$ of the ϕ-field, which is obtained by integrating over the fermionic fields in Eq. (3.6), does not contain a term linear in the fluctuation $\Delta\phi_Q$. To do this, we define the matrix $\mathbf{G}_0^{-1}$ which includes the self-energy correction due to the vacuum expectation value $\bar{\phi}$,

$$[\mathbf{G}_0^{-1}]_{KK'} = \delta_{K,K'}[i\omega - \epsilon_k - \bar{\phi} + \mu] \ , \tag{3.10}$$

---

[1]Because the the symbol ρ_Q denotes the Fourier components of the real density field, we obtain $\rho_Q^* = \rho_{-Q}$. On the other hand, the Hubbard-Stratonovich field ϕ_Q should have the same symmetry, since it couples to ρ_Q [49].

and write

$$\mathbf{G}^{-1} = \mathbf{G}_0^{-1} - \mathbf{V}\,, \qquad\qquad [\mathbf{V}]_{KK'} = i\Delta\phi_{K-K'}\,. \tag{3.11}$$

Integrating in Eq. (3.6) over the fermion fields, we obtain the formally exact expression,

$$\frac{\mathcal{Z}}{\mathcal{Z}_0} = e^{-\beta(\Omega_1-\Omega_0)}\frac{\int\mathcal{D}[\Delta\phi]e^{-S_{\rm eff}[\Delta\phi]}}{\int\mathcal{D}[\phi]e^{-S_0[\phi]}}\,, \tag{3.12}$$

where $\Omega_1 - \Omega_0$ is the change of the grand canonical potential due to the vacuum expectation value ignoring fluctuations,

$$\Omega_1 - \Omega_0 = \frac{1}{\beta}\mathrm{Tr}\ln[\mathbf{G}_0(\bar{\phi})\mathbf{G}_0^{-1}(\bar{\phi}=0)] - V\frac{\bar{\phi}^2}{2f_0}\,. \tag{3.13}$$

Here we have used the "trace-log" formula, see Ref. [52],

$$\det B = \exp[\mathrm{Tr}\ln B]\,. \tag{3.14}$$

The effective action for the fluctuations of the bosonic field is

$$\begin{aligned}
S_{\rm eff}[\Delta\phi] &=& S_0[\phi_Q \to -i\delta_{Q,0}\bar{\phi} + \Delta\phi_Q] + \beta V\frac{\bar{\phi}^2}{2f_0} - \mathrm{Tr}\ln[1 - \mathbf{G}_0\mathbf{V}] \\
&=& \frac{1}{2}\int_Q f_q^{-1}\Delta\phi_{-Q}\Delta\phi_Q - if_0^{-1}\bar{\phi}\Delta\phi_0 + \sum_{n=1}^{\infty}\frac{\mathrm{Tr}[\mathbf{G}_0\mathbf{V}]^n}{n}\,.
\end{aligned} \tag{3.15}$$

We now fix the vacuum expectation value $\bar{\phi}$ from the saddle point condition

$$\frac{\partial\Omega_1}{\partial\bar{\phi}} = -V\frac{\bar{\phi}}{f_0} + V\rho_0 = 0\,, \qquad\Rightarrow\qquad \bar{\phi} = f_0\rho_0\,. \tag{3.16}$$

Here ρ_0 is the density and $G_0(K)$ the fermionic Green function in self-consistent Hartree approximation, i.e.,

$$\rho_0 = \int_K G_0(K) = \frac{1}{V}\sum_k \Theta(\mu - \epsilon_k - f_0\rho_0)\,, \tag{3.17}$$

$$G_0(K) = \frac{1}{i\omega - \epsilon_k - f_0\rho_0 + \mu}\,. \tag{3.18}$$

Note that Eq. (3.18) agrees with Eq. (2.41) if we take into account that within self-consistent Hartree approximation the Fermi momentum k_F is defined via

$$\frac{k_F^2}{2m} = \mu - f_0\rho_0\,. \tag{3.19}$$

Eq. (3.16) guarantees that the terms linear in the fluctuations $\Delta\phi_Q$ in Eq. (3.15) cancel, so that our final result for the effective action for the fluctuations of the Hubbard-Stratonovich field is

$$S_{\rm eff}[\Delta\phi] = \frac{1}{2}\int_Q f_q^{-1}\Delta\phi_{-Q}\Delta\phi_Q + \sum_{n=2}^{\infty}\frac{\mathrm{Tr}[\mathbf{G}_0\mathbf{V}]^n}{n} = S_2[\Delta\phi] + S_{\rm int}[\Delta\phi]\,, \tag{3.20}$$

with the Gaussian part given by

$$S_2[\Delta\phi] = \frac{1}{2}\int_Q [f_q^{-1} + \Pi_0(Q)]\Delta\phi_{-Q}\Delta\phi_Q\,, \qquad (3.21)$$

and the interaction part

$$S_{\text{int}}[\Delta\phi] = \sum_{n=3}^{\infty}\frac{1}{n!}\int_{Q_1}\cdots\int_{Q_n}\delta_{Q_1+\ldots+Q_n,0}\Gamma_0^{(n)}(Q_1,\ldots,Q_n)\Delta\phi_{Q_1}\ldots\Delta\phi_{Q_n}\,. \quad (3.22)$$

The vertices $\Gamma_0^{(n)}(Q_1,\ldots,Q_n)$ are proportional to the symmetrized closed fermion loops $L_S^{(n)}(Q_1,\ldots,Q_n)$,

$$\Gamma_0^{(n)}(Q_1,\ldots,Q_n) \;=\; i^n(n-1)!L_S^{(n)}(-Q_1,\ldots,-Q_n)\,, \qquad (3.23)$$

with symmetrized closed fermion loops given by

$$L_S^{(n)}(Q_1,\ldots,Q_n) \;=\; \frac{1}{n!}\sum_{P(1,\ldots,n)}\int_K G_0(K)G_0(K-Q_{P(1)})$$

$$\times\; G_0(K-Q_{P(1)}-Q_{P(2)})\cdots G_0(K-\sum_{j=1}^{n-1}Q_{P(j)})\,, \quad (3.24)$$

where the sum is over all permutations $P(1,\ldots,n)$ of $1,\ldots,n$, and the fermionic Green functions $G_0(K)$ should be calculated within the self-consistent Hartree approximation, see Eq. (3.18). Note that in Eq. (3.21) we have used

$$\Gamma_0^{(2)}(Q_1,-Q_1) = L_S^{(2)}(-Q_1,Q_1) = -\int_K G_0(K)G_0(K+Q) = \Pi_0(Q)\,. \qquad (3.25)$$

A graphical representation of $\Gamma_0^{(n)}(Q_1,\ldots,Q_n)$ is shown in Fig. 3.1. The closed loop theorem states that for the TLM [i.e., in the limit $1/m \to 0$, see Eq. (2.25)], the symmetrized closed fermion loops with more than two external legs vanish [22, 45, 49, 53]. Therefore $S_{\text{eff}}[\Delta\phi]$ reduces to the Gaussian approximation $S_2[\Delta\phi]$, so that the noninteracting bosonized system can be solved exactly. In Chap. 6 we give explicit expressions for the symmetrized n-loops of the FSM [54–56] and show that $L_S^{(n)} \propto (1/m)^{n-2}$ to leading order in $1/m$.

3.2   Irreducible polarization

In analogy with the RPA approximation (2.14), we define the irreducible polarization as

$$\Pi(Q) = \frac{\Pi_*(Q)}{1 + f_q\Pi_*(Q)} = \frac{1}{f_q + \Pi_*^{-1}(Q)}\,. \qquad (3.26)$$
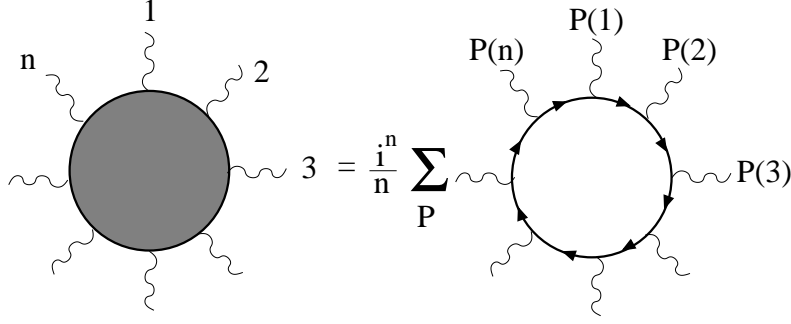
Figure 3.1: Boson vertex with n external legs in the interaction part $S_{\text{int}}[\Delta\phi]$ of the bosonized effective action, see Eq. (3.22). The arrows denote the fermionic Green functions $G_0(K)$ within self-consistent Hartree approximation, see Eq. (3.18). The sum is taken over the $n!$ permutations of the labels of the external legs. For linearized energy dispersion all symmetrized closed fermion loops with more than two external legs vanish.

Applying the Hubbard-Stratonovich transformation (3.2) to Eq. (2.42) we obtain

$$
\begin{aligned}
\Pi(Q) &= \frac{\int \mathcal{D}[\bar{c}, c] \int \mathcal{D}[\phi]\, e^{-S_0[\bar{c},c]-S_0[\phi]-S_1[\bar{c},c,\phi]}\, \rho_Q \rho_{-Q}}{\int \mathcal{D}[\bar{c}, c] \int \mathcal{D}[\phi]\, e^{-S_0[\bar{c},c]-S_0[\phi]-S_1[\bar{c},c,\phi]}} \\
&= -(\beta V)^2 \left. \frac{\partial^2 \mathcal{F}[\tilde{\phi}]}{\partial \tilde{\phi}_{-Q}\, \partial \tilde{\phi}_Q} \right|_{\tilde{\phi}=0},
\end{aligned}
\tag{3.27}
$$

where

$$
\mathcal{F}[\tilde{\phi}] = \frac{\int \mathcal{D}[\bar{c}, c] \int \mathcal{D}[\phi]\, e^{-S_0[\bar{c},c]-S_0[\phi]-S_1[\bar{c},c,\phi+\tilde{\phi}]}}{\int \mathcal{D}[\bar{c}, c] \int \mathcal{D}[\phi]\, e^{-S_0[\bar{c},c]-S_0[\phi]-S_1[\bar{c},c,\phi]}}
\tag{3.28}
$$

is a generating functional depending on the external real source fields $\tilde{\phi}_Q$. Performing the transformation $\phi_Q \to \phi_Q - \tilde{\phi}_Q$ in the numerator of Eq (3.2), we get

$$
\mathcal{F}[\tilde{\phi}] = \frac{\int \mathcal{D}[\bar{c}, c] \int \mathcal{D}[\phi]\, e^{-S_0[\bar{c},c]-S_0[\phi-\tilde{\phi}]-S_1[\bar{c},c,\phi]}}{\int \mathcal{D}[\bar{c}, c] \int \mathcal{D}[\phi]\, e^{-S_0[\bar{c},c]-S_0[\phi]-S_1[\bar{c},c,\phi]}}\, .
\tag{3.29}
$$

We apply now the derivatives with respect to $\tilde{\phi}_Q$ and $\tilde{\phi}_{-Q}$ given in (3.27). After a short calculation, it is easy to show that

$$
\begin{aligned}
\frac{1}{f_q^{-1} + \Pi_*(Q)} &= f_q^2 \Pi(Q) - f_q \\
&= \frac{\int \mathcal{D}[\bar{c}, c] \int \mathcal{D}[\phi]\, e^{-S_0[\bar{c},c]-S_0[\phi]-S_1[\bar{c},c,\phi]}\, \phi_Q \phi_{-Q}}{\int \mathcal{D}[\bar{c}, c] \int \mathcal{D}[\phi]\, e^{-S_0[\bar{c},c]-S_0[\phi]-S_1[\bar{c},c,\phi]}}\, .
\end{aligned}
\tag{3.30}
$$

Integrating the fermions out, the irreducible polarization can be obtained from the fluctuation propagator of the Hubbard-Stratonovich field,

$$
\langle \Delta\phi_Q \Delta\phi_{Q'} \rangle = \frac{\int \mathcal{D}[\Delta\phi] e^{-S_{\text{eff}}[\Delta\phi]} \Delta\phi_Q \Delta\phi_{Q'}}{\int \mathcal{D}[\Delta\phi] e^{-S_{\text{eff}}[\Delta\phi]}} = \delta_{Q+Q',0} \frac{1}{f_q^{-1} + \Pi_*(Q)}\, ,
\tag{3.31}
$$
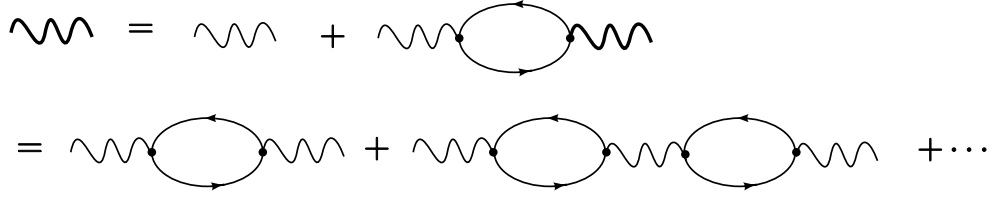
Figure 3.2: Diagrammatic definition of RPA interaction which is denoted by the thick wavy line. The thin wavy lines have the same meaning as in Fig. 2.3 while the solid arrows here represent the Hartree Green function defined in (3.18).

where the vacuum expectation value $\bar{\phi}$ is given by (3.16) and the effective action $S_{\text{eff}}[\Delta\phi]$ is defined in Eq. (3.20). We have pointed out that for the TLM ($1/m \to 0$) the closed fermion loops with more than two external legs do not contribute to the bosonized effective action $S_{\text{eff}}[\Delta\phi]$ and consequently instead of Eq. (3.31), we get

$$\langle \Delta\phi_Q \Delta\phi_{Q'} \rangle_{S_2} \;\; = \;\; \delta_{Q+Q',0} \frac{1}{f_q^{-1} + \Pi_0(Q)} \equiv \delta_{Q+Q',0} f_{\text{RPA}}(Q) \,, \qquad (3.32)$$

where $f_{\text{RPA}}(Q)$ is called the RPA interaction. A diagrammatic representation of $f_{\text{RPA}}(Q)$ is shown in Fig. 3.2.

We have shown that for a linearized energy dispersion the irreducible polarization $\Pi_*(Q)$ agrees with the noninteracting one $\Pi_0(Q)$ and therefore according to to Eq. (3.26) the RPA polarization is exact.

For the quadratic energy dispersion, $\Pi_0(Q)$ will be replaced by the irreducible polarization $\Pi_*(Q)$. The corrections to the RPA can now be calculated systematically in powers of the interaction $S_{\text{int}}[\Delta\phi]$ using the Wick theorem. The RPA interaction thereby plays the role of the Gaussian propagator, so that we naturally obtain an expansion in powers of the RPA interaction.

Chapter 4

Functional renormalization group

In this chapter we give a short review of the functional renormalization group (FRG) and its application to the FSM [7,57–63]. The renormalization group (RG) methods are important to describe systems where fluctuations on many time and length scales lead to divergencies within the perturbation theory. The FRG based on the generating functionals is an elegant strategy to implement the Wilson's idea of the RG and to eliminate unphysical divergences via exact flow equations.

In the first section of this chapter we present a general formalism of FRG, introducing generating functionals and irreducible vertices. In Sec. 4.2 we set up the exact FRG expansions for the irreducible vertices such as one-particle self-energy. In Sec. 4.3 we show how the FRG flow equations change in symmetry broken systems where the field has a finite expectation value.

In Sec. 4.4 we apply the FRG to the FSM, using mixed Bose-Fermi fields. This section is based on the FRG approach to one dimensional fermionic systems [7,57], where we drop the spin indices and take into account that the Hubbard-Stratonovich field ϕ_Q has a finite expectation value, see Ref. [58,59]. However the evaluation of the density-density correlation function in the context of the FRG requires extensive numerical calculation which we have not been able to carry out.

4.1 Generating functionals

Lets assume that the action of the system is given in the following form

$$S[\Phi] = S_0[\Phi] + S_1[\Phi]\,, \tag{4.1}$$

where the Gaussian part is

$$S_0[\Phi] = -\frac{1}{2}\int_\alpha\int_{\alpha'}\Phi_\alpha[\mathbf{G}_0^{-1}]_{\alpha\alpha'}\Phi_{\alpha'} \equiv -\frac{1}{2}(\Phi,\mathbf{G}_0^{-1}\Phi)\,. \tag{4.2}$$

The super-field Φ consists of fermionic as well as bosonic elements Φ_α depending on α. The super-label α includes in addition to the fields classification, all labels necessary to specify the field configuration such as energy, momentum and spin. The symbol $\int_\alpha$ represents summation (for discrete α) or integration (for continuous

α) over all values of α. The Gaussian propagator is assumed to have following symmetry,

$$\mathbf{G}_0^T = \mathbf{Z}\mathbf{G}_0 = \mathbf{G}_0\mathbf{Z} , \tag{4.3}$$

where the infinite diagonal matrix $\mathbf{Z}$ is defined by,

$$\mathbf{Z}_{\alpha\alpha'} = \delta_{\alpha\alpha'}\zeta_\alpha , \qquad \text{with} \quad \zeta_\alpha = \begin{cases} 1 & \text{if } \Phi_\alpha \text{ denotes a boson,} \\ -1 & \text{if } \Phi_\alpha \text{ denotes a fermion.} \end{cases} \tag{4.4}$$

As example we consider the bosonized FSM. Due to Eq. (3.6), we have

$$S_0[\Phi] = S_0[\bar{c}, c] + S_0[\phi] = -\frac{1}{2}(\Phi, \mathbf{G}_0^{-1}\Phi) , \tag{4.5}$$

with $\Phi = [c, \bar{c}, \phi]$ and

$$\mathbf{G}_0 = \begin{pmatrix} 0 & \hat{G}_0 & 0 \\ \zeta\hat{G}_0^T & 0 & 0 \\ 0 & 0 & -\hat{F}_0 \end{pmatrix} , \tag{4.6}$$

where $\zeta = -1$ and $\hat{G}_0$ and $\hat{F}_0$ are infinite matrices in momentum and frequency space,

$$[\hat{G}_0]_{K,K'} = \delta_{K,K'}G_0(K) , \qquad\qquad [\hat{F}_0]_{Q,Q'} = \delta_{Q+Q',0'}f_q . \tag{4.7}$$

We start with the generating functional of the Green functions,

$$\mathcal{G}[J] = \frac{1}{\mathcal{Z}} \int \mathcal{D}[\Phi]\, e^{-S[\Phi]+(J,\Phi)} , \tag{4.8}$$

where

$$(J, \Phi) = \int_\alpha J_\alpha \Phi_\alpha \tag{4.9}$$

and J is the super-source field whose components J_α for a fixed α have the same character (bosonic or fermionic) as Φ_α. The coefficient $\mathcal{Z}$ represents here the partition function which is given by

$$\mathcal{Z} = \int \mathcal{D}[\Phi]\, e^{-S[\Phi]} . \tag{4.10}$$

The Green functions are the expectation value of the product of fields, i.e.,

$$\mathcal{G}^{(n)}_{\alpha_1\cdots\alpha_n} = \langle \Phi_{\alpha_n}\cdots\Phi_{\alpha_1} \rangle = \frac{\int \mathcal{D}[\Phi] e^{-S[\Phi]}\, \Phi_{\alpha_n}\cdots\Phi_{\alpha_1}}{\int \mathcal{D}[\Phi] e^{-S[\Phi]}} = \frac{\delta^n \mathcal{G}[J]}{\delta J_{\alpha_n}\cdots\delta J_{\alpha_1}}\bigg|_{J=0} , \tag{4.11}$$

where the super-script denotes that the Green function has n external legs and $\frac{\delta}{\delta J_\alpha}$ represents the functional derivative with respect to J_α. For FSM, it is convenient to write

$$
\begin{aligned}
(J, \Phi) &= (\bar{j}, c) + (\bar{c}, j) + (J^*, \phi) \\
&= \int_K \bar{j}_K c_K + \int_K \bar{c}_K j_K + \int_Q J_Q^* \phi_Q \,,
\end{aligned} \tag{4.12}
$$

where this notation is equivalent to the definition of source terms $J = (\bar{j}, \zeta j, \phi)$. A comparison between Eqs. (4.9) and (4.12) shows that [see Eq. (2.33)],

$$
\frac{\delta}{\delta J_\alpha} = \beta V \frac{\partial}{\partial J_\alpha} \,. \tag{4.13}
$$

Eq. (4.11) is equivalent to the functional Taylor expansion,

$$
\mathcal{G}[J] = \sum_{n=0}^{\infty} \frac{1}{n!} \int_{\alpha_1} \cdots \int_{\alpha_n} \mathcal{G}_{\alpha_1 \cdots \alpha_n}^{(n)} J_{\alpha_1} \cdots J_{\alpha_n} \,. \tag{4.14}
$$

Likewise we introduce the generating functional for the *connected Green functions* (see Refs. [28, 57] for a proof),

$$
\mathcal{G}_c[J] = \ln \left(\frac{\mathcal{Z}}{\mathcal{Z}_0} \mathcal{G}[J] \right) = \ln \left(\frac{1}{\mathcal{Z}_0} \int \mathcal{D}[\Phi] \, e^{-S[\Phi] + (J, \Phi)} \right) \,, \tag{4.15}
$$

where

$$
\mathcal{Z}_0 = \int \mathcal{D}[\Phi] \, e^{-S_0[\Phi]} \tag{4.16}
$$

is the partition function without interaction. Analogous to Eq. (4.14) we obtain

$$
\mathcal{G}_c[J] = \sum_{n=0}^{\infty} \frac{1}{n!} \int_{\alpha_1} \cdots \int_{\alpha_n} \mathcal{G}_{c,\alpha_1 \cdots \alpha_n}^{(n)} J_{\alpha_1} \cdots J_{\alpha_n} \,, \tag{4.17}
$$

where

$$
\mathcal{G}_{c,\alpha_1 \cdots \alpha_n}^{(n)} = \left. \frac{\delta^n \mathcal{G}_c[J]}{\delta J_{\alpha_n} \cdots \delta J_{\alpha_1}} \right|_{J=0} \,. \tag{4.18}
$$

In particular the exact Green function can be generated by $\mathcal{G}_c[J]$ as follows,

$$
[\mathbf{G}]_{\alpha\alpha'} = - \left. \frac{\delta^2 \mathcal{G}_c[J]}{\delta J_\alpha \, \delta J_{\alpha'}} \right|_{J=0} = -\mathcal{G}_{c,\alpha'\alpha}^{(2)} \,. \tag{4.19}
$$

It is clear that the total Green function $\mathbf{G} = -\frac{\delta^2 \mathcal{G}_c[J]}{\delta J_\alpha \, \delta J_{\alpha'}}$ has the same symmetry as the noninteracting one given by Eq. (4.3),

$$
\mathbf{G}^T = \mathbf{Z}\mathbf{G} = \mathbf{G}\mathbf{Z} \,. \tag{4.20}
$$

In order to derive the irreducible vertex functions, we perform a Legendre transformation of $\mathcal{G}_c[J]$,

$$\mathcal{L}[\langle\Phi\rangle] = (J[\langle\Phi\rangle], \Phi) - \mathcal{G}_c[J[\langle\Phi\rangle]] \,, \tag{4.21}$$

where $\langle\Phi\rangle$ is the expectation value of the super-field Φ which depends on the source field via

$$\langle\Phi_\alpha\rangle = \frac{\delta\mathcal{G}_c}{\delta J_\alpha} \,, \qquad \Leftrightarrow \qquad \langle\Phi\rangle = \frac{\delta\mathcal{G}_c}{\delta J} \,. \tag{4.22}$$

Redefining

$$\Phi \equiv \langle\Phi\rangle \,, \tag{4.23}$$

from the chain role, it is evident that

$$\frac{\delta\mathcal{L}}{\delta\Phi_\alpha} = \zeta_\alpha J_\alpha + \left(\frac{\delta J}{\delta\Phi_\alpha}, \Phi\right) - \sum_{\alpha'} \frac{\delta J_{\alpha'}}{\delta\Phi_\alpha}\frac{\delta\mathcal{G}_c}{\delta J_{\alpha'}} = \zeta_\alpha J_\alpha \,. \tag{4.24}$$

Consequently, we obtain according to Eq. (4.4),

$$J = \mathbf{Z}\frac{\delta\mathcal{L}}{\delta\Phi} \,. \tag{4.25}$$

Additionally, using again the chain role, we have

$$\mathbf{1} = \frac{\delta\Phi}{\delta\Phi} = \frac{\delta\Phi}{\delta J}\frac{\delta J}{\delta\Phi} = \frac{\delta^2\mathcal{G}_c}{\delta J\,\delta J}\mathbf{Z}\frac{\delta^2\mathcal{L}}{\delta\Phi\,\delta\Phi} \,, \tag{4.26}$$

which yields for vanishing fields Φ and J

$$\left.\frac{\delta^2\mathcal{L}}{\delta\Phi\,\delta\Phi}\right|_{\Phi=J=0} = -\mathbf{Z}\mathbf{G}^{-1} = -[\mathbf{G}^{-1}]^T \,. \tag{4.27}$$

To obtain the generating functionals of the irreducible vertices, it is suitable to subtract the Gaussian action from the Legendre transformation (4.21),

$$\Gamma[\Phi] = \mathcal{L}[\Phi] - S_0[\Phi] = \mathcal{L}[\Phi] + \frac{1}{2}(\Phi, \mathbf{G}_0^{-1}\Phi) \,. \tag{4.28}$$

Therefore, we get according to the Dyson's equation,

$$\left.\frac{\delta^2\Gamma}{\delta\Phi\,\delta\Phi}\right|_{\Phi=0} = \left.\frac{\delta^2\mathcal{L}}{\delta\Phi\,\delta\Phi}\right|_{\Phi=0} + \mathbf{G}_0^{-1} = -\mathbf{G}^{-1} + \mathbf{G}_0^{-1} = \mathbf{\Sigma} \,, \tag{4.29}$$

where $\mathbf{\Sigma}$ is the self-energy matrix. Using the functional Taylor expansion, the generating functional $\Gamma[\Phi]$ can be expressed in terms of the irreducible vertices,

$$\Gamma[\Phi] = \sum_{n=0}^{\infty} \frac{1}{n!} \int_{\alpha_1} \cdots \int_{\alpha_n} \Gamma^{(n)}_{\alpha_1\cdots\alpha_n} \Phi_{\alpha_1} \cdots \Phi_{\alpha_n} \,, \tag{4.30}$$
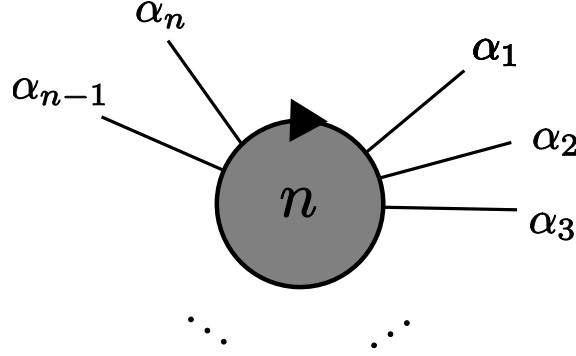
Figure 4.1: The irreducible vertices with n external legs defined in Eq. (4.31) are shown with shaded circles. The external legs associated with the indices are either bosonic or fermionic. The arrow on the circle shows the ordering of the indices $(\alpha_1 \cdots \alpha_n)$ in the vertex function. Note that for purely bosonic systems this arrow can be omitted because the vertex is completely symmetric.

where the irreducible vertex functions with n external legs are given by

$$\Gamma^{(n)}_{\alpha_1 \cdots \alpha_n} = \left. \frac{\delta^n \Gamma[J]}{\delta\Phi_{\alpha_n} \cdots \delta\Phi_{\alpha_1}} \right|_{J=0}. \tag{4.31}$$

Fig. 12.5 shows a graphical representation of $\Gamma^{(n)}_{\alpha_1 \cdots \alpha_n}$.

Finally, we note that the connected Green functions can be expressed in terms of the irreducible vertices as follows,

$$\frac{\delta^2 \mathcal{G}_c[J]}{\delta J \, \delta J} = -\sum_{l=0}^{\infty} \mathbf{Z}\mathbf{G}^T (\mathbf{U}^T \mathbf{G}^T)^l, \tag{4.32}$$

where

$$\begin{aligned}
\mathbf{U} &= \left[\frac{\delta^2 \Gamma}{\delta\Phi \, \delta\Phi} - \left. \frac{\delta^2 \Gamma}{\delta\Phi \, \delta\Phi} \right|_{\Phi=0} \right]^T = \left[\frac{\delta^2 \Gamma}{\delta\Phi \, \delta\Phi} \right]^T - \mathbf{\Sigma} \\
&= \sum_{n=0}^{\infty} \frac{1}{n!} \int_{\alpha_1} \cdots \int_{\alpha_n} \mathbf{\Gamma}^{(n+2)}_{\alpha_1 \cdots \alpha_n} \Phi_{\alpha_1} \cdots \Phi_{\alpha_n},
\end{aligned} \tag{4.33}$$

with the matrix

$$\left[\mathbf{\Gamma}^{(n+2)}_{\alpha_1 \cdots \alpha_n} \right]_{\alpha\alpha'} = \Gamma^{(n+2)}_{\alpha\alpha'\alpha_1 \cdots \alpha_n}. \tag{4.34}$$

The proof of Eq. (4.32) is not cumbersome. From definition (4.33) of $\mathbf{U}$ we obtain

$$\frac{\delta^2 \mathcal{L}}{\delta\Phi \, \delta\Phi} = \mathbf{U}^T - [\mathbf{G}^{-1}]^T, \tag{4.35}$$

and therefore

$$\left[\frac{\delta^2 \mathcal{L}}{\delta\Phi \, \delta\Phi} \right]^{-1} = -\mathbf{G}^T [\mathbf{1} - \mathbf{U}^T \mathbf{G}^T]^{-1} = -\sum_{l=0}^{\infty} \mathbf{G}^T (\mathbf{U}^T \mathbf{G}^T)^l. \tag{4.36}$$

We can hence drive Eq. (4.32) using (4.26) and (4.36). This equation gives rise to the so-called tree expansion which we will not describe here.

4.2   Exact flow equations

The renormalization group idea was proposed in order to eliminate the infrared divergences, arising in the context of the diagrammatic perturbation theory. As Wilson has proposed, one starts with higher energy regimes and in the next steps iteratively one takes lower energies into account. In FRG we suppress the fluctuations with low energies by imposing a cutoff scale in the free propagator of the action,

$$\mathbf{G}_0 \to \mathbf{G}_{0,\Lambda}, \qquad \Rightarrow \qquad S_0[\Phi] \to S_{0,\Lambda}[\Phi]. \tag{4.37}$$

There are two possibilities introducing the FRG cutoff:

$$\mathbf{G}_{0,\Lambda} = \mathbf{\Theta}_\Lambda \mathbf{G}_0 \qquad \text{with} \qquad \mathbf{\Theta}_\Lambda \sim \begin{cases} 1 & \text{for } \Lambda \to 0, \\ 0 & \text{for } \Lambda \to \infty \end{cases} \tag{4.38}$$

or

$$\mathbf{G}_{0,\Lambda}^{-1} = \mathbf{G}_0^{-1} - \mathbf{R}_\Lambda \qquad \text{with} \qquad |\mathbf{R}_\Lambda| \sim \begin{cases} 0 & \text{for } \Lambda \to 0, \\ \infty & \text{for } \Lambda \to \infty. \end{cases} \tag{4.39}$$

In any case we obtain the boundary conditions,

$$\mathbf{G}_{0,\Lambda} \sim \begin{cases} \mathbf{G}_0 & \text{for } \Lambda \to 0, \\ 0 & \text{for } \Lambda \to \infty. \end{cases} \tag{4.40}$$

These conditions are equivalent to the fact that for the low energy modes Λ the Gaussian propagator is switched off, $\mathbf{G}_{0,\Lambda} \approx 0$ while for high energy modes we obtain the original Gaussian propagator, $\mathbf{G}_{0,\Lambda} \approx \mathbf{G}_0$. By this construction, the Green functions and the irreducible vertices depends also on the FRG cutoff Λ,

$$\mathcal{G}_c[J] \to \mathcal{G}_{c,\Lambda}[J], \qquad\qquad \Gamma[\Phi] \to \Gamma_\Lambda[\Phi]. \tag{4.41}$$

The important point is that because in the limit $\Lambda \to \infty$ the free propagator vanishes, the generating functional of the irreducible vertices reduces to the non-Gaussian part of the action in the original physical model, i.e.,

$$\lim_{\Lambda \to \infty} \Gamma_\Lambda[\Phi] = S_1[\Phi]. \tag{4.42}$$

Now, we write the flow equation of the irreducible vertex functions without proving this [7, 57],

$$
\begin{aligned}
\partial_\Lambda \Gamma_{\Lambda,\alpha_1,\cdots,\alpha_n}^{(n)} &= -\frac{1}{2} \sum_{l=1}^\infty \sum_{m_1=1}^\infty \sum_{m_2=1}^\infty \cdots \sum_{m_l=1}^\infty \delta_{n,m_1+\ldots+m_l} \\
&\times \; \mathcal{S}_{\alpha_1,\cdots,\alpha_{m_1};\alpha_{m_1+1},\cdots,\alpha_{m_1+m_2};\cdots;\alpha_{m_1+\cdots+m_{l-1}+1},\cdots,\alpha_n} \operatorname{Tr}\left[\mathbf{Z}\dot{\mathbf{G}}_\Lambda^T \mathbf{\Gamma}_{\Lambda,\alpha_1,\cdots,\alpha_{m_1}}^{(m_1+2)\,T} \right. \\
&\times \; \left. \mathbf{G}_\Lambda^T \mathbf{\Gamma}_{\Lambda,\alpha_{m_1+1},\cdots,\alpha_{m_1+m_2}}^{(m_2+2)\,T} \mathbf{G}_\Lambda^T \ldots \mathbf{\Gamma}_{\Lambda,\alpha_{m_1+\cdots+m_{l-1}+1},\cdots,\alpha_n}^{(m_l+2)\,T} \right],
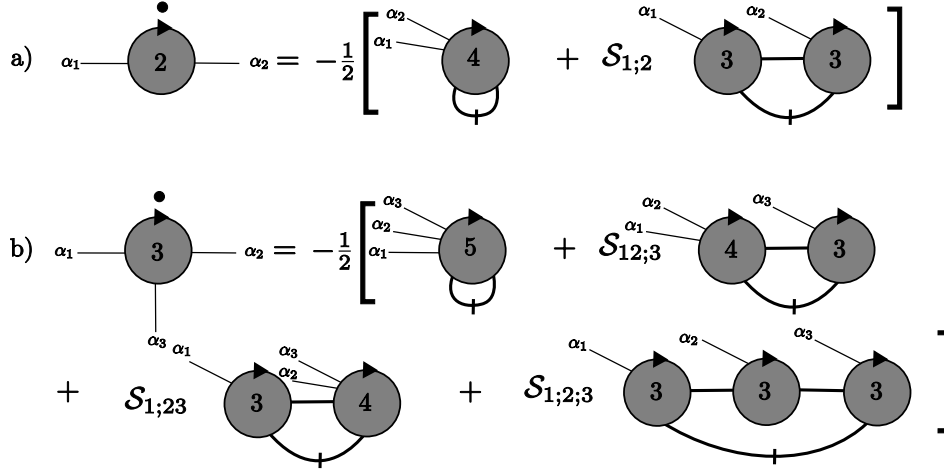\end{aligned}
\tag{4.43}
$$

Figure 4.2: Exact flow equations for the irreducible vertices: a) $\Gamma^{(2)}_{\Lambda,\alpha_1,\alpha_2}$, b) $\Gamma^{(3)}_{\Lambda,\alpha_1,\alpha_2,\alpha_3}$. The dots above the vertices denote the derivative with respect to Λ. The fat lines represent the propagator $\mathbf{G}_\Lambda$ and the slashed fat lines display the single scale propagators $\dot{\mathbf{G}}_\Lambda$.

where $n \geq 1$ and the so-called *single scale propagator* is defined by

$$\dot{\mathbf{G}}_\Lambda = -\mathbf{G}_\Lambda \left(\partial_\Lambda \mathbf{G}^{-1}_{0,\Lambda} \right) \mathbf{G}_\Lambda = [\mathbf{1} - \mathbf{\Sigma}\mathbf{G}_0]^{-1} \left(\partial_\Lambda \mathbf{G}^{-1}_{0,\Lambda} \right) [\mathbf{1} - \mathbf{\Sigma}\mathbf{G}_0]^{-1} . \tag{4.44}$$

Furthermore $\mathcal{S}$ is the symmetrization operator, i.e.,

$$\mathcal{S}_{\alpha_1,\cdots,\alpha_{m_1};\alpha_{m_1+1},\cdots,\alpha_{m_1+m_2};\cdots;\alpha_{m_1+\cdots+m_{l-1}+1}} = \frac{1}{\prod_{i=1}^{l} m_i!} \sum_P \mathrm{sgn}_\zeta(P) A_{\alpha_{P(1)}\cdots\alpha_{P(n)}} ,$$

$$\tag{4.45}$$

where P denotes any permutation and $\mathrm{sgn}_\zeta(P)$ is defined via the equation

$$\Phi_{\alpha_1}\Phi_{\alpha_2}\cdots\Phi_{\alpha_n} = \mathrm{sgn}_\zeta(P)\Phi_{\alpha_{P(1)}}\Phi_{\alpha_{P(2)}}\cdots\Phi_{\alpha_{P(n)}} . \tag{4.46}$$

It is clear that the vertices $\Gamma^{(n)}_{\alpha_1,\cdots,\alpha_n}$ are symmetric with respect to the exchange of indices. According to Eq. (4.45), the operator $\mathcal{S}$ makes a total symmetric expression from a partly symmetric one. The flow equation of a vertex function with n external legs depends on other vertices whose external legs are bigger than n. Diagrammatic representations of these flow equations for $n = 2$ and $n = 3$ are shown in Fig. 4.2. We can now evaluate the differential equations given by (4.43), choosing $\Lambda = \Lambda_0$ as initial condition and taking eventually the limit $\Lambda \to 0$ to calculate the result.

4.3 FRG with symmetry breaking

In this section we generalize our FRG expansion for the case of nonvanishing expectation value of the super-field Φ [58], i.e.,

$$\left. \frac{\delta\mathcal{G}_c}{\delta J_\alpha} \right|_{J\to 0} = \langle\Phi_\alpha\rangle|_{J\to 0} \equiv \Phi^0_\alpha \neq 0 \tag{4.47}$$

The flow equation (4.43) was driven by assuming that $\Phi_\alpha = 0$. If the super-field Φ has a finite expectation value, we define the generating functionals of irreducible vertices as follows,

$$\Gamma[\Phi] = \mathcal{L}[\Phi] + \frac{1}{2}(\Delta\Phi, \mathbf{G}_0^{-1}\Delta\Phi)\,, \qquad (4.48)$$

where

$$\Delta\Phi_\alpha = \Phi_\alpha - \Phi_\alpha^0\,. \qquad (4.49)$$

Obviously by this construction Γ is extremal at $\Phi_\alpha = \Phi_\alpha^0$,

$$\left.\frac{\delta\Gamma[\Phi]}{\delta\Phi_\alpha}\right|_{\Phi=\Phi^0}. \qquad (4.50)$$

The analogue functional Taylor expansion to Eq. (4.30) is given by

$$\Gamma[\Phi] = \sum_{n=0}^{\infty} \frac{1}{n!} \int_{\alpha_1} \cdots \int_{\alpha_n} \Gamma_{\alpha_1\cdots\alpha_n}^{(n)} \Delta\Phi_{\alpha_1} \cdots \Delta\Phi_{\alpha_n}\,. \qquad (4.51)$$

Note that the vertices $\Gamma_{\alpha_1\cdots\alpha_n}^{(n)}$ implicitly depend on the vacuum expectation value Φ_α^0. In the symmetry breaking case, the FRG flow equation of irreducible vertex function with one external leg is given by

$$\partial_\Lambda \Gamma_{\Lambda,\alpha}^{(1)} = -\frac{1}{2}\mathrm{Tr}\left[\mathbf{Z}\dot{\mathbf{G}}_\Lambda^T \mathbf{\Gamma}_{\Lambda,\alpha}^{(3)\,T}\right] - \int_{\alpha'}\left[\mathbf{G}_\Lambda^{-1}\right]_{\alpha\alpha'}\left(\partial_\Lambda\Phi_{\Lambda,\alpha'}^0\right) - \int_{\alpha'}\left[\partial_\Lambda\mathbf{G}_\Lambda^{-1}\right]_{\alpha\alpha'}\Phi_{\Lambda,\alpha'}^0\,, \qquad (4.52)$$

while flow equations of irreducible vertices with more than one external legs are similar to Eq. (4.43) with the difference that they contains an additional term arising because of the finite value of $\Phi_{\Lambda,\alpha}^0$,

$$\begin{aligned}
\partial_\Lambda\Gamma_{\Lambda,\alpha_1,\cdots,\alpha_n}^{(n)} &= \int_\alpha \left(\partial_\Lambda\Phi_{\Lambda,\alpha}^0\right)\Gamma_{\Lambda,\alpha\alpha_1,\ldots,\alpha_n}^{(n+1)} - \frac{1}{2}\sum_{l=1}^{\infty}\sum_{m_1=1}^{\infty}\sum_{m_2=1}^{\infty}\cdots\sum_{m_l=1}^{\infty}\delta_{n,m_1+\ldots+m_l} \\
&\times\quad \mathcal{S}_{\alpha_1,\cdots,\alpha_{m_1};\alpha_{m_1+1},\cdots,\alpha_{m_1+m_2};\cdots;\alpha_{m_1+\cdots+m_{l-1}+1},\cdots,\alpha_n}\,\mathrm{Tr}\left[\mathbf{Z}\dot{\mathbf{G}}_\Lambda^T\mathbf{\Gamma}_{\Lambda,\alpha_1,\cdots,\alpha_{m_1}}^{(m_1+2)\,T}\right. \\
&\times\quad \left.\mathbf{G}_\Lambda^T\mathbf{\Gamma}_{\Lambda,\alpha_{m_1+1},\cdots,\alpha_{m_1+m_2}}^{(m_2+2)\,T}\mathbf{G}_\Lambda^T\ldots\mathbf{\Gamma}_{\Lambda,\alpha_{m_1+\cdots+m_{l-1}+1},\cdots,\alpha_n}^{(m_l+2)\,T}\right]\,. \qquad (4.53)
\end{aligned}$$

Note that the matrix $\mathbf{\Gamma}_{\Lambda,\alpha_1\cdots\alpha_m}^{(m+2)}$ is defined as in Eq. (4.34). The parameter $\Phi_{\Lambda,\alpha}^0$ describes the flowing order parameter. Demanding that the FRG does not generate vertices with only one external leg (i.e., $\Gamma_{\Lambda,\alpha}^{(1)} = 0$) and choosing $\mathbf{G}_{\Lambda,0}$ such that

$$\mathbf{G}_{0,\Lambda}^{-1}\Phi_\Lambda^0 = 0\,, \qquad\qquad \left[\partial_\Lambda\mathbf{G}_{0,\Lambda}^{-1}\right]\Phi_\Lambda^0 = 0\,, \qquad (4.54)$$

we obtain for the flow equation of the order parameter due to Eq.(4.52),

$$\int_{\alpha'}[\mathbf{\Sigma}_\Lambda]_{\alpha\alpha'}\partial_\Lambda\Phi_{\Lambda,\alpha'}^0 = \frac{1}{2}\mathrm{Tr}\left[\mathbf{\Gamma}_{\Lambda,\alpha}^{(3)}\dot{\mathbf{G}}_\Lambda\right]\,. \qquad (4.55)$$

Fig. 4.3 shows diagrammatic representations of the flow equation for $\Gamma_\alpha^{(1)}$ and $\Gamma_{\alpha_1,\alpha_2}^{(2)}$ in the case of $\Phi_\alpha^0 \neq 0$.
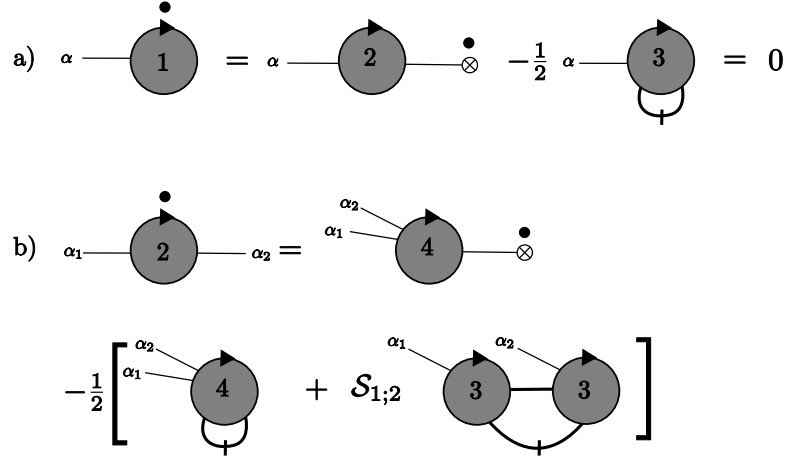
Figure 4.3: Exact flow equations for a) $\Gamma^{(1)}_{\Lambda,\alpha}$ and b) $\Gamma^{(2)}_{\Lambda,\alpha_1\alpha_2}$ in the case of finite vacuum expectation value. The symbols have the same meaning as in Fig. 4.2. Because one-legged vertices are not generated by FRG, we set $\partial_\Lambda\Gamma^{(1)}_{\Lambda,\alpha} = 0$. The smalls dotted circles with cross denote $\partial_\Lambda\Phi^0_\Lambda$.

4.4 Application of FRG to the forward scattering model

In this section we derive a formally FRG equation for the irreducible polarization $\Pi_*(Q)$ of the FSM. Demanding that the particle number is conserved, the Green function matrix has the same block structure as the free propagator given by (4.6),

$$\mathbf{G} = [\mathbf{G}]_{\alpha\alpha'} = -\left.\frac{\delta^2 \mathcal{G}_c[J]}{\delta J_\alpha \, \delta J'_\alpha}\right|_{J=0} = \begin{pmatrix} 0 & \hat{G} & 0 \\ \zeta\hat{G}^T & 0 & 0 \\ 0 & 0 & -\hat{F} \end{pmatrix}, \tag{4.56}$$

where the source field J is introduced in Eq. (4.12). Due to Dyson's equation (4.29), the self-energy $\boldsymbol{\Sigma}$ has the same block structure as the inverse Green function $\mathbf{G}^{-1}$. It involves the fermionic self-energy as well as the the irreducible polarization as follows,

$$\boldsymbol{\Sigma} = \begin{pmatrix} 0 & \zeta[\hat{\Sigma}]^T & 0 \\ \hat{\Sigma} & 0 & 0 \\ 0 & 0 & \hat{\Pi}_*(Q) \end{pmatrix}. \tag{4.57}$$

Here, $\hat{G}$, $\hat{F}$, $\hat{\Sigma}$ and $\hat{\Pi}_*$ are infinite matrices, which are defined by

$$[\hat{G}]_{K,K'} = \delta_{K,K'}G(K), \qquad\qquad [\hat{F}]_{Q,Q'} = \delta_{Q+Q',0}f_*(Q), \tag{4.58}$$

$$[\hat{\Sigma}]_{K,K'} = \delta_{K,K'}\Sigma(K), \qquad\qquad [\hat{\Pi}_*]_{Q,Q'} = \delta_{Q+Q',0}\Pi_*(Q). \tag{4.59}$$

Thus, we get

$$G(K) = \left[G^{-1}(K) - \Sigma(K)\right]^{-1}, \tag{4.60}$$

$$f_*(Q) = \left[f_q^{-1} + \Pi_*(Q)\right]^{-1}. \tag{4.61}$$

We use the momentum-transfer cutoff scheme proposed in Ref. [7], where only the free bosonic part $S_0[\phi]$ is regularized by suppressing bosonic fluctuations with momenta q smaller than a certain cutoff Λ. Considering the sharp momentum transfer cutoff given in Eq. (2.35), one possibility is to introduce the cutoff as a multiplicative Θ-function [64] by replacing in Eq. (3.4)

$$f_q \rightarrow \Theta(|q| - \Lambda)\, f_q = \Theta(|q| - \Lambda)\, \Theta(q_0 - |q|)\, f_0\,. \tag{4.62}$$

We see that $\Theta(|q| - \Lambda)$ satisfies the condition (4.38). Alternatively, we may insert an additive cutoff $R_\Lambda(q)$ [see Eq. (4.39)] in the inverse propagator [65, 66],

$$f_q^{-1} \rightarrow f_q^{-1} + R_\Lambda(q)\,, \tag{4.63}$$

where $R_\Lambda(q) = \nu_0 R(q^2/\Lambda^2)$ with $R(0) = 1$ and $R(\infty) = 0$. A convenient choice is the Litim regulator $R(x) = (1 - x)\Theta(1 - x)$, see Ref. [67]. All correlation functions then depend on the cutoff Λ. Denoting the flowing irreducible polarization by $\Pi_{*,\Lambda}(Q)$, the true irreducible polarization of our model is recovered in the limit

$$\lim_{\Lambda \to 0} \Pi_{*,\Lambda}(Q) = \Pi_*(Q)\,. \tag{4.64}$$

An exact hierarchy of FRG flow equations for the one-line irreducible vertices of our model can then be obtained by differentiating the corresponding generating functional $\Gamma_\Lambda[\langle \bar{c} \rangle, \langle c \rangle, \langle \phi \rangle]$ with respect to Λ and expanding Γ_Λ in powers of the expectation values of the fields

$$\begin{aligned}
\Gamma_\Lambda[\bar{\psi}, \psi, \phi^0 + \delta\phi] \;=\; & \sum_{n=0}^{\infty} \sum_{m=0}^{\infty} \frac{1}{(m!)^2 n!} \int_{K_1'} \cdots \int_{K_m'} \int_{K_1} \cdots \int_{K_m} \int_{Q_1} \cdots \int_{Q_n} \\
\times\; & \delta_{K_1' + \ldots + K_m', K_1 + \ldots + K_m + Q_1 + \ldots + Q_n} \\
\times\; & \Gamma_\Lambda^{(2m,n)}(K_1', \ldots, K_m'; K_1, \ldots, K_m; Q_1, \ldots, Q_n) \\
\times\; & \bar{\psi}_{K_1'} \cdots \bar{\psi}_{K_m'} \psi_{K_1} \cdots \psi_{K_m} \Delta\phi_{Q_1} \cdots \Delta\phi_{Q_n}\,,
\end{aligned} \tag{4.65}$$

where

$$\bar{\psi} = \langle \bar{c} \rangle\,, \qquad\qquad \psi = \langle c \rangle\,, \qquad\qquad \Delta\phi = \langle \phi \rangle - \phi^0\,. \tag{4.66}$$

In our model, the vacuum expectation value ϕ_Q^0 in the absence of the sources is related to the exact density $\rho = \int_K \langle \bar{c}_K c_K \rangle$ via the Poisson equation [58, 59],

$$\phi_Q^0 = \delta_{Q,0}\bar{\phi}\,, \qquad\qquad\qquad \bar{\phi} = -i f_0 \rho\,. \tag{4.67}$$

Following Ref. [58, 59], it is convenient to include the contribution $(2\beta V f_0)^{-1}(\Delta\phi_0)^2$ arising from the fluctuation of the zero mode in the Gaussian part of the bosonic action (3.4) into the definition of the irreducible vertex $\Gamma_\Lambda^{(0,2)}(-Q, Q)$ with two external bosonic legs, so that

$$\Gamma_\Lambda^{(0,2)}(-Q, Q) = (\beta V)^{-1}\delta_{Q,0} f_0^{-1} + \Pi_{*,\Lambda}(Q)\,. \tag{4.68}$$

The flowing irreducible polarization $\Pi_{*,\Lambda}(Q)$ then satisfies the exact flow equation (4.53),

$$
\begin{aligned}
\partial_\Lambda \Pi_{*,\Lambda}(Q) &= \frac{1}{2} \int_{Q'} \dot{F}_\Lambda(Q') \Gamma_\Lambda^{(4)}(Q', -Q', Q, -Q) + \Gamma_\Lambda^{(3)}(Q, -Q, 0) \partial_\Lambda \bar{\phi}_\Lambda \\
&\quad - \int_{Q'} \dot{F}_\Lambda(Q') F_\Lambda(Q + Q') \Gamma_\Lambda^{(3)}(-Q, Q + Q', -Q') \Gamma_\Lambda^{(3)}(Q', -Q - Q', Q) \, .
\end{aligned}
$$
(4.69)

Here for a sharp momentum-transfer cutoff the bosonic propagator is

$$
F_\Lambda(Q) = \Theta(|q| - \Lambda) \frac{f_q}{1 + f_q \Pi_\Lambda(Q)} \, ,
$$
(4.70)

and the corresponding single-scale propagator is

$$
\dot{F}_\Lambda(Q) = -\delta(|q| - \Lambda) \frac{f_q}{1 + f_q \Pi_\Lambda(Q)} \, .
$$
(4.71)

Alternatively, if we work with a smooth additive cutoff then

$$
F_\Lambda(Q) = \frac{f_q}{1 + f_q [\Pi_\Lambda(Q) + R_\Lambda(q)]} \, ,
$$
(4.72)

and

$$
\dot{F}_\Lambda(Q) = [-\partial_\Lambda R_\Lambda(q)][F_\Lambda(Q)]^2 \, .
$$
(4.73)

The vertices

$$
\Gamma_\Lambda^{(n)}(Q_1, \ldots, Q_n) \equiv \Gamma_\Lambda^{(0,n)}(Q_1, \ldots, Q_n)
$$
(4.74)

are the totally symmetrized one-interaction-line irreducible vertices with n external bosonic legs. A graphical representation of Eq. (4.69) is shown in Fig. 4.4. The flow of the vacuum expectation value $\bar{\phi}_\Lambda$ of the bosonic field is determined by the exact FRG equation

$$
[f_0^{-1} + \Pi_\Lambda(0)] \partial_\Lambda \bar{\phi}_\Lambda = -\frac{1}{2} \int_{Q'} \dot{F}_\Lambda(Q') \Gamma_\Lambda^{(3)}(Q', -Q', 0) \, ,
$$
(4.75)

which follows from Eq. (4.55). A graphical representation of Eq. (4.75) is shown in Fig. 4.5. We may use Eq. (4.75) to eliminate the derivative of the flowing vacuum expectation value in the flow equation (4.69) to obtain the following exact FRG flow equation for the irreducible polarization

$$
\begin{aligned}
\partial_\Lambda \Pi_\Lambda(Q) &= \frac{1}{2} \int_{Q'} \dot{F}_\Lambda(Q') \Gamma_\Lambda^{(4)}(Q', -Q', Q, -Q) \\
&\quad - \frac{1}{2} \frac{f_0}{1 + f_0 \Pi_\Lambda(0)} \Gamma_\Lambda^{(3)}(Q, -Q, 0) \int_{Q'} \dot{F}_\Lambda(Q') \Gamma_\Lambda^{(3)}(Q', -Q', 0) \\
&\quad - \int_{Q'} \dot{F}_\Lambda(Q') F_\Lambda(Q + Q') \Gamma_\Lambda^{(3)}(-Q, Q + Q', -Q') \Gamma_\Lambda^{(3)}(Q', -Q - Q', Q) \, .
\end{aligned}
$$
(4.76)

Figure 4.4: Graphical representation of the exact FRG flow equation (4.69) for the irreducible polarization in the momentum-transfer cutoff scheme. The shaded circles represent the one-interaction-line irreducible vertices, the thick wavy lines denote the exact cutoff-dependent boson propagator (effective interaction) defined in Eq. (4.70), the small crossed circle is the flowing vacuum expectation value of the bosonic field ϕ, and the small black dot denotes the derivative with respect to the flow parameter Λ. The slashed wavy lines represent the single-scale propagator given in Eqs. (4.71, 4.73).

Figure 4.5: Graphical representation of the exact FRG flow equation (4.69) for the vacuum expectation value of the bosonic Hubbard-Stratonovich field. The symbols are explained in the caption of Fig. 4.4.

As shown in Refs. [58,59], in the momentum-transfer cutoff scheme the vertices at the initial scale $\Lambda = \Lambda_0 \equiv q_0$ satisfy nontrivial initial conditions. The requirement that the vertex $\Gamma_{\Lambda_0}^{(0,1)}$ with one bosonic leg vanishes at $\Lambda = \Lambda_0$ implies that the fermionic self-energy $\Sigma_{\Lambda_0}(K) = \Gamma_{\Lambda_0}^{(2,0)}(K,K)$ at the initial scale is given by the self-consistent Hartree approximation,

$$\Sigma_{\Lambda_0} = f_0 \rho_0 \,, \tag{4.77}$$

where the initial density ρ_0 satisfies the Hartree self-consistency condition (3.17). The initial conditions for the purely bosonic vertices $\Gamma_{\Lambda_0}^{(0,n)} \equiv \Gamma_{\Lambda_0}^{(n)}$ are for $n = 2$,

$$\Gamma_{\Lambda_0}^{(0,2)}(-Q,Q) = (\beta V)^{-1}\delta_{Q,0}f_0^{-1} - L_S^{(2)}(Q,-Q)\,, \tag{4.78}$$

and for $n > 2$,

$$\Gamma_{\Lambda_0}^{(0,n)}(Q_1,\ldots,Q_n) = i^n(n-1)!\, L_S^{(n)}(-Q_1,\ldots,-Q_n)\,, \tag{4.79}$$

where $L_S^{(n)}(Q_1,\ldots,Q_n)$ are the symmetrized closed fermion loops with n external legs defined in Eq. (3.24). A graphical representation of Eq. (4.79) is shown in Fig. 3.1. By definition, the symmetrized two loop is (up to a minus sign) given by the noninteracting polarization $\Pi_0(Q)$,

$$L_S^{(2)}(-Q,Q) = \int_K G_0(K)G_0(K+Q) = -\Pi_0(Q)\,. \tag{4.80}$$

However, in contrast to Eq. (2.43), the fermionic Green functions in Eq. (4.80) are self-consistent Hartree Green functions as defined in Eq. (3.18). Finally, in the momentum-transfer cutoff scheme the initial value of the three-legged vertex $\Gamma_{\Lambda_0}^{(2,1)}(K';K;Q)$ is

$$\Gamma_{\Lambda_0}^{(2,1)}(K';K;Q) = i\,, \tag{4.81}$$

which follows from Eq. (3.5). All other vertices vanish at the initial scale $\Lambda = \Lambda_0$.

The above RG equation (4.76) is exact but not closed and should be augmented by FRG flow equations for the vertices $\Gamma_{\Lambda}^{(3)}$ and $\Gamma_{\Lambda}^{(4)}$ which in turn involve higher order bosonic vertices. Only for linearized energy dispersion, the closed loop theorem guarantees that $\Gamma_{\Lambda}^{(n)}(Q_1,\ldots,Q_n) = 0$, so that we recover the well known result that the RPA is exact for the Tomonaga-Luttinger model. To motivate a sensible truncation procedure for quadratic energy dispersion, we note that the vertices $\Gamma_{\Lambda}^{(n)}$ with $n \geq 3$ are irrelevant in the renormalization group sense: If we assign to the momentum-independent part of the interaction $f_0 = f_{q=0}$ a vanishing scaling dimension, then in D dimensions the vertices $\Gamma_{\Lambda}^{(n)}$ have scaling dimensions $-(D+z_\phi)(n/2-1)$, where z_ϕ is the dynamic exponent of the bosonic field mediating the forward scattering interaction. In one dimension $z_\phi = 1$ due to the linear dispersion of the ZS mode, so that in $D = 1$ the vertex $\Gamma^{(3)}$ is irrelevant with scaling dimension -1, while $\Gamma^{(4)}$ is irrelevant with scaling dimension -2. Because the renormalization group flow of irrelevant couplings is usually not important, it

is reasonable to truncate the infinite hierarchy of flow equations by approximating the vertices $\Gamma_\Lambda^{(3)}$ and $\Gamma_\Lambda^{(4)}$ in Eq. (4.69) by their initial values at $\Lambda = \Lambda_0$,

$$\Gamma_\Lambda^{(n)}(Q_1, \ldots, Q_n) \approx \Gamma_{\Lambda_0}^{(n)}(Q_1, \ldots, Q_n) = i^n(n-1)! L_S^{(n)}(-Q_1, \ldots, -Q_n), \quad (4.82)$$

where the symmetrized closed fermion loops are defined in Eq. (3.24). Then Eq. (4.76) becomes a closed integro-differential equation for $\Pi_\Lambda(Q)$, the solution of which gives for $\Lambda \to 0$ a nonperturbative estimate for the irreducible polarization. Note that even with the truncation (4.82) the FRG flow equation (4.76) is nonperturbative, because the renormalization of the polarization is self-consistently taken into account in the bosonic loop integrations. It should be interesting to analyze Eq. (4.76) numerically and try to extract the spectral line shape. Possibly, one can check in this way whether the resummation procedure proposed by Pustilnik *et al.* [3] is justified also for nonintegrable models. But because of the difficult numerical calculation we can not handle this equation anymore. On the other hand, the perturbative approach which is derived in Chap. 3 [see Eq. (3.31)] will be evaluated analytically in Chap. 7, using some approximations.

Chapter 5

RPA for the forward scattering model

For the TLM, i.e., for a linearized energy dispersion, the symmetrized closed fermion loops with more than two external legs vanish [22, 45, 49, 53]. Hence, in this limit the RPA yields the exact dynamic structure factor and seems to be a reasonable starting point for the perturbative calculation of $S(\omega, q)$ in the FSM. However we will see in this chapter that the RPA result for $S(\omega, q)$ exhibits some unphysical features which are related to the fact that the effect of interactions on the energy scale of the single-pair particle-hole continuum is not included in the RPA. The first section of this chapter is based on Ref. [29]. In this section we outline briefly the RPA within the quadratic energy dispersion and show how the relative weight of the ZS peak to particle-hole continuum changes by modifying the interaction. In Sec. 5.2 we expand the inverse noninteracting polarization $\Pi_0^{-1}(Q)$ in powers of the inverse mass $1/m$. This expansion gives rise to so-called mass-shell singularities. We then use a simple procedure which was proposed by Samokhin [5] to regularize these singularities.

5.1 Dynamic structure factor within RPA

In the context of RPA [see Eq. (2.14)], the irreducible polarization defined in (3.26) is approximated by the noninteracting one,

$$\Pi_{\mathrm{RPA}}(Q) = \frac{1}{f_q + \Pi_0^{-1}(Q)}, \tag{5.1}$$

where the noninteracting polarization $\Pi_0(Q)$ for quadratic energy dispersion is calculated in (2.43),

$$\Pi_0(Q) = \frac{m}{\pi q} \ln \left| \frac{i\bar{\omega} + v_F q + \frac{q^2}{2m}}{i\bar{\omega} + v_F q - \frac{q^2}{2m}} \right| . \tag{5.2}$$

In the regime $q \ll q_0$ [see Eqs. (2.35,2.36)], the corresponding RPA dynamic structure factor consists of two contributions,

$$S_{\text{RPA}}(\omega, q) = \frac{1}{\pi} \text{Im} \Pi_{\text{RPA}}(Q) = Z_q \delta(\omega - \omega_q) + S_{\text{RPA}}^{\text{inc}}(\omega, q), \qquad (5.3)$$

where the first term represents the undamped ZS mode with weight,

$$Z_q \approx \left[f_0^2 \left. \frac{\partial \text{Re} \Pi_0}{\partial \omega} \right|_{\omega = \omega_q} \right]^{-1} = \frac{v_F q^2}{2\pi \omega_q} W_q, \qquad (5.4)$$

and energy

$$
\begin{aligned}
\omega_q &= v_F |q| \sqrt{1 + \frac{q}{k_F} \coth\left(\frac{q}{k_F g_0}\right) + \left[\frac{q}{2k_F}\right]^2} \\
&= v_0 |q| \left\{ 1 + \frac{g_0(4 + 3g_0)}{6x_0^2} \left[\frac{q}{2k_F g_0}\right]^2 + \mathcal{O}(q^4) \right\}. \qquad (5.5)
\end{aligned}
$$

Note that the dimensionless interaction g_0 is defined in (2.21). The dimensionless function

$$W_q = \frac{\left[\frac{q}{k_F g_0}\right]^2}{\sinh^2\left(\frac{q}{k_F g_0}\right)} \qquad (5.6)$$

can be identified with the relative contribution of the ZS peak to the f-sum rule [29],

$$\int_0^\infty d\omega \, \omega S(\omega, q) = \frac{v_F q^2}{2\pi}. \qquad (5.7)$$

The second part $S_{\text{RPA}}^{\text{inc}}(\omega, q)$ in Eq. (5.3) represents the incoherent continuum due to excitations involving a single particle-hole pair (single-pair continuum). For finite g_0, the shape of $S_{\text{RPA}}^{\text{inc}}(\omega, q)$ is modified as shown quantitatively in Fig. 5.1. It is obvious that the ZS mode never touches the single-pair continuum and ZS mode remains undamped or rather the so-called *Landau damping* [2] does not occur in the FSM. The damping of the ZS mode is thus due to the excitations involving more than a single particle-hole pair (multi-pair excitations) which are neglected in RPA.

For $|q|/k_F \ll g_0$, the relative weight of the single-pair continuum is negligibly small, so that the ZS peak carries most of the spectral weight. For example, the relative contribution of the single-pair continuum to the f-sum rule vanishes as $(q/g_0 k_F)^2 \ll 1$ and the dynamic structure factor reduces to $S_{\text{TLM}}(\omega, q)$ which is given by Eq. (2.18). Note that in the limit $g_0 \to 0$ the ZS mode disappears and the incoherent part $S_{\text{RPA}}^{\text{inc}}(\omega, q)$ becomes a box function (for $q < 2k_F$) according to Eq. (2.44).
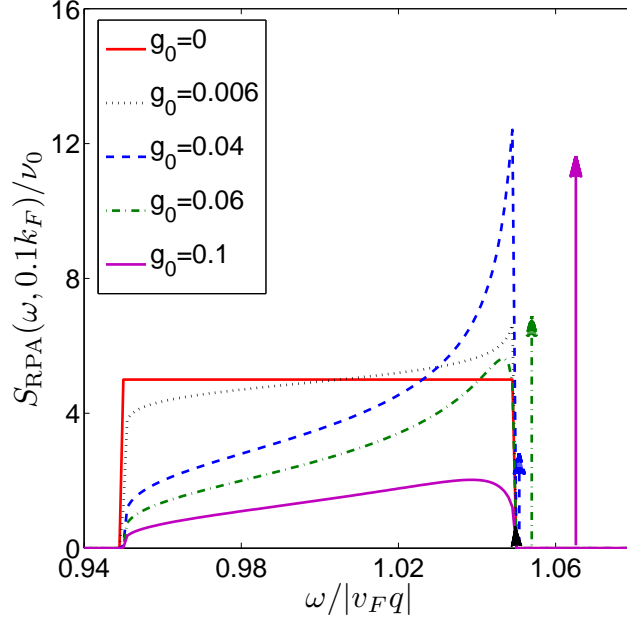
Figure 5.1: RPA dynamic structure factor for forward scattering model, $q/k_F = 0.1$ and different values of $g_0 = \nu_0 f_0$ according to Eq. (5.3). The arrows represent the ZS mode $Z_q \delta(\omega - \omega_q)$, where the position of the arrows is given by the ZS energy ω_q and the length of the arrows is proportional to the weight W_q. Note that for $q/k_F \ll g_0 \ll 1$, the distance between the upper edge of the single-pair particle-hole continuum and the position of the ZS peak is $g_0/2$ which is much larger than the width of the particle-hole continuum or rather q^2/m.

5.2 Expansion of inverse noninteracting polarization in powers of $1/m$

It is instructive to see which features of $S_{\mathrm{RPA}}(\omega, q)$ are recovered if we expand the inverse noninteracting polarization $\Pi_0^{-1}(Q)$ in powers of the inverse mass m^{-1}. Therefore we introduce the dimensionless variables,

$$iy = \frac{i\bar{\omega}}{v_F q}, \qquad\qquad p = \frac{q}{2k_F}, \qquad (5.8)$$

and rewrite Eq. (5.2) as

$$\Pi_0(i\omega, q) = \nu_0 \tilde{\Pi}_0(iy, p), \qquad (5.9)$$

with the dimensionless function

$$\tilde{\Pi}_0(iy, p) = \frac{1}{2p} \ln \left| \frac{iy + 1 + p}{iy + 1 - p} \right| = \frac{1}{4p} \ln \left[\frac{y^2 + (1+p)^2}{y^2 + (1-p)^2} \right]. \qquad (5.10)$$

For an interaction with momentum-transfer cutoff $q_0 \ll k_F$ the relevant dimension-less momenta satisfy $|p| \ll 1$, so that we expand $\tilde{\Pi}_0^{-1}(iy, p)$ in powers of p. From Eq. (5.10) we find

$$\tilde{\Pi}_0^{-1}(iy, p) = 1 + y^2 - \frac{p^2}{3} \frac{1 - 3y^2}{1 + y^2} + \mathcal{O}(p^4). \tag{5.11}$$

For later reference, we note that the correction of order p^2 in Eq. (5.11) can be written as

$$-\frac{p^2}{3} \frac{1 - 3y^2}{(1 + y^2)} = p^2 \left[1 - \frac{4}{3(1 + y^2)} \right] = p^2 - \frac{2p^2}{3} \left[\frac{1}{1 - iy} + \frac{1}{1 + iy} \right]. \tag{5.12}$$

For $p \to 0$ we recover the result for linearized dispersion,

$$\lim_{p \to 0} \tilde{\Pi}_0^{-1}(iy, p) \equiv \tilde{\Pi}_0^{-1}(iy) = 1 + y^2, \tag{5.13}$$

which yields the dynamic structure factor of the TLM given in Eq. (2.18). However, after analytic continuation to real frequencies $iy \to x + i0 = \frac{\omega}{v_F q} + i0$, the correction term of order p^2 in the expansion (5.11) is singular on the mass-shell $|\omega| = v_F|q|$. Although in the noninteracting limit we know that this mass-shell singularity has been artificially generated by expanding the logarithm in Eq. (5.10), it is not clear how to regularize a similar singularity in the interacting system. Therefore, a formal expansion in powers of the band curvature $1/m$ using either a purely fermionic approach [6] or conventional bosonization [38] is not reliable close to the mass-shell after analytic continuation. Fortunately, within the functional bosonization approach used in this work this problem does not arise, because the effective expansion parameter in functional bosonization is not $1/m$, but the combination $g_0 q_0/(m v_F)$, see Refs. [45, 49]. In particular, in the noninteracting limit functional bosonization yields the exact structure factor of the free Fermi gas with quadratic dispersion, containing all orders in $1/m$.

It is instructive to examine the RPA dynamic structure factor if we nevertheless use the expansion (5.11) for the noninteracting polarization. Then we obtain after analytic continuation $iy \to x + i0 = \omega/(v_F q) + i0$ for small $|q| \ll g_0 k_F$,

$$S_{\mathrm{RPA}}(\omega, q) \approx \frac{\nu_0}{\pi} \mathrm{Im} \left[\frac{1}{g_0 + \tilde{\Pi}_0^{-1}(x + i0, p)} \right] = Z_q^+ \delta(\omega - \tilde{\omega}_q^+) + Z_q^- \delta(\omega - \tilde{\omega}_q^-), \tag{5.14}$$

where Z_q^+ and $\tilde{\omega}_q^+$ reduce for small q to the corresponding expressions Z_q and $v_0|q|$ for linear dispersion [see Eq. (2.20)], and the weight and the dispersion of the other mode $\tilde{\omega}_q^-$ is for $|q| \ll k_F g_0$,

$$Z_q^- \approx \frac{2|q|}{3\pi} \left[\frac{q}{2 k_F g_0} \right]^2, \tag{5.15}$$

$$\tilde{\omega}_q^- \approx v_F|q| \left[1 - \frac{2}{3 g_0} \left(\frac{q}{2 k_F} \right)^2 \right]. \tag{5.16}$$

This peak is associated with the incoherent part $S_{\mathrm{RPA}}^{\mathrm{inc}}(\omega, q)$ of the dynamic structure factor discussed above which in the approximation (5.11) is replaced by a single peak with the same weight. From Eqs. (5.15) and (2.20) one easily verifies that for $|q| \ll g_0 k_F$ the relative weight of the peak associated with the incoherent part is indeed small,

$$\frac{Z_q^-}{Z_q^+} = \frac{4x_0}{3} \left[\frac{q}{2k_F g_0} \right]^2 = \frac{4\pi^2 x_0 p_0^2}{3} \left[\frac{v_F q}{f_0 q_0} \right]^2 , \tag{5.17}$$

where we have used $p_0 = q_0/(2k_F)$, see Eqs. (2.37). Hence, for $|q| \ll g_0 k_F$ most of the weight of $S_{\mathrm{RPA}}(\omega, q)$ is carried by the ZS mode $\tilde{\omega}_q^+ \approx v_0|q|$, so that the incoherent part corresponding to the mode $\tilde{\omega}_q^- \approx v_F|q|$ can be neglected. Note that the limits $q \to 0$ and $g_0 \to 0$ do not commute and that only for $|q|/(2k_F) \ll g_0$ the weight of the mode $\tilde{\omega}_q^-$ can be neglected.

Mathematically, the second peak in Eq. (5.14) is due to the pole arising from the term of order p^2 in the expansion (5.11) of the inverse free polarization. Although after the analytic continuation $iy \to x + i0$ this term is singular for $x = 1$, we know from the exact result (5.10) how this singularity should be regularized: we simply should smooth out the corresponding δ-function peak over an interval of width $\mathrm{w}_q \propto q^2/m$. In fact, we can self-consistently calculate w_q by noting that after analytic continuation the singular term in the expansion (5.11) gives rise to the following formally infinite imaginary part of the inverse noninteracting polarization,

$$\mathrm{Im}\tilde{\Pi}_0^{-1}(x + i0, p) = -\Gamma_0(x, p) = -\frac{2\pi}{3} p^2 [\delta(1 - x) - \delta(1 + x)] . \tag{5.18}$$

Ignoring the renormalization arising from the (singular) real part of $\tilde{\Pi}_0^{-1}(x + i0, p)$ and approximating the resulting dynamic structure factor in this regime by a Lorentzian centered at $\omega = v_F|q|$, we find for the full width at half maximum in the limit $g_0 \ll 1$,

$$\mathrm{w}_q = \frac{v_F|q|}{2} \Gamma_0(1, p = q/(2k_F)) . \tag{5.19}$$

To obtain a self-consistent estimate for w_q we follow Samokhin [5] and regularize the singularity in $\Gamma_0(1, p)$ by replacing $\delta(\omega = 0)$ by the height of a normalized Lorentzian of width w_q on resonance,

$$\delta(x - 1)|_{x=1} = v_F|q| \, \delta(\omega - v_F|q|)|_{\omega = v_F|q|} \to \frac{v_F|q|}{\pi \mathrm{w}_q} . \tag{5.20}$$

Hence, our self-consistent regularization is

$$\Gamma_0(1, p) \to \frac{2p^2 v_F|q|}{3\mathrm{w}_q} . \tag{5.21}$$

Substituting this into Eq. (5.19) we obtain the self-consistency equation

$$\mathrm{w}_q = \frac{1}{3} \left(\frac{q}{2k_F} \right)^2 \frac{(v_F q)^2}{\mathrm{w}_q} , \tag{5.22}$$

which leads to the following estimate for the width of the single-pair particle-hole continuum,

$$\mathrm{w}_q = \frac{1}{2\sqrt{3}} \frac{q^2}{m}. \tag{5.23}$$

On the other hand, it is known $[3, 4, 35]$ that the shape of the single-pair continuum cannot be approximated by a Lorentzian, but the order of magnitude of its width obtained within the above regularization is correct for sufficiently small q. Hence, the mass-shell singularity arising after analytic continuation $iy \to x+i0$ in the expansion of the inverse noninteracting polarization (5.11) in powers of $p = q/(2k_F)$ is simply related to the single-pair particle-hole continuum. This singularity can be regularized by smearing out the δ-function in the imaginary part over a finite interval of width $\mathrm{w}_q \propto q^2/m$. However, the width w_q should not be confused with the damping of the ZS mode which remains sharp within RPA. Note that because of the unphysical mass-shell singularities occurring within RPA, a better starting point would be the so-called RPAE or "time-dependent Hartree-Fock approximation", because it takes the renormalization of the single-pair particle-hole continuum approximately into account $[37, 39]$.

In order to obtain the ZS damping, one should calculate interaction corrections to the irreducible polarization. The finite overlap between the continuum due to particle-hole excitations involving more than a single particle-hole pair (multi-pair excitations) then determines the ZS damping. To this end, in the next chapter we first calculate the symmetrized fermion closed loops arising in the bosonized effective action $S_{\mathrm{eff}}[\Delta\phi]$. In Chap. 7 we show that by expanding the inverse irreducible polarization analogue to (5.11), our approach does not suffer from the mass-shell singularities discussed above. Moreover, we show that the distinction between the ZS energy $v_0|q|$ and the energy scale $v_F|q|$ associated with the single-pair continuum shown in Fig. 5.1 is an unphysical artifact of the RPA which disappears once the corrections to the RPA are self-consistently taken into account.

Chapter 6

Symmetrized fermion loops

For a perturbative expansion of the irreducible polarization $\Pi_*(Q)$ in the bosonic language, we need to determine symmetrized closed fermion loops which are defined in (3.24). In the first section of this chapter we analyze these loops explicitly and show that they vanish for a linearized energy dispersion, i.e., $1/m \to 0$. Secs. 6.2 and 6.3 are devoted to the calculation of the symmetrized three and four loops, which we require in Chap. 7 to obtain perturbatively the dynamic structure factor.

The important point is that we would like to examine all corrections to the RPA to second order of the small parameter $p_0 = q_0/(2k_F) \propto 1/m$, which is naturally generated using the functional bosonization approach [45, 49]. Therefore by the diagrammatic expansion we consider only a few number of diagrams which behave as p_0^2 for $p_0 \to 0$. We have then to neglect contributions to the bosonic self-energy which are proportional to p_0^n with $n > 2$. But this calculation will be described accurately in the next chapter.

6.1 Fermion loops for quadratic energy dispersion

For fermions with quadratic energy dispersion in one dimension, the symmetrized fermion loops (3.24) can be calculated exactly. Neumayr and Metzner [54, 55] (see also Ref. [56]) have derived reduction formulas for quadratic dispersion in D dimensions which allow to express the nonsymmetrized loops

$$
\begin{aligned}
\bar{L}^{(n)}(\bar{Q}_1, \ldots, \bar{Q}_n) &= \int_K \prod_{i=1}^n G_0(K - \bar{Q}_i) \\
&= \int_K G_0(K - \bar{Q}_1) G_0(K - \bar{Q}_2) \cdots G_0(K - \bar{Q}_n), \quad (6.1)
\end{aligned}
$$

for $n > D+1$ in terms of linear combinations of the more elementary loop $\bar{L}^{(D+1)}(\bar{Q}_1, \ldots, \bar{Q}_{D+1})$. In particular, in $D = 1$ the nonsymmetrized loops $\bar{L}^{(n)}(\bar{Q}_1, \ldots, \bar{Q}_n)$ with $n > 2$ can be expressed in terms of the two loop,

$$
\bar{L}^{(2)}(0, -Q) = L_S^{(2)}(-Q, Q) = -\Pi_0(Q). \quad (6.2)
$$

41

Given explicit expressions for the nonsymmetrized loops $\bar{L}^{(n)}(\bar{Q}_1, \ldots, \bar{Q}_n)$, we may construct the corresponding symmetrized loops $L_S^{(n)}(Q_1, \ldots, Q_n)$ by shifting the labels,

$$
\begin{aligned}
\bar{Q}_1 &= 0\,, \\
\bar{Q}_2 &= Q_1\,, \\
\bar{Q}_3 &= Q_1 + Q_2\,, \\
&\cdots \\
\bar{Q}_n &= \sum_{j=1}^{n-1} Q_j\,,
\end{aligned}
\tag{6.3}
$$

so that $\bar{Q}_{i+1} - \bar{Q}_i = Q_i$, and defining

$$
L^{(n)}(Q_1, \ldots, Q_n) = \bar{L}^{(n)}(\bar{Q}_1, \ldots, \bar{Q}_n)\,.
\tag{6.4}
$$

Then the symmetrized loops are

$$
L_S^{(n)}(Q_1, \ldots, Q_n) = \frac{1}{n!} \sum_{P(1,\ldots,n)} L^{(n)}(Q_{P(1)}, \ldots, Q_{P(n)})\,.
\tag{6.5}
$$

In one dimension, the reduction formula for the nonsymmetrized loop $\bar{L}^{(n)}(\bar{Q}_1, \ldots, \bar{Q}_n)$ given by Neumayr and Metzner [55] can be obtained using a straightforward partial fraction decomposition. Performing the frequency integration in Eq. (6.1) and introducing the notation $\bar{Q}_i = (i\bar{\omega}_i, \bar{q}_i)$ we obtain after some algebra,

$$
\bar{L}^{(n)}(\bar{Q}_1, \ldots, \bar{Q}_n) = \sum_{i=1}^{n} \int_{-k_F}^{k_F} \frac{dk}{2\pi} \prod_{\substack{j=1 \\ j \neq i}}^{n} \frac{1}{\Omega_{ij}(k)}\,,
\tag{6.6}
$$

where [see Eq.(3.19)],

$$
\Omega_{ij}(k) = i(\bar{\omega}_i - \bar{\omega}_j) + \xi_k - \xi_{k + \bar{q}_i - \bar{q}_j}\,,
\tag{6.7}
$$

$$
\xi_k = \frac{k^2}{2m} + f_0 \rho_0 - \mu = \frac{k^2 - k_F^2}{2m}\,.
\tag{6.8}
$$

Defining

$$
k_{ij} = \frac{\bar{q}_j - \bar{q}_i}{2} + im \frac{\bar{\omega}_j - \bar{\omega}_i}{\bar{q}_j - \bar{q}_i}\,,
\tag{6.9}
$$

we may alternatively write Eq. (6.6) as

$$
\bar{L}^{(n)}(\bar{Q}_1, \ldots, \bar{Q}_n) = \sum_{i=1}^{n} \int_{-k_F}^{k_F} \frac{dk}{2\pi} \prod_{\substack{j=1 \\ j \neq i}}^{n} \frac{m}{(\bar{q}_j - \bar{q}_i)(k - k_{ij})}\,.
\tag{6.10}
$$

We can now perform another partial fraction expansion to obtain

$$\bar{L}^{(n)}(\bar{Q}_1,\ldots,\bar{Q}_n) = \sum_{\substack{i,j=1\\i\neq j}}^{n} \left[\prod_{\substack{l=1\\l\neq i,j}}^{n} H_{ijl}\right]^{-1} \frac{m}{\bar{q}_j - \bar{q}_i} \int_{-k_F}^{k_F} \frac{dk}{2\pi} \frac{1}{k - k_{ij}},\qquad(6.11)$$

with

$$H_{ijl} = -\frac{(\bar{q}_l - \bar{q}_i)(\bar{q}_l - \bar{q}_j)}{2m} + i(\bar{\omega}_i - \bar{\omega}_l) + i(\bar{\omega}_j - \bar{\omega}_i)\frac{\bar{q}_l - \bar{q}_i}{\bar{q}_j - \bar{q}_i}.\qquad(6.12)$$

In the special case $n = 2$ this yields

$$\bar{L}^{(2)}(\bar{Q}_1,\bar{Q}_2) = \frac{m}{\pi(\bar{q}_1 - \bar{q}_2)} \ln\left|\frac{k_F + k_{12}}{k_F - k_{12}}\right|.\qquad(6.13)$$

In order to give an explicit formula for the function $L^{(n)}(Q_1,\ldots,Q_n)$ defined in Eq. (6.4), which depends on the external momenta and frequencies $Q_i = (i\omega_i, q_i)$, we introduce the notation

$$q_{ij} = \bar{q}_i - \bar{q}_j = \begin{cases} \sum_{l=j}^{i-1} q_l, & i > j \\ -\sum_{l=i}^{j-1} q_l, & j > i \end{cases},\qquad(6.14)$$

and similarly for $\omega_{ij} = \bar{\omega}_i - \bar{\omega}_j$. These quantities fulfill $q_{ij} = q_{il} + q_{lj}$ and $\omega_{ij} = \omega_{il} + \omega_{lj}$, such that H_{ijl} can be reexpressed as

$$H_{ijl} = \frac{1}{q_{ij}}\left[i(\omega_{il}q_{lj} - q_{il}\omega_{lj}) - \frac{q_{li}q_{lj}q_{ij}}{2m}\right],\qquad(6.15)$$

which is manifestly symmetric under exchange of i and j, i.e., $H_{jil} = H_{ijl}$. This yields

$$L^{(n)}(Q_1,\ldots,Q_n) = -\sum_{\substack{i,j=1\\i<j}}^{n} \left[\prod_{\substack{l=1\\l\neq i,j}}^{n} H_{ijl}\right]^{-1} \Pi_0(Q_{ij}),\qquad(6.16)$$

with

$$Q_{ij} = (i\omega_{ij}, q_{ij}).\qquad(6.17)$$

This result is equivalent with Eq. (19) of Ref. [55]. Finally, in order to obtain the symmetrized loops $L_S^{(n)}(Q_1,\ldots,Q_n)$ in Eq. (6.5), an additional summation over the $n!$ permutations is necessary. Evidently, the resulting expressions are rather complicated. In the following two sections we shall therefore discuss the symmetrized three loop and the symmetrized four loop separately. However, without explicitly evaluating the loops the following two general properties can be established:

1. The symmetrized n-loops $L_S^{(n)}(Q_1,\ldots,Q_n)$ are finite for all values of their arguments [55]. This guarantees that in the perturbative expansion of the irreducible polarization $\Pi_*(Q)$ in powers of the RPA interaction no infrared singularities are encountered.

2. In the limit $1/m \to 0$ the symmetrized n-loop is proportional to $(1/m)^{n-2}$. More precisely, the dimensionless symmetrized n-loops $\tilde{L}_S^{(n)}(Q_1, \ldots, Q_n)$, defined via

$$(n-1)! L_S^{(n)}(Q_1, \ldots, Q_n) = \frac{\nu_0}{(mv_F^2)^{n-2}} \tilde{L}_S^{(n)}(Q_1, \ldots, Q_n), \qquad (6.18)$$

have finite limits for $1/m \to 0$. For large m the vertices $\Gamma_0^{(n)}(Q_1, \ldots, Q_n)$ in the interaction part $S_{\text{int}}[\Delta\phi]$ of our effective action (3.22) are therefore proportional to increasing powers of the small parameter $1/m$, which justifies the perturbative treatment of these vertices.

6.2   Symmetrized three loop

The explicit expression for the symmetrized three loop can be written as

$$L_S^{(3)}(i\omega_1, q_1; i\omega_2, q_2; -i\omega_1 - i\omega_2, -q_1 - q_2) = -\text{Re}\left[\frac{1}{i\omega_1 q_2 - i\omega_2 q_1 - q_1 q_2 \frac{q_1 + q_2}{2m}}\right]$$
$$\times \left[q_1 \Pi_0(i\omega_1, q_1) + q_2 \Pi_0(i\omega_2, q_2) - (q_1 + q_2)\Pi_0(i\omega_1 + i\omega_2, q_1 + q_2)\right]. \qquad (6.19)$$

Introducing again the variables $iy_1 = i\omega_1/(v_F q_1)$, $p_1 = q_1/(2k_F)$ (and similarly for iy_2 and p_2) and the dimensionless function $\tilde{\Pi}_0(iy, p) = \nu_0^{-1} \Pi_0(i\omega, q)$ [see Eqs. (5.8) and (5.9)], we may write the symmetrized three loop in the dimensionless form (6.18),

$$L_S^{(3)}(i\omega_1, q_1; i\omega_2, q_2; -i\omega_1 - i\omega_2, -q_1 - q_2) = \frac{\nu_0}{mv_F^2} \tilde{L}_S^{(3)}(iy_1, p_1; iy_2, p_2), \qquad (6.20)$$

with

$$\tilde{L}_S^{(3)}(iy_1, p_1; iy_2, p_2) = \frac{1}{(y_1 - y_2)^2 + (p_1 + p_2)^2}\left[\frac{1}{s_2}\tilde{\Pi}_0(iy_1, p_1) + \frac{1}{s_1}\tilde{\Pi}_0(iy_2, p_2)\right.$$
$$\left. - \left(\frac{1}{s_1} + \frac{1}{s_2}\right)\tilde{\Pi}_0(iy_1 s_1 + iy_2 s_2, p_1 + p_2)\right], \qquad (6.21)$$

where we have defined

$$s_1 = \frac{p_1}{p_1 + p_2} = \frac{r}{r+1}, \qquad\qquad s_2 = \frac{p_2}{p_1 + p_2} = \frac{1}{r+1}, \qquad (6.22)$$

with

$$r = \frac{p_1}{p_2}. \qquad (6.23)$$

For later convenience we also define

$$r_1 = \frac{p_1}{p_1 - p_2} = \frac{r}{r-1}, \qquad\qquad r_2 = \frac{p_2}{p_2 - p_1} = \frac{-1}{r-1}. \qquad (6.24)$$
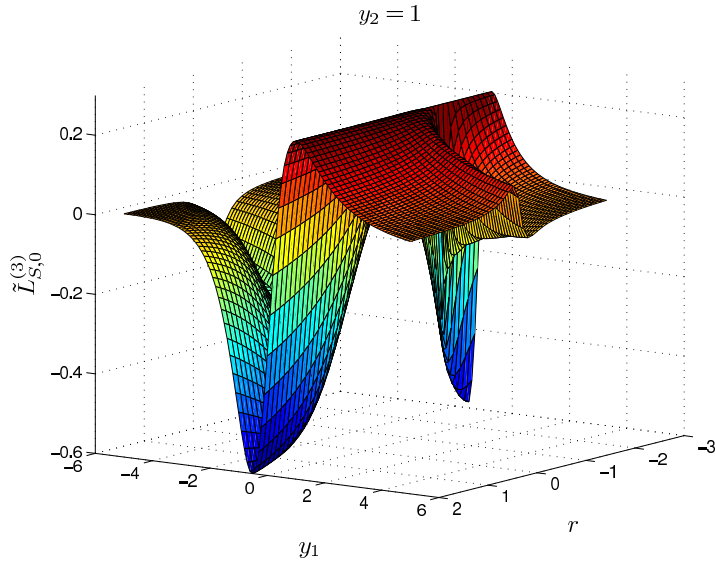
Figure 6.1: Graph of the function $\tilde{L}_{S,0}^{(3)}(iy_1, iy_2, r)$ given in Eq. (6.26) for $y_2 = 1$ as a function of y_1 and $r = p_1/p_2$.

Note that by this construction $s_1 + s_2 = r_1 + r_2 = 1$.

At the first sight it seems that the symmetrized three loop diverges for $|p_1/p_2| \to 0$ or $|p_2/p_1| \to 0$. Moreover, the prefactor in Eq. (6.19) diverges in the special limit $p_1 \to -p_2$ and $y_1 \to y_2$. It turns out, however, that all divergencies cancel and the symmetrized three loop is everywhere of the order of unity. This nontrivial cancellation cannot be obtained by power counting and can be viewed to be a consequence of the asymptotic Ward identity associated with the separate conservation of left- and right-moving particles for linearized energy dispersion [22, 53]. We shall show in Sec. 6.3 that a similar cancellation protects also the symmetrized four loop from divergencies. The symmetrization of the loops is crucial to cancel the divergencies. In diagrammatic language, the symmetrization properly takes vertex and self-energy corrections into account.

The limiting behavior of the function $\tilde{L}_S^{(3)}(iy_1, p_1; iy_2, p_2)$ for $p_1 \to 0$ and $p_2 \to 0$ is not unique but depends on the ratio $r = p_1/p_2$. Using Eq. (5.13) we obtain after some algebra,

$$\lim_{p_i \to 0, p_1/p_2 = r} \tilde{L}_S^{(3)}(iy_1, p_1; iy_2, p_2) = \tilde{L}_{S,0}^{(3)}(iy_1, iy_2, r) \,, \tag{6.25}$$

with

$$\tilde{L}_{S,0}^{(3)}(iy_1, iy_2, r) = -\frac{1 - y_1 y_2 - (y_1 + y_2)(s_1 y_1 + s_2 y_2)}{[1 + y_1^2][1 + y_2^2][1 + (s_1 y_1 + s_2 y_2)^2]} \,, \tag{6.26}$$

which is manifestly finite for all values of its arguments. A graph of the function $\tilde{L}_{S,0}^{(3)}(iy_1, iy_2, r)$ is shown in Fig. 6.1. Note that a finite limit of the dimensionless function $\tilde{L}_S^{(3)}(iy_1, p_1; iy_2, p_2)$ for small momenta does not contradict the loop cancellation theorem [22, 45, 49, 53–55], because according to Eq. (6.20) the physical

symmetrized three loop $L_S^{(3)}(i\omega_1, q_1; i\omega_2, q_2; -i\omega_1 - i\omega_2, -q_1 - q_2)$ involves an extra factor of $1/m$, so that it vanishes for $1/m \to 0$.

6.3   Symmetrized four loop

The symmetrized four loop is more complicated than the three loop. However, the four loop determines the correction to the irreducible polarization to the first order in the the RPA interaction [29], so that we need it for our calculation. Actually, we shall see in the next chapter that we need the four loop only for the special arguments $Q_3 = -Q_1$ and $Q_4 = -Q_2$. It is useful to introduce the notation

$$y_\pm = y_1 \pm y_2, \qquad\qquad p_\pm = p_1 \pm p_2, \qquad\qquad (6.27)$$

and the complex functions

$$C_\pm(iy_-, p_1, p_2) = \frac{1}{p_1 p_2 [iy_- - p_\pm]}, \qquad\qquad (6.28)$$

$$W(iy, p) = \frac{1}{2p}\left[\frac{1}{iy + 1 + p} - \frac{1}{iy + 1 - p}\right]. \qquad\qquad (6.29)$$

We also need

$$\mathrm{Re} W(iy, p) = \frac{y^2 - 1 + p^2}{[y^2 + (1+p)^2][y^2 + (1-p)^2]}, \qquad\qquad (6.30)$$

$$\mathrm{Im} W(iy, p) = \frac{2y}{[y^2 + (1+p)^2][y^2 + (1-p)^2]}. \qquad\qquad (6.31)$$

The functions $C_\pm(iy_-, p_1, p_2)$ are singular for $p_i \to 0$, while $W(iy, p)$ has a finite limit for $p \to 0$,

$$\lim_{p\to 0} W(iy, p) = -\frac{1}{(1 + iy)^2}. \qquad\qquad (6.32)$$

Using our general result (6.16) for the nonsymmetrized n-loops $L^{(n)}(Q_1, \ldots, Q_n)$ and performing the sum (6.5) over all permutations of the external labels, we obtain for the dimensionless symmetrized four loop (as defined in Eq. (6.18) for $n = 4$) for the special combination $Q_1 = -Q_3$ and $Q_2 = -Q4$,

$$6L_S^{(4)}(i\omega_1, q_1; -i\omega_1, -q_1; i\omega_2, q_2; -i\omega_2, -q_2) = \frac{\nu_0}{(mv_F^2)^2}\tilde{L}_S^{(4)}(iy_1, p_1; iy_2, p_2), \quad (6.33)$$

with

$$
\begin{aligned}
\tilde{L}_S^{(4)}(iy_1, p_1; iy_2, p_2) &= \frac{p_1}{2}\mathrm{Re}\left[p_+ C_+^2 + p_- C_-^2 + 2p_1 C_+^* C_-\right]\tilde{\Pi}_0(iy_1, p_1) \\
&+ \frac{p_2}{2}\mathrm{Re}\left[p_+ C_+^2 - p_- C_-^2 - 2p_2 C_+ C_-\right]\tilde{\Pi}_0(iy_2, p_2) \\
&- p_+^2[\mathrm{Re}C_+]^2\tilde{\Pi}_0(iy_1 s_1 + iy_2 s_2, p_+) \\
&- p_-^2[\mathrm{Re}C_-]^2\tilde{\Pi}_0(iy_1 r_1 + iy_2 r_2, p_-) \\
&+ \frac{1}{2}\mathrm{Im}[C_+ - C_-]\mathrm{Im}[W(iy_1, p_1) - W(iy_2, p_2)] \\
&- \mathrm{Re}[W(iy_1, p_1)W(iy_2, p_2)],
\end{aligned}
\tag{6.34}
$$

where we have written

$$
C_\pm = C_\pm(iy_-, p_1, p_2).
\tag{6.35}
$$

After some algebra Eq. (6.34) can be cast into the form

$$
\begin{aligned}
\tilde{L}_S^{(4)}(iy_1, p_1; iy_2, p_2) &= 2\frac{(p_1^2 + 3p_2^2)y_-^4 + 2(p_1^2 - p_2^2)^2 y_-^2 + (p_1^2 - p_2^2)^3}{p_2^2[y_-^2 + p_+^2]^2[y_-^2 + p_-^2]^2}\tilde{\Pi}_0(iy_1, p_1) \\
&+ 2\frac{(p_2^2 + 3p_1^2)y_-^4 + 2(p_2^2 - p_1^2)^2 y_-^2 + (p_2^2 - p_1^2)^3}{p_1^2[y_-^2 + p_+^2]^2[y_-^2 + p_-^2]^2}\tilde{\Pi}_0(iy_2, p_2) \\
&- \frac{\tilde{\Pi}_0(iy_1 s_1 + iy_2 s_2, p_+)}{s_1^2 s_2^2[y_-^2 + p_+^2]^2} - \frac{\tilde{\Pi}_0(iy_1 r_1 + iy_2 r_2, p_-)}{r_1^2 r_2^2[y_-^2 + p_-^2]^2} \\
&+ \frac{2y_-\mathrm{Im}[W(iy_1, p_1) - W(iy_2, p_2)]}{[y_-^2 + p_+^2][y_-^2 + p_-^2]} \\
&- \mathrm{Re}[W(iy_1, p_1)W(iy_2, p_2)].
\end{aligned}
\tag{6.36}
$$

Naive power counting would suggest that this expression is singular for $y_1 \to y_2$ or $|p_1| \to |p_2|$, or if p_1/p_2 approaches either zero or infinity. However, similar to the symmetrized three loop, all singularities cancel in Eq. (6.36), so that the symmetrized four loop remains finite and of the order of unity for all values of its arguments.

For simplicity, consider again the limit $p_1 \to 0$ and $p_2 \to 0$ with constant $r = p_1/p_2$. Then

$$
\lim_{p_i \to 0, p_1/p_2 = r} \tilde{L}_S^{(4)}(iy_1, p_1, iy_2, p_2) = \tilde{L}_{S,0}^{(4)}(iy_1, iy_2, r),
\tag{6.37}
$$

with

$$
\begin{aligned}
\tilde{L}_{S,0}^{(4)}(iy_1, iy_2, r) &= \frac{1}{(y_1 - y_2)^4}\left[\frac{2(r^2 + 3)}{1 + y_1^2} + \frac{2(r^{-2} + 3)}{1 + y_2^2} - \frac{1}{s_1^2 s_2^2[1 + (s_1 y_1 + s_2 y_2)^2]}\right. \\
&\left. - \frac{1}{r_1^2 r_2^2[1 + (r_1 y_1 + r_2 y_2)^2]} + \frac{4y_-^2[1 - 2y_1 y_2 - y_1 y_2(y_1^2 + y_2^2 + y_1 y_2)]}{[1 + y_1^2]^2[1 + y_2^2]^2}\right] \\
&+ \frac{4y_1 y_2 - (1 - y_1^2)(1 - y_2^2)}{[1 + y_1^2]^2[1 + y_2^2]^2}.
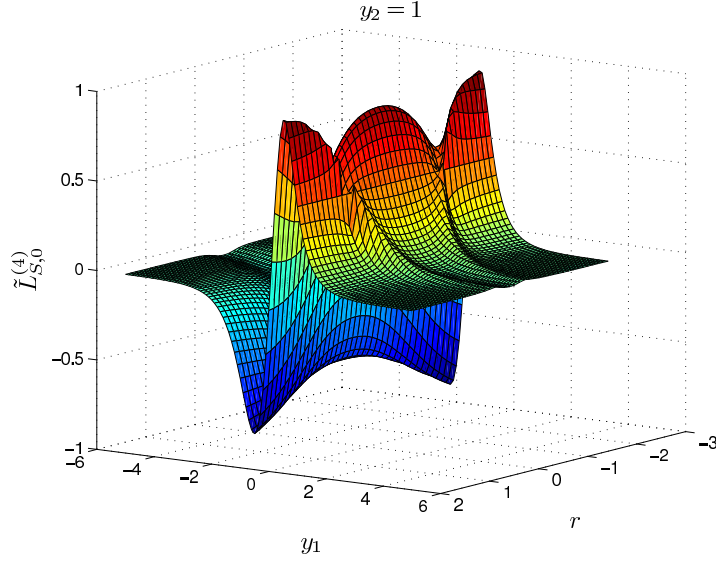\end{aligned}
\tag{6.38}
$$

Figure 6.2: Graph of the function $\tilde{L}_{S,0}^{(4)}(iy_1, iy_2, r)$ given in Eq. (6.38) for $y_2 = 1$ as a function of y_1 and $r = p_1/p_2$.

The important point is now that the singular prefactor $1/(y_1 - y_2)^4$ in Eq. (6.38) is compensated by a factor of $(y_1 - y_2)^4$ arising from the sum of the five terms in the square braces. In fact, we can explicitly cancel this singularity by combining these terms differently,

$$
\tilde{L}_{S,0}^{(4)}(iy_1, iy_2, r) = -\frac{[1 - y_1^2][1 - y_2^2]}{[1 + y_1^2]^2[1 + y_2^2]^2}
$$

$$
+ \frac{1}{[1 + y_1^2]^2[1 + y_2^2]^2[1 + (s_1 y_1 + s_2 y_2)^2][1 + (r_1 y_1 + r_2 y_2)^2]}
$$

$$
\times \left\{ -1 + 6y_1 y_2 + t_1 t_2 (y_1 - y_2)^2 [y_1^2 + y_2^2 + 6y_1 y_2] + 2(t_1 y_1 + t_2 y_2)^2 y_1 y_2 (4 - y_1 y_2) \right.
$$

$$
+ 2(t_1 y_1 + t_2 y_2)\Big[(t_1 y_1 - t_2 y_2)(y_1^2 - y_2^2) + (t_1 y_2 + t_2 y_1)\Big]
$$

$$
\left. + (t_1 y_1^2 + t_2 y_2^2)^2 + (t_1 y_1^2 + t_2 y_2^2)(2 - y_1^2 y_2^2) + (t_1 y_2^2 + t_2 y_1^2) \right\}. \tag{6.39}
$$

where the coefficients r_1 and r_2 are defined in (6.24) and we have introduced

$$
t_1 = s_1 r_1 = \frac{p_1^2}{p_1^2 - p_2^2} = \frac{r^2}{r^2 - 1}, \tag{6.40}
$$

$$
t_2 = s_2 r_2 = \frac{p_2^2}{p_2^2 - p_1^2} = \frac{-1}{r^2 - 1}. \tag{6.41}
$$

so that $t_1 + t_2 = 1$. A graph of the function $\tilde{L}_{S,0}^{(4)}(iy_1, iy_2, r)$ is shown in Fig. 6.2.

Chapter 7

Calculation of $S(\omega, q)$ using functional bosonization

In this chapter we use the bosonization approach developed in Chap. 3 to calculate the propagator (3.31), where $\Pi_*(Q) - \Pi_0(Q)$ plays the role of the bosonic self-energy. Therefore, we expand the irreducible polarization in powers of the RPA interaction, which is the Gaussian propagator of our boson field $\Delta\phi_Q$.

In Sec. 7.1 we expand diagrammatically the irreducible polarization to second order in the RPA interaction. We present furthermore a procedure to calculate the dynamic structure factor by taking the renormalization of the ZS velocity into account. In this context, Schönhammer [37] has shown that within the so-called RPAE approximation the relative position of the collective mode energy and the energy of the single-pair particle-hole continuum is different from the RPA prediction for the FSM. In Sec. 7.2 we expand similar to Eq. (5.11) the irreducible polarization to second order in p_0. To this end we introduce an approximation, where we replace also the symmetrized fermion loops by their asymptotic limit for small momenta, which we have calculated in Secs. 6.2 and 6.3. In addition we perform the approximation given by (5.13) to simplify the RPA interaction $f_{\text{RPA}}(Q)$. Fortunately in our approach the frequency integrations can be carried out analytically. Eventually, in Sec. 7.3 we show that the unphysical mass-shell singularities appearing in Eq.(5.11), cancel each other out in our approximation, so that our expansion in powers of $p_0 \propto 1/m$ is reasonable.

7.1   One loop self-consistency equation for $\Pi_*(Q)$

The diagrams contributing to $\Pi_*(Q)$ up to second order in the RPA interaction are shown in Fig. 7.1. The relevant dimensionless parameter for this expansion is the ratio $p_0 = q_0/(2k_F)$, because by assumption the range of the interaction in momentum space has a cutoff $q_0 \ll k_F$ so that each additional bosonic loop integration gives rise to a factor of p_0^2. Hence, the diagram (d) involving two bosonic loops is of order p_0^4, because according to Eq. (6.18) the symmetrized fermion loop with six external legs is proportional to $1/m^4$ and the two bosonic loop integrations generate a factor of q_0^4. Because the other three diagrams are proportional to p_0^2, it
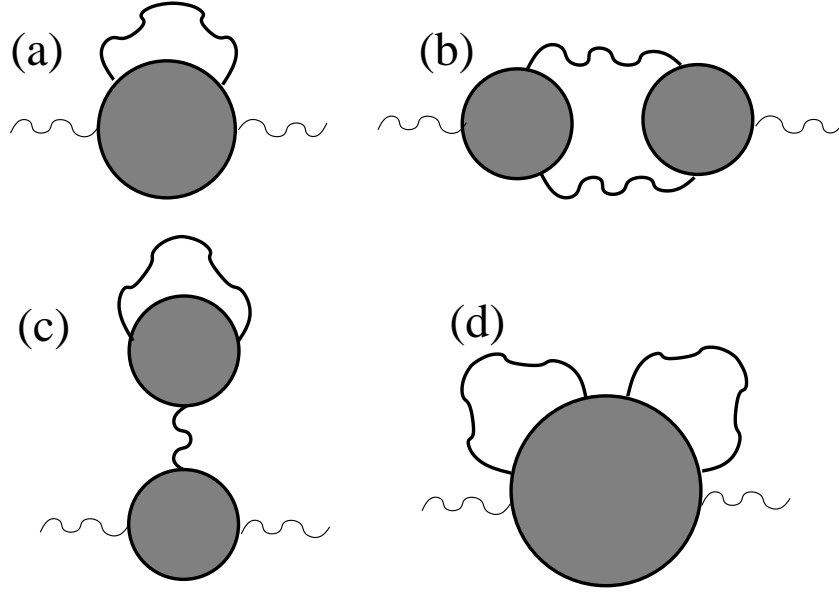
Figure 7.1: Diagrams arising in the perturbative expansion of the irreducible polarization to second order in the RPA interaction. The shaded circles represent the vertices of $S_{\text{eff}}[\delta\phi]$, which are related to symmetrized closed fermion loops as defined in Fig. 3.1. Diagram (a) is equivalent to the three fermionic diagrams shown in Fig. 7.2 and diagram (b) is the so-called Aslamasov-Larkin diagram which corresponds to the two fermionic diagrams in Fig. 7.3. Diagram (c) can be viewed as a higher order self-energy correction which renormalizes the relation between density and chemical potential while diagram (d) involving two bosonic loops and the symmetrized fermionic six loop is of fourth order in $p_0 = q_0/(2k_F)$ and can be neglected to order p_0^2.

is consistent to neglect diagram (d) as long as we retain all terms up to order p_0^2. Evaluating the diagrams (a)–(c) in Fig. 7.1 we obtain the following expression for the irreducible polarization,

$$
\begin{aligned}
\Pi_*(Q) \quad \approx \quad & \Pi_0(Q) + \frac{1}{2} \int_{Q'} f_{\text{RPA}}(Q') \Bigg\{ 6 L_S^{(4)}(Q', -Q', Q, -Q) \\
& + \quad 4 f_{\text{RPA}}(0) L_S^{(3)}(Q, -Q, 0) L_S^{(3)}(Q', -Q', 0) \\
& + \quad 4 f_{\text{RPA}}(Q + Q') L_S^{(3)}(-Q, Q + Q', -Q') L_S^{(3)}(Q', -Q - Q', Q) \Bigg\}. \quad (7.1)
\end{aligned}
$$

The properties of the symmetrized three and four loops appearing in this expression have been discussed in detail in Chap. 6. In addition the corresponding fermionic diagrams are shown in Figs. 7.2 and 7.3.

It turns out, however, that in order to cure the unphysical features of the RPA discussed at the end of Chap. 5 (in particular, within RPA the energy scale $v_F|q|$ of the single-pair continuum erroneously involves the bare Fermi velocity), we should
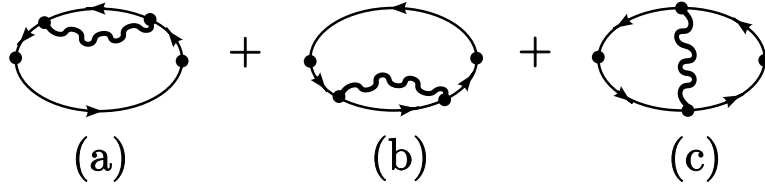
Figure 7.2: Corrections to the irreducible polarization in an expansion to first order in powers of the RPA interaction. The thick wavy lines denote $f_{\mathrm{RPA}}(Q)$, see Fig. 3.2. Diagrams (a) and (b) describe the self-energy correction while the diagram (c) describe the vertex correction.
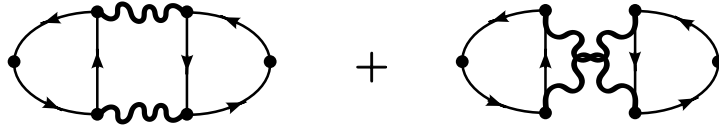

Figure 7.3: Aslamasov-Larkin contributions [68, 69] to the irreducible polarization $\Pi_*(Q)$. The thick wavy lines are the screened RPA interactions, see Fig. 3.2.

self-consistently dress the Gaussian propagator $f_{\mathrm{RPA}}(Q)$ in Eq. (7.1) by self-energy corrections. Formally, this amounts to replacing the RPA interaction by the exact effective interaction,

$$f_{\mathrm{RPA}}(Q) \to f_*(Q) = \frac{f_q}{1 + f_q \Pi_*(Q)} \, . \tag{7.2}$$

In Sec. 4.4 we have justified this procedure using a functional renormalization group approach [7, 58]. With this substitution, Eq. (7.1) becomes a complicated integral equation for the irreducible polarization, which cannot be solved analytically. Fortunately, this integral equation can again be simplified by noting that on the right-hand side it is not necessary to retain the full Q-dependence of $\Pi_*(Q)$, but to keep only those terms which contribute to the self-consistent renormalization of the ZS velocity. To explain this, let us introduce again the dimensionless variables $iy = i\omega/(v_F q)$ and $p = q/(2k_F)$ and define the dimensionless irreducible polarization

$$\Pi_*(i\omega, q) = \nu_0 \tilde{\Pi}_*(iy, p) \, . \tag{7.3}$$

The corresponding dimensionless effective interaction is then

$$\tilde{f}_*(iy, p) = \frac{g_p}{1 + g_p \tilde{\Pi}_*(iy, p)} \, , \tag{7.4}$$

where $g_p = \nu_0 f_{q=pk_F}$, see also Eqs. (5.8) and (5.9). The dynamic structure factor can then be written as

$$S(\omega, q) = \frac{1}{\pi} \mathrm{Im} \left[\frac{1}{f_q + \Pi_*^{-1}(\omega + i0, q)} \right] = \frac{\nu_0}{\pi} \mathrm{Im} \left[\frac{1}{g_p + \tilde{\Pi}_*^{-1}(x + i0, p)} \right] \, , \tag{7.5}$$

where $x = \omega/(v_F q)$. For our purpose it is now sufficient to approximate the dimensionless inverse irreducible polarization by

$$\tilde{\Pi}_*^{-1}(iy, p) = Z_1 + Z_2 y^2 \,, \tag{7.6}$$

where the dimensionless renormalization factors Z_1 and Z_2 should be determined as a function of the interaction such that the approximation (7.6) yields the true ZS velocity v. Within RPA, where the nonlinear terms in the energy dispersion do not renormalizes the ZS velocity, the irreducible polarization is approximated by the noninteracting one, so that $Z_1 = Z_2 = 1$. If we approximate the inverse polarization in Eq. (7.5) by Eq. (7.6) we obtain for $\omega > 0$ and $q \to 0$,

$$S(\omega, q) \approx \frac{v_F |q|}{2\pi v Z_2} \delta(\omega - v|q|) \,, \tag{7.7}$$

where the renormalized ZS velocity is

$$\frac{v}{v_F} = \sqrt{\frac{Z_1 + g_0}{Z_2}} \equiv x_0 \equiv \sqrt{1 + g} \,, \tag{7.8}$$

with renormalized coupling constant

$$g = \frac{g_0 + Z_1}{Z_2} - 1 \,. \tag{7.9}$$

In order to avoid the unphysical splitting of the spectral weight in $S(\omega, q)$ (as discussed at the end of Chap. 5, this is an artifact of the RPA) it is crucial that the true ZS velocity v appears in the bosonic propagators. Therefore, a naive expansion in powers of the RPA interaction is not sufficient. However, we may further reduce the complexity of the calculation by noting that Eq. (7.7) still contains the correct velocity if we set $Z_2 \to 1$ in the prefactor. Within this approximation, the velocity renormalization implied by Eq. (7.6) can be simply taken into account via a redefinition of the coupling constant, $g_0 \to g$. It is therefore sufficient to replace the RPA interaction in Eq. (7.1) by an effective interaction of the same form but with a renormalized effective coupling g instead of g_0, which should be chosen such that all interaction corrections to the ZS velocity are self-consistently taken into account.

In field-theoretical language the constants Z_1 and Z_2 are counterterms which guarantee that our Gaussian propagator depends on the true ZS velocity. In Chap. 8 we shall explicitly calculate the factors Z_1, Z_2 and the corresponding renormalized ZS velocity v to second order in our small parameter p_0. A similar procedure is necessary to self-consistently calculate the true Fermi surface of an interacting Fermi system [70,71]. The expansion of the modified dimensionless interaction $\tilde{g}_p$ for small p is then [see Eq. (2.38)]

$$\tilde{g}_p = g + \frac{1}{2} g_0'' p^2 + \mathcal{O}(p^4) \,, \tag{7.10}$$

where

$$g_0'' = (2k_F)^2 \nu_0 f_0'' = \operatorname{sign} f_0'' \frac{2}{\pi p_c} \,, \tag{7.11}$$

with

$$p_c \equiv \frac{q_c}{2k_F} \, . \tag{7.12}$$

In this approximation, our dimensionless effective interaction is

$$\tilde{f}_*(iy, p) \approx \tilde{f}_g(iy, p) = \frac{\tilde{g}_p}{1 + \tilde{g}_p \tilde{\Pi}_0(iy, p)} \, , \tag{7.13}$$

which differs from the RPA interaction, because the function $\tilde{g}_p$ includes the renormalization of the ZS velocity due to fluctuations beyond the RPA.

Collecting all terms, our final result for the dimensionless irreducible polarization to one bosonic loop can be written as

$$\tilde{\Pi}_*(iy, p) \approx \tilde{\Pi}_0(iy, p) + \tilde{\Pi}_1(iy, p) + \tilde{\Pi}_2(iy, p) \, , \tag{7.14}$$

where the noninteracting polarization is given in Eq. (5.10), and the subscripts indicate the powers of $\tilde{g}_p$. The term $\tilde{\Pi}_1(iy, p)$ corresponding to diagram (a) in Fig. 7.1 can be written as

$$\tilde{\Pi}_1(iy, p) = -\int_{-\infty}^{\infty} dp' |p'| \int_{-\infty}^{\infty} \frac{dy'}{2\pi} \tilde{f}_g(iy', p') \tilde{L}_S^{(4)}(iy, p, iy', p') \, , \tag{7.15}$$

where the dimensionless symmetrized four loop $\tilde{L}_S^{(4)}(iy, p, iy', p')$ is defined in Eq. (6.36). The term $\tilde{\Pi}_2(iy, p)$ involving two powers of the effective interaction is of the form

$$\tilde{\Pi}_2(iy, p) = \tilde{\Pi}_2^{\mathrm{AL}}(iy, p) + \tilde{\Pi}_2^{\mathrm{H}}(iy, p) \, , \tag{7.16}$$

where the contribution from the Aslamasov-Larkin (AL) diagram [68,69] in Fig. 7.1 (b) is

$$\begin{aligned}
\tilde{\Pi}_2^{\mathrm{AL}}(iy, p) = & -\int_{-\infty}^{\infty} dp' |p'| \int_{-\infty}^{\infty} \frac{dy'}{2\pi} \tilde{f}_g(iy', p') \\
& \times \tilde{f}_g \left(\frac{iyp + iy'p'}{p + p'}, p + p' \right) [\tilde{L}_S^{(3)}(iy, p, iy', p')]^2 \, ,
\end{aligned} \tag{7.17}$$

and the contribution from the Hartree diagram in Fig. 7.1 (c) can be written as

$$\begin{aligned}
\tilde{\Pi}_2^{\mathrm{H}}(iy, p) = & -\frac{g}{1 + g} \tilde{L}_S^{(3)}(iy, p, iy, -p) \int_{-\infty}^{\infty} dp' |p'| \int_{-\infty}^{\infty} \frac{dy'}{2\pi} \\
& \times \tilde{f}_g(iy', p') \tilde{L}_S^{(3)}(iy', p', iy', -p') \, .
\end{aligned} \tag{7.18}$$

Here, the dimensionless symmetrized three loop $\tilde{L}_S^{(3)}(iy, p, iy', p')$ is defined in Eq. (6.21). The parameters Z_1 and Z_2 hidden in the effective interaction $\tilde{f}_g(iy, p)$ should be determined self-consistently by evaluating Eqs.(7.14–7.18) and demanding that the resulting renormalized ZS velocity is consistent with the result obtained from Eq. (7.6). We emphasize again that the above expression for $\Pi_*(Q)$ is not based on an expansion in powers of $1/m$: all functions appearing in Eqs. (7.15–7.18) depend on $1/m$ in a rather complicated nonlinear manner.

7.2   Approximation A: neglecting $1/m$-corrections to $\Pi_0(Q)$

Eqs. (7.15–7.18) are still too complicated to admit an analytic evaluation. In order to explicitly calculate the dynamic structure factor without resorting to elaborate numerics, we shall further simplify the above expressions by making the following *approximation A: We replace the noninteracting polarization $\Pi_0(Q)$ appearing in the effective interaction and the symmetrized closed fermion loops on the right-hand sides of Eqs. (7.15–7.18) by its asymptotic limit for small momenta given in Eq. (5.13).* Keeping in mind that in one dimension the closed fermion loops with $n > 2$ external legs can all be expressed in terms of $\Pi_0(Q)$, the symmetrized three and four loops are then approximated by Eqs. (6.26) and (6.39). For consistency, we should also expand the dimensionless free polarization $\tilde\Pi_0(iy, p)$ on the right-hand side of Eq. (7.14) to second order in p, see Eq. (5.11).

It turns out that with this simplification the y'-integrations in Eqs. (7.15), (7.17) and (7.18) can be done analytically for general $\tilde g_p$ using the method of residues. The form of Eq. (7.5) suggests that it is natural to expand the *inverse* irreducible polarization in powers of p and p_0. This procedure can be formally justified within functional bosonization [29, 49], where the interaction corrections to the *inverse* irreducible polarization play the role of the self-energy corrections in the effective bosonized theory. But it is usually better to expand the self-energy rather than the Green function in powers of the relevant small parameter, because the direct expansion of the Green function usually leads to unphysical singularities. Using Eqs. (5.11) and (7.15–7.18) we obtain for the expansion of the inverse irreducible polarization to order p_0^2,

$$
\tilde\Pi_*^{-1}(iy, p) = 1 + y^2 - \frac{p^2}{3}\frac{1 - 3y^2}{1 + y^2} - (1 + y^2)^2\tilde\Pi_1(iy, p) - (1 + y^2)^2\tilde\Pi_2(iy, p) + \mathcal{O}(p_0^3)\,,
$$
(7.19)

where p is assumed to be smaller than the dimensionless momentum-transfer cutoff $p_0 = q_0/(2k_F)$. It is convenient to introduce the notation

$$
\begin{aligned}
x_p &= \sqrt{1 + \tilde g_p}\,, & \text{(7.20a)}\\
a_p &= x_p + 1 = \sqrt{1 + \tilde g_p} + 1\,, & \text{(7.20b)}\\
b_p &= x_p - 1 = \sqrt{1 + \tilde g_p} - 1\,, & \text{(7.20c)}
\end{aligned}
$$

so that $a_p b_p = \tilde g_p$. The contribution involving the symmetrized four loop can then be written as

$$
\begin{aligned}
-(1 + y^2)^2\tilde\Pi_1(iy, p) = \mathrm{Re}\int_0^\infty dp'\Bigg\{&\frac{|p'|}{x_{p'}}\frac{p'^4 F_1(iy, p') + p'^2 p^2 F_2(iy, p') + p^4 F_3(iy, p')}{[a_{p'}^2 p'^2 - (1 + iy)^2 p^2][b_{p'}^2 p'^2 - (1 - iy)^2 p^2]}\\
&-p'^2\tilde g_{p'}(1 + iy)^2\Big[\frac{2p'}{p(1 - iy)} + 1\Big]\frac{|p + p'|}{x_{p'}^2 p'^2 - [(1 - iy)p + p']^2} + (p' \to -p')\Bigg\}\,,
\end{aligned}
$$
(7.21)

with

$$F_1(iy, p) = 4\tilde{g}_p(x_p + iy)^2 + \tilde{g}_p^2 \left[\frac{8x_p}{1 - iy} - 4x_p - \tilde{g}_p - (2 + x_p - \frac{\tilde{g}_p}{2})(1 + y^2) \right], \quad (7.22)$$

$$F_2(iy, p) = \tilde{g}_p \left[-(1 + iy)^4 + \tilde{g}_p(2 - y^2 + y^4) - 4b_p iy(1 - y^2) \right]$$
$$- 2b_p^2 x_p \frac{1 + iy}{1 - iy}(3 - 6y^2 - y^4), \quad (7.23)$$

$$F_3(iy, p) = -4b_p^2(1 + y^2) \left[1 - \frac{1 + y^2}{2} - \frac{(1 + y^2)^2}{8} \right]. \quad (7.24)$$

Both functions $F_1(iy, p)$ and $F_2(iy, p)$ contain a singular term proportional to $(1 - iy)^{-1}$, which after analytic continuation give rise to a mass-shell singularity at the energies $\pm v_F q$ associated with the bare Fermi velocity. Fortunately, these singularities cancel when Eq. (7.21) is combined with the corresponding contributions from the expansion of $\tilde{\Pi}_0^{-1}(iy, p)$ in Eq. (7.19) and from the AL diagram given in Eq. (7.31) below. To show this explicitly, it is useful to isolate the singular term in Eqs. (7.22) and (7.23) by setting

$$F_1(iy, p) = \frac{8\tilde{g}_p^2 x_p}{1 - iy} + \tilde{F}_1(iy, p), \quad (7.25)$$

$$F_2(iy, p) = -8b_p^2 x_p \frac{(1 + iy)^2}{1 - iy} + \tilde{F}_2(iy, p). \quad (7.26)$$

$\tilde{F}_1(iy, p)$ and $\tilde{F}_2(iy, p)$ are now analytic functions of y,

$$\tilde{F}_1(iy, p) = 4\tilde{g}_p(x_p + iy)^2 - \tilde{g}_p^2 \left[4x_p + \tilde{g}_p + (2 + x_p - \frac{\tilde{g}_p}{2})(1 + y^2) \right], \quad (7.27)$$

$$\tilde{F}_2(iy, p) = \tilde{g}_p \left[-(1 + iy)^4 + \tilde{g}_p(2 - y^2 + y^4) + 4b_p iy(1 + 2iy + y^2) \right]$$
$$+ 2b_p^2(1 + iy) \left[x_p(1 + iy)(1 + y^2) - 4iy \right]. \quad (7.28)$$

Eq. (7.21) can then be written as

$$-(1 + y^2)^2 \tilde{\Pi}_1(iy, p) = \text{Re} \int_0^\infty dp' \left\{ \frac{p'^5 \tilde{F}_1(iy, p') + p'^3 p^2 \tilde{F}_2(iy, p') + p' p^4 F_3(iy, p')}{x_{p'}[a_{p'}^2 p'^2 - (1 + iy)^2 p^2][b_{p'}^2 p'^2 - (1 - iy)^2 p^2]} \right.$$
$$+ \frac{8p'}{1 - iy} + \frac{8p' p^2 (1 - iy)}{b_{p'}^2 p'^2 - (1 - iy)^2 p^2} - p'^2 \tilde{g}_{p'}(1 + iy)^2 \left[\frac{2p'}{p(1 - iy)} + 1 \right]$$
$$\times \frac{|p' + p|}{x_{p'}^2 p'^2 - [p' + (1 - iy)p]^2} + (p \to -p) \right\}. \quad (7.29)$$

Next, consider the contribution $\tilde{\Pi}_2^{\text{AL}}(iy, p)$ from the Aslamasov-Larkin diagram in Eq. (7.17). Adopting again approximation A, the symmetrized three loop $\tilde{L}_S^{(3)}(iy, p,$

$iy', p')$ is replaced by its limit $\tilde{L}_{S,0}^{(3)}(iy, iy', p/p')$ for $1/m \to 0$ given in Eq. (6.26). Then we obtain

$$-(1+y^2)^2 \tilde{\Pi}_2^{\mathrm{AL}}(iy, p) = \int_{-\infty}^{\infty} dp' |p'| \tilde{g}_{p'} \tilde{g}_{p'+p}$$

$$\times \int_{-\infty}^{\infty} \frac{dy'}{2\pi} \frac{\left[1 - yy' - (y+y')\frac{py+p'y'}{p+p'}\right]^2}{\left[1+y'^2\right] \left[x_{p'}^2 + y'^2\right] \left[1 + \left(\frac{py+p'y'}{p+p'}\right)^2\right] \left[x_{p'+p}^2 + \left(\frac{py+p'y'}{p+p'}\right)^2\right]} \, . \, (7.30)$$

The y'-integration can now be carried out using the theorem of residues. The result can be cast into the following form,

$$-(1+y^2)^2 \tilde{\Pi}_2^{\mathrm{AL}}(iy, p) = \mathrm{Re} \int_0^{\infty} dp' p' \frac{|p' + p|}{2}$$

$$\times \left\{ \frac{\tilde{g}_{p'+p} |p'+p| \left[(p'+p)(1 + 2iyx_{p'} + x_{p'}^2) - p(y^2 + x_{p'}^2)\right]^2}{x_{p'} \left[(p'+p)^2 - \left(x_{p'}p' + iyp\right)^2\right] \left[x_{p'+p}^2 (p'+p)^2 - \left(x_{p'}p' + iyp\right)^2\right]} \right.$$

$$+ \frac{\tilde{g}_{p'} p' \left[p'(1 + 2iyx_{p'+p} + x_{p'+p}^2) + p(y^2 + x_{p'+p}^2)\right]^2}{x_{p'+p} \left[p'^2 - \left(x_{p'+p}(p'+p) - iyp\right)^2\right] \left[x_{p'}^2 p'^2 - \left(x_{p+p'}(p+p') - iyp\right)^2\right]}$$

$$- \left[\frac{2(p'+p)}{p(1-iy)} - 1\right] \frac{\tilde{g}_{p'+p} |p'+p| (1+iy)^2}{x_{p'+p}^2 (p'+p)^2 - [p'+p-(1-iy)p]^2}$$

$$+ \left[\frac{2p'}{p(1-iy)} + 1\right] \frac{\tilde{g}_{p'} p' (1+iy)^2}{x_{p'}^2 p'^2 - [p' + (1-iy)p]^2} \right\} + (p \to -p) \, . \quad (7.31)$$

Finally, the contribution (7.18) of the Hartree-type of diagram (c) in Fig. 7.1 is[1]

$$-(1+y^2)^2 \tilde{\Pi}_2^{\mathrm{H}}(iy, p) = I_H(1 - y^2) \, , \quad (7.32)$$

with

$$I_H = -\frac{2g}{1+g} \int_0^{\infty} dp\, p \left[\frac{1 + \frac{\tilde{g}_p}{2}}{\sqrt{1 + \tilde{g}_p}} - 1\right] = -\frac{g}{1+g} \int_0^{\infty} dp\, p \frac{(x_p - 1)^2}{x_p} \, . \quad (7.33)$$

For Θ-function cutoff this reduces to

$$I_H = -\frac{p_0^2 g}{1+g} \left[\frac{1 + \frac{g}{2}}{\sqrt{1+g}} - 1\right] \, , \quad (7.34)$$

---

[1] The three loop $\tilde{L}_S^{(3)}(iy, p, iy, -p)$ appearing in the Hartree-type of contribution (7.18) to the irreducible polarization is ambiguous for the required combination of arguments: The value of $\lim_{y' \to y, p' \to p} \tilde{L}_S^{(3)}(iy, p, iy', p')$ depends on order of limits. Because Hartree interactions should be static, we define $\tilde{L}_S^{(3)}(iy, p, iy, -p)$ as the limit of $\tilde{L}_S^{(3)}(iy, p, iy', p')$ where we first set the frequency sum $\omega + \omega' = v_F(qy + q'y')$ equal to zero and then take the limit $p' \to -p$.

while for Lorentzian cutoff,

$$I_H = -\frac{p_0^2 g}{1+g} \left[1 + \frac{g}{2} - \sqrt{1+g}\right] . \tag{7.35}$$

Combining all terms we obtain the following expansion of the inverse irreducible polarization to second order in p_0^2,

$$\tilde{\Pi}_*^{-1}(iy, p) = 1+y^2+p^2 - \frac{2p^2}{3}\left[\frac{1}{1-iy} + \frac{1}{1+iy}\right] + I_H(1-y^2) + I(iy, p) + \mathcal{O}(p_0^3), \tag{7.36}$$

where we have used Eqs. (5.11) and (5.12) to clearly exhibit the mass-shell singularity generated by the expansion of the inverse free polarization. The dimensionless integral $I(iy, p)$ can be written as

$$I(iy, p) = \frac{1}{2}\int_0^\infty dp' p' \left[J(iy, p, p') + J(-iy, p, p')\right], \tag{7.37}$$

where the complex function $J(iy, p, p')$ is given by

$$
\begin{aligned}
J(iy, p, p') &= \frac{p'^4 \tilde{F}_1(iy, p') + p'^2 p^2 \tilde{F}_2(iy, p') + p^4 F_3(iy, p')}{x_{p'}[a_{p'}^2 p'^2 - (1+iy)^2 p^2][b_{p'}^2 p'^2 - (1-iy)^2 p^2]} \\
&+ \frac{8}{1-iy} + \frac{8p^2(1-iy)}{b_{p'}^2 p'^2 - (1-iy)^2 p^2} + \frac{|p'+p|}{2} \\
&\times \left\{ \frac{\tilde{g}_{p'+p}|p'+p|\left[(p'+p)(1+2iyx_{p'} + x_{p'}^2) - p(y^2 + x_{p'}^2)\right]^2}{x_{p'}\left[(p'+p)^2 - (x_{p'}p' + iyp)^2\right]\left[x_{p'+p}^2(p'+p)^2 - (x_{p'}p' + iyp)^2\right]} \right. \\
&+ \frac{\tilde{g}_{p'}p'\left[p'(1+2iyx_{p'+p} + x_{p'+p}^2) + p(y^2 + x_{p'+p}^2)\right]^2}{x_{p'+p}\left[p'^2 - (x_{p'+p}(p'+p) - iyp)^2\right]\left[x_{p'}^2 p'^2 - (x_{p+p'}(p+p') - iyp)^2\right]} \\
&- \left[\frac{2(p'+p)}{p(1-iy)} - 1\right]\frac{\tilde{g}_{p'+p}|p'+p|(1+iy)^2}{x_{p'+p}^2(p'+p)^2 - [p'+p-(1-iy)p]^2} \\
&- \left.\left[\frac{2p'}{p(1-iy)} + 1\right]\frac{\tilde{g}_{p'}p'(1+iy)^2}{x_{p'}^2 p'^2 - [p'+(1-iy)p]^2}\right\} + (p \to -p). \tag{7.38}
\end{aligned}
$$

Although it is not obvious from Eq. (7.38), the function $J(iy, p, p')$ vanishes as $\tilde{g}_{p'}^2$ for $p' \gg p_0$, so that the integral (7.37) is ultraviolet convergent as long as $\tilde{g}_p$ vanishes faster than $1/p$ for $p \to \infty$.

7.3 Cancellation of the mass-shell singularities at $\omega = \pm v_F q$

We now show that the mass-shell singularities at $iy \to x = \pm 1$ (corresponding to frequencies $\omega = \pm v_F q$) arising from the expansion of the noninteracting polarization

in Eq. (7.36) are *exactly cancelled* by corresponding singularities in $I(x, p)$, because for $x \to \pm 1$ the integral $I(x, p)$ diverges as

$$I(x, p) \sim \frac{2p^2}{3} \frac{1}{1 \mp x}, \qquad x \to \pm 1. \tag{7.39}$$

To proof this, it is sufficient to calculate the residues

$$R_\pm(p) = \lim_{x \to \pm 1} [(1 \mp x)I(x, p)] = \frac{1}{2} \int_0^\infty dp' p' \lim_{x \to \pm 1} [(1 \mp x)J(\pm x, p, p')] . \tag{7.40}$$

Using $x_p^2 - 1 = \tilde{g}_p$ we find from Eq. (7.38),

$$\lim_{x \to \pm 1} [(1 \mp x)J(\pm x, p, p')] = 8 - 4\frac{|p' + p| - |p' - p|}{p} = 8\Theta(|p| - p')(1 - p'/|p|) . \tag{7.41}$$

Hence,

$$R_\pm(p) = 4 \int_0^{|p|} dp' p'(1 - p'/|p|) = \frac{2p^2}{3}, \tag{7.42}$$

which proofs Eq. (7.39). We conclude that the expansion (7.36) of the inverse irreducible polarization to second order in p_0^2 does not exhibit any mass-shell singularities at frequencies $\omega = \pm v_F q$ corresponding to the excitation energy of noninteracting particle-hole pairs. This cancellation also corrects the unphysical feature of the RPA that the single particle-hole pair continuum is centered at the energy $v_F |q|$ involving the bare Fermi velocity v_F.

It is convenient to explicitly cancel the mass-shell singularities arising from the expansion of the free polarization in Eq. (7.36) against the corresponding singularities in $I(iy, p)$. Therefore we use the identity

$$\frac{2p^2}{3} \left[\frac{1}{1 - iy} + \frac{1}{1 + iy} \right] = \frac{1}{2} \int_0^\infty dp' p' [J_0(iy, p, p') + J_0(-iy, p, p')], \tag{7.43}$$

where

$$J_0(iy, p, p') = \frac{8}{1 - iy} \left[1 - \frac{p' + p + |p' + p|}{2p} + (p \to -p) \right], \tag{7.44}$$

to write Eq. (7.36) as follows,

$$\tilde{\Pi}_*^{-1}(iy, p) = 1 + y^2 + p^2 + I_H(1 - y^2) + \tilde{I}(iy, p) + \mathcal{O}(p_0^3). \tag{7.45}$$

The integral $\tilde{I}(iy, p)$ can again be written as

$$\tilde{I}(iy, p) = \frac{1}{2} \int_0^\infty dp' p' \left[\tilde{J}(iy, p, p') + \tilde{J}(-iy, p, p') \right], \tag{7.46}$$

with

$$\tilde{J}(iy, p, p') = J(iy, p, p') - J_0(iy, p, p'). \tag{7.47}$$

We may now explicitly cancel the mass-shell singularities in the regularized integrand $\tilde{J}(iy, p, p')$ and obtain after some algebra,

$$
\tilde{J}(iy, p, p') = \frac{p'^4 \tilde{F}_1(iy, p') + p'^2 p^2 \tilde{F}_2(iy, p') + p^4 F_3(iy, p')}{x_{p'}[a_{p'}^2 p'^2 - (1 + iy)^2 p^2][b_{p'}^2 p'^2 - (1 - iy)^2 p^2]} + \frac{8p^2(1 - iy)}{b_{p'}^2 p'^2 - (1 - iy)^2 p^2}
$$

$$
+ \frac{\tilde{g}_{p'+p}(p' + p)^2 \left[(p' + p)(1 + 2iyx_{p'} + x_{p'}^2) - p(y^2 + x_{p'}^2) \right]^2}{2x_{p'} \left[(p' + p)^2 - (x_{p'}p' + iyp)^2 \right] \left[x_{p'+p}^2 (p' + p)^2 - (x_{p'}p' + iyp)^2 \right]}
$$

$$
+ \frac{\tilde{g}_{p'}|p' + p|p' \left[p'(1 + 2iyx_{p'+p} + x_{p'+p}^2) + p(y^2 + x_{p'+p}^2) \right]^2}{2x_{p'+p} \left[p'^2 - \left(x_{p'+p}(p' + p) - iyp \right)^2 \right] \left[x_{p'}^2 p'^2 - \left(x_{p+p'}(p + p') - iyp \right)^2 \right]}
$$

$$
+ \frac{(p' + p) \left[8(p' + p) - 4(1 - iy)p + \tilde{g}_{p'+p}(p' + p) \left[\frac{p'+p}{p}(3 + iy) + \frac{1}{2}(1 + iy)^2 \right] \right]}{x_{p'+p}^2 (p' + p)^2 - [p' + p - (1 - iy)p]^2}
$$

$$
+ \frac{|p' + p| \left[-8p' - 4(1 - iy)p + \tilde{g}_{p'}p' \left[\frac{p'}{p}(3 + iy) - \frac{1}{2}(1 + iy)^2 \right] \right]}{x_{p'}^2 p'^2 - [p' + (1 - iy)p]^2} + (p \to -p) \,. \, (7.48)
$$

Despite the cancellation of the mass-shell singularities at $x = \pm 1$, the interaction with sharp momentum transfer generates a new mass-shell singularity at $x = \pm x_0$. However we shall argue in Chap. 9 that the above approximation A is *not* sufficient to calculate the line shape of the dynamic structure factor for momenta $q \lesssim q_c = 1/(m|f_0''|)$ [see Eq. (2.39)], because in this regime the spectral line shape is dominated by the terms neglected in approximation A. On the other hand, for $q \gtrsim q_c$ the line shape of $S(\omega, q)$ is essentially determined by the quadratic term in the expansion of f_q for small q, so that in this regime A is justified.

Chapter 8

Interaction with sharp momentum-transfer cutoff

In this chapter we assume that the dimensionless interaction g_p is of the form

$$g_p = g_0 \Theta(p_0 - |p|). \tag{8.1}$$

In this case the p'-integration in Eq. (7.37) is elementary and can be carried out exactly. Note that all derivatives of the interaction (8.1) vanish at $p = 0$ so that $f_0'' = 0$, which is certainly an unphysical feature of the Θ-function cutoff. The length q_c defined in Eq. (2.39) is then formally infinite, so that the regime (2.40) does not exist. In the next chapter we will show that for such an interaction approximation A discussed in Sec. 7.2 (i.e., replacing $\tilde{\Pi}_0(iy, p) \approx \tilde{\Pi}_0(iy, 0) = [1 + y^2]^{-1}$ in loop integrations) is never justified. But it is still interesting to evaluate Eq. (7.45), because it allows us to explicitly see the partial cancellation between contributions arising from the first-order diagram in Fig. 7.1 (a) and the AL diagram in Fig. 7.1 (b). We show in the first section of this chapter that the irreducible polarization exhibits a new mass-shell singularity at $\omega = v|q|$ if we use the interaction defined in (8.1). This feature is an artifact of the non-analyticity of step function. In Sec. 8.2 we calculate the renormalization of the ZS velocity according to Eq. (7.8) for $q \to 0$ and in Sec. 8.3 we use again the Samokhin regularization method for the mass-shell singularity, which we have applied in Sec. 5.2 to estimate the ZS damping.

8.1 Explicit evaluation of the irreducible polarization

In order to clearly exhibit the cancellation of mass-shell singularities, it is instructive to evaluate the contributions $\tilde{\Pi}_1(iy, p)$ (first-order in the effective interaction) and $\tilde{\Pi}_2(iy, p)$ (second order in the effective interaction) separately. Therefore, we specify $\tilde{g}_p = g\Theta(p_0 - |p|)$ in Eqs. (7.37, 7.38) and perform the p'-integration exactly. Recall that the effective coupling constant g is defined as a function of the bare coupling g_0 via Eq. (7.9). The $p \to 0$ limits of the coefficients x_p, a_p and b_p given in Eqs. (7.20a–

7.20c) are now denoted by

$$x_0 = \sqrt{1+g}, \tag{8.2a}$$
$$a = x_0 + 1, \tag{8.2b}$$
$$b = x_0 - 1. \tag{8.2c}$$

Note that for small g,

$$a = 2 + \frac{g}{2} - \frac{g^2}{8} + \frac{g^3}{16} + O(g^4), \tag{8.3}$$

$$b = a - 2 = \frac{g}{2} - \frac{g^2}{8} + \frac{g^3}{16} + O(g^4). \tag{8.4}$$

After some tedious algebra we find that the contribution from the diagram (a) in Fig. 7.1 to the expansion (7.19) can be written as

$$
\begin{aligned}
-(1+y^2)^2 \tilde{\Pi}_1(iy, p) = & -p_0^2 \frac{b^2(3+x_0)}{2ax_0}(2+g-\Delta) \\
& + p^2 \left\{ \frac{2}{3}\frac{1-3y^2}{1+y^2} + \frac{(2+g)}{g}(4-g) - \frac{4\Delta}{g^2}\left[4+g-\frac{g^2}{4}\right] \right. \\
& + \frac{\Delta-g}{x_0} \mathrm{Re}\left[-\frac{a^2}{b^3}(1-iy)(x_0+iy)\ln\left(\frac{1+iy}{x_0+iy}\right)\right. \\
& \left.\left. + \frac{b^2}{a^3}(1-iy)(x_0-iy)\ln\left(\frac{p_0^2 a^2 - p^2(1+iy)^2}{p^2(1+iy)(x_0-iy)}\right)\right]\right\},
\end{aligned}
\tag{8.5}
$$

where we have defined

$$\Delta = 1 + g + y^2 = x_0^2 + y^2. \tag{8.6}$$

If we neglect at this point the contribution $\tilde{\Pi}_2(iy, p)$ involving two powers of the effective interaction,

$$\tilde{\Pi}_{*,1}^{-1}(iy, p) \equiv \nu_0 \Pi_{*,1}^{-1}(i\omega, q) = 1 + y^2 - \frac{p^2}{3}\frac{1-3y^2}{1+y^2} - (1+y^2)^2 \tilde{\Pi}_1(iy, p), \tag{8.7}$$

we recover from Eq. (7.5) the previous estimate [29] of the dynamic structure factor for ω close to $v|q|$ and $q \to 0$

$$S(q, \omega \approx v|q|) = \frac{\nu_0}{\pi} \mathrm{Im}\left[\frac{\Pi_{*,1}(\omega+i0, q)}{1+f_q \Pi_{*,1}(\omega+i0, q)}\right] = \frac{Z_q \gamma_q}{\pi\left[(\omega-v|q|)^2 + \gamma_q^2\right]}, \tag{8.8}$$

where the last logarithmic term in Eq. (8.5) gives rise to the ZS damping

$$\gamma_q = \mathrm{Im}\Pi_{*,1}(q, v|q|)\left[\frac{\partial \mathrm{Re}\Pi_{*,1}}{\partial\omega}\bigg|_{\omega=v|q|}\right]^{-1} \approx \frac{\pi}{8}\frac{g^3}{x_0 a^4}\frac{|q|^3}{v_F m^2}. \tag{8.9}$$

In view of the discussion at the end of Sec. 5.2 this result should not be surprising: within our approximation the ZS mode is located at higher energy than the single-pair continuum and is immersed in the multi-pair continuum, whose spectral weight Z_q is generated by the logarithmic terms in Eq. (8.5). The overlap of the multi-pair continuum with the ZS mode leads to the q^3-damping, in agreement with the arguments by Teber [6].

Unfortunately, the term in Eq. (8.5) which is responsible for the ZS damping given by (8.9) is exactly cancelled by a similar term in $-(1+y^2)\tilde{\Pi}_2^{\mathrm{AL}}(iy,p)$. Explicitly carrying out the p'-integration in Eq. (7.31) and adding the contribution (7.32) from the Hartree-type of term, we obtain for $|p| < p_0$,

$$
-(1+y^2)^2\tilde{\Pi}_2(iy,p) = p_0^2\frac{b^2}{2x_0^3}g(2+g-\Delta)
$$

$$
+p_0(p_0-|p|)\frac{b^2}{ax_0^3}\Big[g(2+g) - b\big(1+\frac{g}{4}\big) - \Delta x_0^2\Big]
$$

$$
+p^2\bigg\{-\frac{1-3y^2}{3(1+y^2)} + \frac{g}{2x_0} - \frac{(2+g)}{2g}\Big[4-g+\frac{4}{x_0}\Big]
$$

$$
+\frac{2\Delta}{g^2}\Big[4+g-\frac{g^2}{4}+\frac{3g^2}{4x_0}+x_0(4-g)\Big] - \frac{(4+g)^2+8g(2+g-\Delta)}{12x_0\Delta}
$$

$$
+\frac{g^2\Delta}{16x_0^5}\ln\Big(\frac{4p_0(p_0-|p|)x_0^2+p^2\Delta}{p^2\Delta}\Big) + \frac{\Delta-g}{x_0}\mathrm{Re}\Big[\frac{a^2}{b^3}(1-iy)(x_0+iy)\ln\Big(\frac{1+iy}{x_0+iy}\Big)
$$

$$
-\frac{b^2}{a^3}(1-iy)(x_0-iy)\ln\Big(\frac{p_0(p_0-|p|)a^2+p^2(1+iy)(x_0-iy)}{p^2(1+iy)(x_0-iy)}\Big)\Big]\bigg\}. \qquad (8.10)
$$

Adding Eqs. (8.5) and (8.10) and rearranging terms, we obtain for the expansion (7.19) of the inverse irreducible polarization for sharp momentum-transfer cutoff

$$
\begin{aligned}
\tilde{\Pi}_*^{-1}(iy,p) = {}& 1 + p_0^2 g_1 + (1+p_0^2 g_2)y^2 + p_0|p|[g_3+g_4 y^2] \\
& + \frac{p^2}{2}\bigg\{\frac{4g}{3x_0} - 2 + \frac{b}{gx_0}[8+4g-g^2] + \frac{\Delta}{g^2}\big[16b-4ga+g^2(1+3/x_0)\big] \\
& - \frac{(4+3g)^2}{6x_0\Delta} + \frac{g^2\Delta}{8x_0^5}\ln\Big(\frac{4p_0(p_0-|p|)x_0^2+p^2\Delta}{p^2\Delta}\Big) \\
& - (1+y^2)\frac{b^2}{a^3x_0}2\mathrm{Re}\Big[(1-iy)(x_0-iy)\ln\Big(\frac{p_0 a-|p|(x_0-iy)}{p_0 a+|p|(1+iy)}\Big)\Big]\bigg\},
\end{aligned}
$$

$$(8.11)$$

where

$$g_1 \;=\; -\frac{b^2}{2x_0^3}\left[3+\frac{g}{2}\frac{x_0+3}{x_0+1}\right]-\frac{3}{8}g^2+\frac{5}{8}g^3+\mathcal{O}(g^4)\,, \tag{8.12a}$$

$$g_2 \;=\; \frac{b^2}{2x_0^3}=\frac{1}{8}g^2-\frac{1}{4}g^3+\mathcal{O}(g^4)\,, \tag{8.12b}$$

$$g_3 \;=\; \frac{b^2}{ax_0^3}\left[x_0+\frac{g}{4}b\right]=\frac{1}{8}g^2-\frac{7}{32}g^3+\mathcal{O}(g^4)\,, \tag{8.12c}$$

$$g_4 \;=\; \frac{b^2}{ax_0}=\frac{1}{8}g^2-\frac{5}{32}g^3+\mathcal{O}(g^4)\,. \tag{8.12d}$$

Eq. (8.11) has three important properties:

- The logarithmic term in Eq. (8.5) which is responsible for the q^3-dependence of γ_q in Eq. (8.9), is exactly cancelled by a similar term with opposite sign arising from the AL diagram.

- The mass-shell singularity at $\omega = \pm v_F q$ associated with the expansion of the free polarization $\Pi_0(\omega, q)$ in Eq. (7.36) has disappeared in Eq. (8.5), in agreement with our general considerations in Chap. 7.

- Eq. (8.11) contains a term proportional to $1/\Delta$, which after analytic continuation gives rise to a mass-shell singularity at the physical energy $\omega = \pm vq$ of the ZS mode.

The mass-shell singularity at $\omega = \pm vq$ is an artifact of the sharp momentum-transfer cutoff used in this chapter in combination with approximation A discussed in Sec. 7.2. In fact, we shall show in the next chapter that a more realistic interaction f_q with finite f_0'' does not lead to any mass-shell singularities, even if we still use approximation A to evaluate Eqs. (7.15–7.18).

8.2   Renormalized ZS velocity

To calculate the renormalized ZS velocity it is sufficient to set $p = 0$ in Eq. (8.11), so that the problems related to the mass-shell singularity do not arise. Comparing Eq. (8.11) at $p = 0$ with the defining equation (7.6) of the renormalization constants Z_1 and Z_2, we find to order p_0^2,

$$Z_i = 1 + p_0^2 g_i\,, \qquad i = 1, 2\,, \tag{8.13}$$

which are nonlinear self-consistency equations for Z_1 and Z_2, because g_1 and g_2 are defined in terms of the renormalized coupling $g = (g_0 + Z_1 - Z_2)/Z_2$, see Eq. (7.9). However, keeping in mind that the difference $g - g_0$ is proportional to p_0^2 and that Eq. (8.13) is only valid to order p_0^2, we may ignore the self-consistency condition and

set $Z_1 = Z_2 = 1$ in the expressions for g_1 and g_2 on the right-hand side of Eq. (8.13). From Eq. (7.8) we then obtain for the renormalized ZS velocity,

$$\frac{v}{v_F} = \sqrt{\frac{Z_1 + g_0}{Z_2}} = \sqrt{1 + g}\,, \tag{8.14}$$

where

$$g = g_0 - p_0^2 g_5\,, \tag{8.15}$$

with

$$g_5 = x_0^2 g_2 - g_1 = \frac{b^2}{x_0^3}\left[2 + \frac{g}{4}\left(3 + \frac{2}{a}\right)\right] = \frac{1}{2}g^2 - \frac{3}{4}g^3 + \mathcal{O}(g^4)\,. \tag{8.16}$$

To order p_0^2 we thus obtain for the energy of the ZS mode

$$\omega_q \approx v|q|\,, \tag{8.17}$$

with renormalized ZS velocity,

$$v = v_F\sqrt{1 + g_0 - p_0^2 g_5} = v_0\left[1 - p_0^2\frac{g_5}{2x_0^2} + \mathcal{O}(p_0^4)\right]\,, \tag{8.18}$$

where $v_0 = v_F\sqrt{1 + g_0}$ is the RPA result for the ZS velocity. A graph of the relative change of the ZS velocity as a function of the interaction strength g is shown in Fig. 8.1. Obviously, even for large g and $p_0^2 = \mathcal{O}(1)$ the correction to the RPA result v_0 never exceeds more than a few percent.

8.3   Spectral line shape

Although for sharp momentum-transfer cutoff the dynamic structure factor exhibits (within approximation A discussed in Sec. 7.2) a mass-shell singularity at the ZS energy $v|q|$, it is nevertheless instructive to follow Samokhin [5] and regularize the singularity by hand using the procedure outlined in Sec. 5.2. Because the natural scale for the momentum dependence is not $2k_F$ but the scale q_0 set by the momentum-transfer cutoff, it is convenient to express the momentum dependence via $\tilde{q} = q/q_0$. Setting $p = p_0\tilde{q}$ and writing

$$S(\omega, q) = \frac{\nu_0}{\pi}\text{Im}\left[\frac{1}{g_0 + \tilde{\Pi}_*^{-1}(x + i0, \tilde{q})}\right]\,, \tag{8.19}$$

we obtain on the imaginary frequency axis

$$g_0 + \tilde{\Pi}_*^{-1}(iy, \tilde{q}) = \Delta\left[1 + p_0^2(g_2 + g_4|\tilde{q}|)\right] - p_0^2 g_6|\tilde{q}|$$
$$+ p_0^2\tilde{q}^2\left\{h_0 - \frac{h_1}{\Delta} + \Delta\left[g_7 + g_8\ln\left(1 + \frac{4x_0^2(1 - |\tilde{q}|)}{\tilde{q}^2\Delta}\right)\right]\right.$$
$$\left. + (g - \Delta)\frac{b^2}{a^3 x_0}\text{Re}\left[(1 - iy)(x_0 - iy)\ln\left(\frac{a - |\tilde{q}|(x_0 - iy)}{a + |\tilde{q}|(1 + iy)}\right)\right]\right\}\,, \tag{8.20}$$
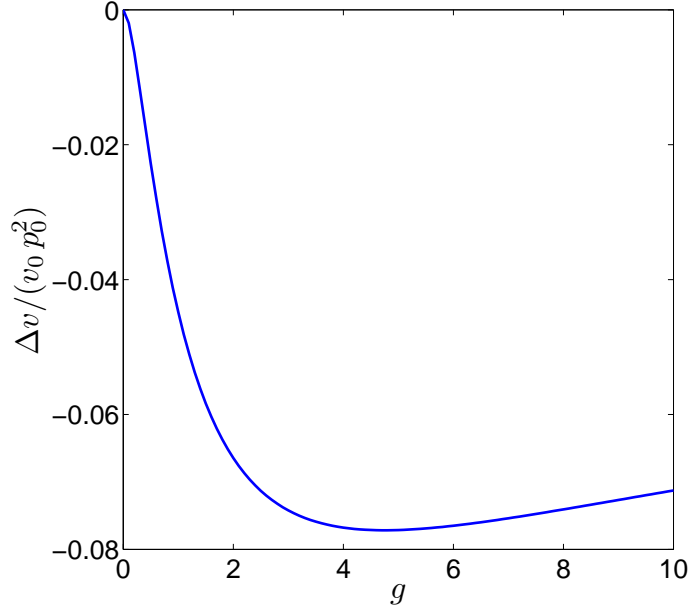
Figure 8.1: Relative renormalization $\Delta v/(v_0 p_0^2) \equiv (v - v_0)/(v_0 p_0^2) = -g_5/(2x_0^2)$ of the ZS velocity in units of p_0^2 as a function of the interaction strength g, see Eq. (8.18).

where

$$g_6 = x_0^2 g_4 - g_3 = \frac{b^2}{ax_0^3} g \left[2 + g - \frac{b}{g} \left(1 + \frac{g}{4} \right) \right] = \frac{3}{16} g^3 + \mathcal{O}(g^4), \quad (8.21a)$$

$$g_7 = \frac{1}{2} + \frac{3}{2x_0} - \frac{8}{g} \left(\frac{a}{4} - \frac{b}{g} \right) = \frac{1}{8} g^2 - \frac{11}{64} g^3 + \mathcal{O}(g^4), \quad (8.21b)$$

$$g_8 = \frac{g^2}{16x_0^5} = \frac{1}{16} g^2 - \frac{5}{32} g^3 + \mathcal{O}(g^4), \quad (8.21c)$$

$$h_0 = -1 + \frac{2g}{3x_0} + \frac{b}{2gx_0} [8 + 4g - g^2] = 1 + \frac{1}{6} g - \frac{1}{12} g^2 + \mathcal{O}(g^3), \quad (8.21d)$$

$$h_1 = \frac{(1 + 3x_0^2)^2}{12x_0} = \frac{(4 + 3g)^2}{12x_0} = \frac{4}{3} + \frac{4}{3} g + \frac{1}{4} g^2 + \mathcal{O}(g^3). \quad (8.21e)$$

From Eq. (8.20) it is obvious that our functional bosonization approach yields a systematic expansion of the inverse irreducible polarization in powers of the small parameter $p_0 = q_0/(2k_F)$. Note that only h_0 and h_1 have finite limits for $g \to 0$, whereas the other couplings $g_1, \ldots, g_8$ vanish at least as g^2 (the coupling g_6 vanishes even as g^3).

In the limit $g \to 0$ Eq. (8.20) correctly reduces to the expansion of the noninteracting inverse polarization given in Eq. (5.11). However, the term h_1/Δ generates a mass-shell singularity at the true collective mode energy $\omega = \pm vq$. Fortunately, this singularity can be avoided if we use a more physical interaction whose Fourier
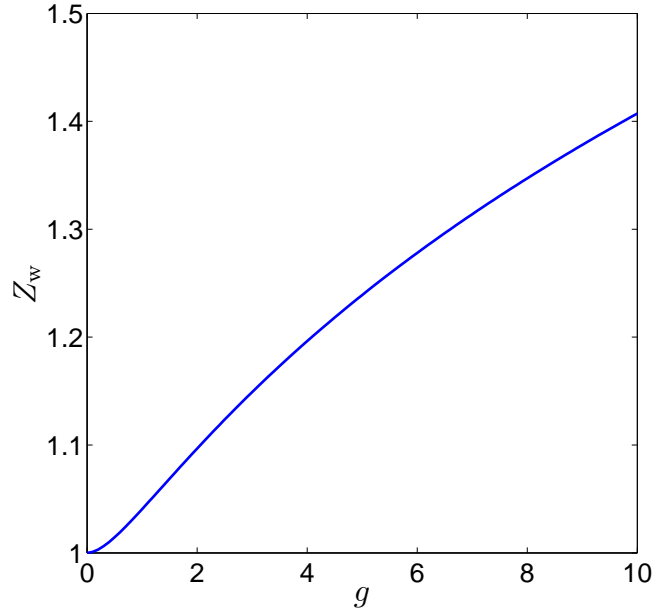
Figure 8.2: Graph of the factor Z_w defined in Eq. (8.23), which estimates the interaction-induced relative change of the width of ZS resonance for $q \ll q_c$, see Eqs. (8.22,8.23).

transform f_q is analytic for small q, as will be shown explicitly in Chap. 9. In this section we shall simply regularize the mass-shell singularity by hand using the self-consistent regularization procedure proposed by Samokhin [5], which we have already described in detail in Sec. 5.2. Repeating the steps leading from Eq. (5.18) to Eq. (5.23), we obtain from the self-consistent regularization of the singular term proportional to h_1/Δ in Eq. (8.20) the following estimate for the width of the ZS mode,

$$\mathrm{w}_q = \frac{\sqrt{h_1}}{2x_0} \frac{q^2}{2m} = Z_\mathrm{w} \frac{q^2}{2\sqrt{3}m}, \tag{8.22}$$

where we have factored out the corresponding estimate in the absence of interactions given in Eq. (5.23), and the dimensionless factor Z_w is given by

$$Z_\mathrm{w} = \sqrt{\frac{3h_1}{4x_0^2}} = \frac{1 + \frac{3}{4}g}{[1 + g]^{3/4}}. \tag{8.23}$$

Note that $Z_\mathrm{w} \sim 1 + \frac{3}{32}g^2 + O(g^3)$ for $g \to 0$, and $Z_\mathrm{w} \sim \frac{3}{4}g^{1/4}$ for $g \to \infty$. A graph of Z_w as a function of the interaction strength g is shown in Fig. 8.2. The estimate (8.22) for the width of the ZS resonance on the frequency axis scales as q^2, which is for small q much larger than our previous estimate (8.9) based on the evaluation of only the first-order diagram (a) in Fig. 7.1. The q^2-scaling of the width of the ZS resonance has already been found by Samokhin [5] and has been confirmed later
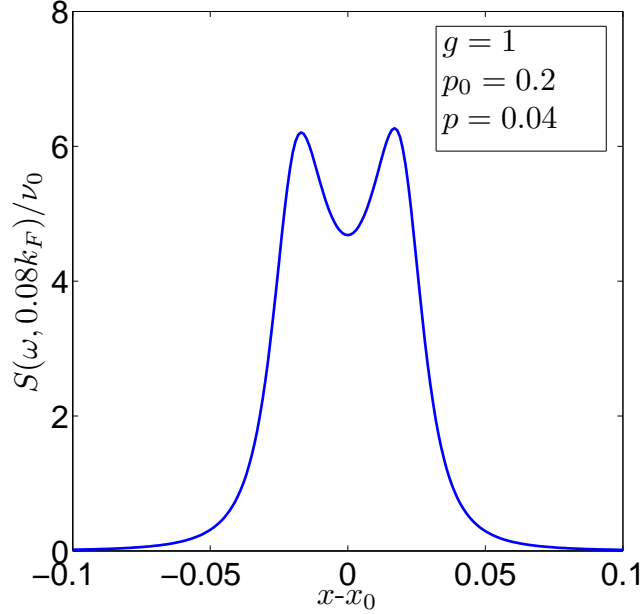
Figure 8.3: Graph of the dynamic structure factor $S(\omega, q)$ as a function of $x - x_0 = (\omega - vq)/(v_F q)$ for fixed $q = 0.08 k_F$. The line shape has been calculated from Eqs. (8.19 ,8.20, 8.22) and (8.24). The distance between the local maxima is proportional to $w_q \propto q^2/m$.

in Refs. [3, 4, 31]. However, the derivation of Eq. (8.22) is based on a rather ad hoc regularization prescription of the mass-shell singularity in Eq. (8.20), which ignores in particular the divergent real part of the term h_1/Δ. Let us nevertheless proceed and calculate the corresponding dynamic structure factor, which can be obtained by replacing the term $h_1/\Delta = h_1/(x_0^2 + y^2)$ on the right-hand side of Eq. (8.20) by

$$\frac{h_1}{\Delta} \rightarrow \frac{h_1}{x_0^2 - \frac{(\omega + iw_q)^2}{(v_F q)^2}}. \tag{8.24}$$

The finite imaginary part w_q in this expression is a rough estimate of the modification of the spectral line shape due to the terms which have been neglected by making the approximation A discussed in Sec. 7.2. The typical form of the dynamic structure factor in the regime $p \ll p_0$ implied by Eqs. (8.20, 8.22) and (8.24) is shown in Fig. 8.3. Obviously, within our approximation the dynamic structure factor does not exhibit any threshold singularities, which according to Refs. [3, 4] are a generic feature of the dynamic structure factor of Luttinger liquids. It turns out that the absence of threshold singularities in Fig. 8.3 is an artifact of the rather simple regularization prescription (8.24) of the unphysical mass-shell singularity in Eq. (8.20). In the following chapter we shall show how to recover the threshold singularities within our functional bosonization approach.

Chapter 9

Interaction with regular momentum dependence

In this chapter we show that for a more realistic interaction whose Fourier transform is for small momenta of the form

$$f_q = f_0 + \frac{1}{2} f_0'' q^2 + \mathcal{O}(q^4), \qquad \text{with } f_0'' \neq 0. \qquad (9.1)$$

we do not encounter any mass-shell singularities. In fact, we believe that even for sharp momentum-transfer cutoff, $f_q = f_0 \Theta(q_0 - q)$, our perturbative result (7.1) does not suffer from mass-shell singularities as long as we do not rely on the approximation A discussed in Chap. 7; in other words, the mass-shell singularity h_1/Δ in Eq. (8.20) is an artifact of the sharp momentum-transfer cutoff in combination with our neglect of curvature corrections to the free polarization in loop integrations. While we are not able to evaluate Eqs. (7.15–7.18) analytically without relying on approximation A, we shall in this chapter abandon the sharp momentum-transfer cutoff and assume that the interaction f_q can be expanded for small q as in Eq. (2.38). Later we shall argue that as long as we rely on approximation A, our result for $S(\omega, q)$ can only be trusted for $q \gtrsim q_c = 1/(m|f_0''|)$, see Eq. (2.39). But if f_0'' is sufficiently large, then there exists a parametrically large regime $q_c \ll q \ll k_F$ of wave-vectors where our calculation is valid. In the last section of this chapter we use a resummation procedure proposed by Pustilnik *et al.* [3] to obtain from a logarithmic singularity in our calculation an algebraic one.

9.1 Imaginary part of $\Pi_*^{-1}(\omega, q)$

Let us first calculate the imaginary part of the dimensionless inverse polarization $\tilde{\Pi}_*^{-1}(x + i0, p)$ given in Eq. (7.45) assuming for simplicity $p > 0$. From Eqs. (7.46) and (7.48) we obtain

$$
\begin{aligned}
\mathrm{Im}\tilde{\Pi}_*^{-1}(x + i0, p) &= \mathrm{Im}\tilde{I}(x + i0, p) \\
&= \frac{1}{2} \int_0^\infty dp' p' \mathrm{Im} \left[\tilde{J}(x + i0, p, p') + \tilde{J}(-x - i0, p, p') \right].
\end{aligned} \quad (9.2)
$$

In order to calculate the imaginary part of $\tilde{J}(x+i0,p,p')$, we first perform a partial fraction decomposition of Eq. (7.48). We then transform some parts of $\tilde{J}(iy,p,p')$ using $iy \to -iy$, because $\tilde{I}(iy,p)$ defined in Eq. (7.46) is symmetric under this transformation. We obtain

$$
\begin{aligned}
\tilde{J}(iy,p,p') \;&=\; \frac{1}{4x_{p'}}\left[\frac{A_2(iy,p,p')+A_1(-iy,p,p')}{a_{p'}p'+p(1-iy)} + \frac{A_2(iy,p,p')-A_1(iy,p,p')}{b_{p'}p'-p(1-iy)}\right] \\
&+\frac{1}{4x_{p'+p}}\left[\frac{B_2(iy,p,p')+B_1(-iy,p,p')}{a_{p'+p}(p'+p)-p(1+iy)} - \frac{B_2(iy,p,p')-B_1(iy,p,p')}{b_{p'+p}(p'+p)+p(1-iy)}\right] \\
&-\frac{1}{4x_{p'}x_{p'+p}}\left[\frac{C_2(iy,p,p')+C_1(-iy,p,p')}{(x_{p'}+x_{p'+p})p'+p(x_{p'+p}-iy)} + \frac{C_2(iy,p,p')-C_1(iy,p,p')}{(x_{p'}-x_{p'+p})p'-p(x_{p'+p}-iy)}\right] \\
&+\;(p\to -p)\,,
\end{aligned}
\tag{9.3}
$$

where

$$
\begin{aligned}
A_1(iy,p,p') \;&=\; \frac{p'}{p'+p}\left[2g_{p'}x_{p'}(5+2iy+y^2)-4(1+2iyx_{p'}-y^2)-g_{p'}^2(-2+y^2)\right] \\
&+\frac{p'p}{p'+p}\left[-32x_{p'}^2+2g_{p'}(1-y^2)[a_{p'}-b_{p'}(1-iy)]\,,\right. \\
&+\;2g_{p'}(1+iy)(10+iy+y^2)+4b_{p'}(1+iy)(-5-y^2)\right] \\
&+\frac{p^2}{p'+p}\left[(1+y^2)^2[b_{p'}^2+1]-4x_{p'}(1+iy)(4+y^2-iy)-4b_{p'}^2\right],
\end{aligned}
\tag{9.4a}
$$

$$
A_2(iy,p,p') \;=\; |p'+p|\left[-16-8(1-iy)\frac{p}{p'}+g_{p'}\left[\frac{p'}{p}(6+2iy)-(1+iy)^2\right]\right],
\tag{9.4b}
$$

$$
\begin{aligned}
B_1(iy,p,p') \;&=\; \left[16(p'+p)-8(1-iy)p\right. \\
&+\;g_{p'+p}(p'+p)\left[\frac{p'+p}{p}(6+2iy)+(1+iy)^2\right]\right],
\end{aligned}
\tag{9.4c}
$$

$$
B_2(iy,p,p') \;=\; |p'+p|\left[(1+2iyx_{p'+p}+x_{p'+p}^2)+\frac{p}{p'}(y^2+x_{p'+p}^2)\right]^2,
\tag{9.4d}
$$

$$
C_1(iy,p,p') \;=\; \frac{1}{p'+p}\left[(p'+p)(1+2iyx_{p'}+x_{p'}^2)-p(y^2+x_{p'}^2)\right]^2,
\tag{9.4e}
$$

$$
C_2(iy,p,p') \;=\; B_2(iy,p,p')\,.
\tag{9.4f}
$$

If we now carry out the analytic continuation to the real frequency axis $iy \to x+i0$, we can take the imaginary part via the relation

$$
\mathrm{Im}\frac{1}{x-a\pm i0} = \mathcal{P}\frac{1}{x-a} \mp i\delta(x-a)\,,
\tag{9.5}
$$

where $\mathcal{P}$ denote the Cauchy principal value. We get after some algebra,

$$
\begin{aligned}
&\operatorname{Im}\left[p'\tilde{J}(x+i0,p,p')\right] = \\
&-\frac{(1+x)^2(2p'+p-px)^2}{4p'^2 x_{p'}}\left[\chi_{p,p'}\delta\big(a_{p'}p'+p(1-x)\big)+\psi_{p,p'}\delta\big(b_{p'}p'-p(1-x)\big)\right] \\
&-\frac{(1+x)^2(2p'+p+px)^2}{4(p'+p)^2 x_{p'+p}} \\
&\times\left[\chi_{p,p'}\delta\big(a_{p'+p}(p'+p)-p(1-x)\big)-\psi_{p,p'}\delta\big(b_{p'+p}(p'+p)+p(1-x)\big)\right] \\
&-\frac{\left[p(1+x^2-2xx_{p'})+p'(1-2xx_{p'}+x_{p'}^2)\right]^2}{4(p'+p)^2 x_{p'}x_{p'+p}}\times \\
&\left[\chi_{p,p'}\delta\big(p'(x_{p'}+x_{p'+p})+p(x_{p'+p}-x)\big)+\psi_{p,p'}\delta\big(p'(x_{p'}-x_{p'+p})-p(x_{p'+p}-x)\big)\right] \\
&+(p\to -p)\,, \tag{9.6}
\end{aligned}
$$

where

$$
\begin{aligned}
\chi_{p,p'} &= p'(p'+p)+p'|p'+p|\,, \tag{9.7}\\
\psi_{p,p'} &= p'(p'+p)-p'|p'+p|\,. \tag{9.8}
\end{aligned}
$$

We have used here

$$
f(x)\,\delta(x-a) = f(a)\,\delta(x-a)\,. \tag{9.9}
$$

Applying the transformation $p' \to p' - p$ and then $p \to -p$ to the first term of Eq. (9.6), it is clear that the first four δ-functions cancel each other out and we can write

$$
\begin{aligned}
\operatorname{Im}\tilde{J}(x+i0,p,p') &= -\frac{\pi|p'+p|}{2x_{p'}x_{p'+p}} \\
&\times\Bigg\{\Theta(p'+p)\left[1-x_{p'}x_{p'+p}-x(x_{p'}-x_{p'+p})\right]^2\delta\big(p'(x_{p'}+x_{p'+p})-p(x-x_{p'+p})\big) \\
&+\Theta(-p'-p)\left[1+x_{p'}x_{p'+p}-x(x_{p'}+x_{p'+p})\right]^2\delta\big(p'(x_{p'}-x_{p'+p})-p(x+x_{p'+p})\big)\Bigg\} \\
&-(p\to -p) \\
&= -\frac{\pi|p'+p|}{2x_{p'}x_{p'+p}}\left[1-x_{p'}\tilde{x}_{p'+p}-x(x_{p'}-\tilde{x}_{p'+p})\right]^2\delta\big(p'(x_{p'}+\tilde{x}_{p'+p})-p(x-\tilde{x}_{p'+p})\big) \\
&-(p\to -p)\,, \tag{9.10}
\end{aligned}
$$

where we have defined

$$
\tilde{x}_{p+p'} = \operatorname{sgn}(p+p')x_{p+p'}\,. \tag{9.11}
$$

In order to perform the p'-integration in Eq. (9.2), we use the fact that by assumption both p and p' are small compared to unity so that we may expand x_p to first order in p^2,

$$
x_p = \sqrt{1+\tilde{g}_p} = \sqrt{1+g+\frac{g_0''}{2}p^2+\mathcal{O}(p^4)} = x_0+\frac{x_0''}{2}p^2+\mathcal{O}(p^4)\,, \tag{9.12}
$$

where from Eq. (7.11),

$$x_0'' \approx \frac{g_0''}{2x_0} = \frac{\mathrm{sgn}f_0''}{\pi x_0 p_c}. \tag{9.13}$$

Note that for small p_c the coefficient x_0'' is large compared to unity. The δ-functions in Eq. (9.10) can then be approximated by

$$\delta\Big(p'(x_{p'} + x_{p'+p}) - p(x - x_{p'+p})\Big) \approx \frac{1}{2x_p}\delta\Big(p' - p\frac{x - x_p}{2x_p}\Big), \tag{9.14}$$

$$\delta\Big(p'(x_{p'} - x_{p'+p}) - p(x + x_{p'+p})\Big) \approx \frac{2}{3|x_0''p|}\delta\Big(p'^2 + p'p + \frac{2(x + x_p)}{3x_0''}\Big). \tag{9.15}$$

In Eq. (9.14) we have expanded the argument of the δ-function to linear order in p and p', assuming that both dimensionless momenta are small. On the other hand, due to the cancellation of the leading term in the difference $x_{p'} - x_{p'+p}$ in the δ-function of Eq. (9.15), the corresponding expansion has to be carried out to cubic order in the momenta. The integration in Eq. (9.10) can now be carried out analytically and we obtain for small $p > 0$,[1]

$$\mathrm{Im}\tilde{\Pi}_*^{-1}(x + i0, p) = -\pi^2 p_c\Bigg[\Theta(x - x_p)\tilde{g}_p^2\tilde{\gamma}_p\frac{x^2 - x_p^2}{6x_0^4} + h_1(x)C_I\Big(-\mathrm{sgn}f_0''\frac{x - x_p}{\tilde{\gamma}_p}\Big)\Bigg], \tag{9.16}$$

where

$$\tilde{\gamma}_p = \frac{3p^2}{8\pi x_0 p_c}, \tag{9.17}$$

and the functions $h_1(x)$ and $C_I(u)$ are given by

$$h_1(x) = \frac{(1 + 2xx_p + x_p^2)^2}{12x_p}, \tag{9.18}$$

$$C_I(u) = \Theta(u)\Theta(1 - u)\frac{u}{\sqrt{1 - u}}. \tag{9.19}$$

Because the Θ-functions in Eq. (9.19) confirm that $|x - x_p| < \tilde{\gamma}_p$, we can replace for $\tilde{\gamma}_p \ll 1$

$$h_1(x) \to h_1(x_p) \approx h_1 = \frac{(1 + 3x_0^2)^2}{12x_0}. \tag{9.20}$$

The coefficient h_1 has also appeared for sharp momentum-transfer cutoff [see Eq. (8.21e)] in form of the residue of the mass-shell singularity h_1/Δ in our expression (8.20) for the irreducible polarization. A graph of $C_I(u)$ is shown as the dashed line in Fig. 9.1. Mathematically, the square-root singularity of $C_I(u)$ for $u \to 1$ originates from the special point $x - x_p = -\mathrm{sgn}f_0''\tilde{\gamma}_p$ where the argument of the Dirac δ-function

---

[1]There are two mistakes in the expression for $\mathrm{Im}\tilde{\Pi}_*^{-1}(x + i0, p)$ given in Eq. (7.7) of Ref. [42]. The factor 6 must be replaced by a factor 12 in denominator of the first part of this equation and the coefficient $-\mathrm{sgn}f_0''$ should be in the argument of the function C_I in the second part of this equation. The correct result for $\mathrm{Im}\tilde{\Pi}_*^{-1}(x + i0, p)$ is given in Eq. (9.16) of this thesis.
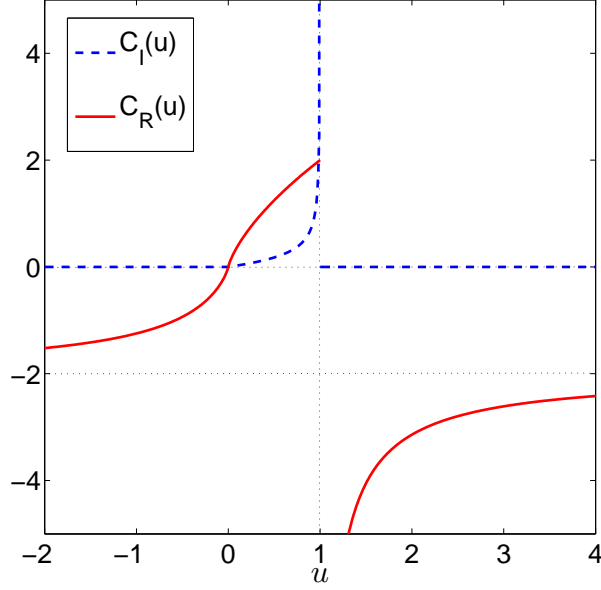
Figure 9.1: Graph of the functions $C_I(u)$ and $C_R(u)$ defined in Eqs. (9.19) and (9.22). The dotted lines indicate asymptotic limits.

on the right-hand side of Eq. (9.14) has a double root. We believe that the divergence of $C_I(u)$ for $u \to 1$ is unphysical and indicates that the approximations leading to Eq. (9.14) are not sufficient in this regime. Hence, within our approximations we can only obtain reliable results for the spectral line shape as long as the ratio $-\text{sgn} f_0''(x - x_p)/\tilde{\gamma}_p$ is not too close to unity.

9.2 Real part of $\Pi_*^{-1}(\omega, q)$

For $p_c \ll 1$ and $p \ll 1$ we can obtain the contribution from $\text{Re}\tilde{I}(x+i0, p)$ analytically from Eqs. (7.46) and (7.48) using the fact that among the corrections of order p^2 only terms proportional to p^2/p_c should be retained. We obtain for $x > 0$ and $p > 0$ after a some lengthy algebra,

$$\text{Re}\tilde{I}(x + i0, p) \approx \int_0^\infty \frac{\mathrm{d}p'^2}{2} \left[2 - \frac{g_{p'}}{x_{p'}} - \frac{(1 + x_{p'}^2)^2}{2x_{p'}^3} - 2u^2(\frac{1}{x_{p'}} - 1) - u^2 \frac{g_{p'}}{x_{p'}} \right]$$
$$+ \frac{h_1(x)}{x_0''} \left[2 - C_R\left(-\text{sgn} f_0'' \frac{x - x_p}{\tilde{\gamma}_p}\right) \right] + \frac{h_1(-x)}{x_0''} \left[2 - C_R\left(-\text{sgn} f_0'' \frac{x + x_p}{\tilde{\gamma}_p}\right) \right], \quad (9.21)$$

where

$$C_R(u) = \frac{u}{\sqrt{|1 - u|}} \left[\Theta(1 - u) \ln \left| \frac{1 + \sqrt{1 - u}}{1 - \sqrt{1 - u}} \right| - 2\Theta(u - 1) \arctan\left(\frac{1}{\sqrt{u - 1}} \right) \right],$$
$$(9.22)$$

and the function $h_1(x)$ is defined in (9.18). A graph of $C_R(u)$ is shown in Fig. 9.1 (solid line). Because for positive p one has $(x + x_p)/\tilde{\gamma}_p \gg 1$ we obtain

$$\text{Re}\tilde{I}(x + i0, p) = I_1 - x^2 I_2 + \pi p_c h_1 \text{sgn} f_0'' C_R\left(-\text{sgn} f_0'' \frac{x - x_p}{\tilde{\gamma}_p}\right), \tag{9.23}$$

with

$$I_1 = -\int_0^\infty dp\, p\frac{(x_p - 1)^2}{2x_p^3}(3x_p^2 + 2x_p + 1) + 2\pi p_c h_1 \text{sgn} f_0'', \tag{9.24}$$

$$I_2 = \int_0^\infty dp\, p\frac{(x_p - 1)^2}{x_p}, \tag{9.25}$$

Note that $C_R(u)$ and $C_I(u)$ can be written as

$$C_R(u) = \text{Re}C(u + i0), \tag{9.26}$$
$$C_I(u) = \text{Im}C(u + i0), \tag{9.27}$$

where the complex function $C(z)$ is

$$C(z) = \frac{z}{i\sqrt{1 - z}} \ln\left(\frac{\sqrt{1 - z} + 1}{\sqrt{1 - z} - 1}\right). \tag{9.28}$$

The real part of our dimensionless inverse polarization can be written as

$$\text{Re}\tilde{\Pi}_*^{-1}(x + i0, p) = Z_1 - Z_2 x^2 + \pi p_c h_1 \text{sgn} f_0'' C_R\left(-\text{sgn} f_0'' \frac{x - x_p}{\tilde{\gamma}_p}\right), \tag{9.29}$$

where

$$Z_1 = 1 + I_1 + I_H, \tag{9.30}$$
$$Z_2 = 1 + I_2 - I_H. \tag{9.31}$$

By assumption, the bare interaction f_q is negligibly small for momentum-transfers exceeding $q_0 \ll k_F$, so that the integrals I_1, I_2 and I_H are proportional to $p_0^2 = [q_0/(2k_F)]^2 \ll 1$ and hence $Z_i = 1 + \mathcal{O}(p_0^2)$. Keeping in mind the self-consistent definition (7.8) of x_0, we finally obtain for positive x and p,

$$g_p + \text{Re}\tilde{\Pi}_*^{-1}(x + i0, p) = Z_2\left[x_p^2 - x^2 + R(x, p)\right], \tag{9.32}$$

where

$$R(x, p) = \frac{\pi p_c h_1}{Z_2} \text{sgn} f_0'' C_R\left(-\text{sgn} f_0'' \frac{x - x_p}{\tilde{\gamma}_p}\right). \tag{9.33}$$

9.3 Spectral line shape of $S(\omega, q)$

To discuss the line shape of the dynamic structure factor, it is convenient to introduce also the imaginary part of the effective self-energy via

$$\text{Im}\tilde{\Pi}_*^{-1}(x + i0, p) = -Z_2 \Gamma(x, p), \tag{9.34}$$

or explicitly,

$$\Gamma(x, p) = \frac{\pi^2 p_c}{Z_2} \left[\Theta(x - x_p) \tilde{g}_p^2 \tilde{\gamma}_p \frac{x^2 - x_p^2}{6x_0^4} + h_1 C_I \left(-\text{sgn} f_0'' \frac{x - x_p}{\tilde{\gamma}_p} \right) \right]. \tag{9.35}$$

The dynamic structure factor can then we written as

$$S(\omega, q) = \frac{\nu_0}{\pi Z_2} \frac{\Gamma(x, p)}{[x^2 - x_p^2 - R(x, p)]^2 + \Gamma^2(x, p)}. \tag{9.36}$$

The resulting line shape for $f_0'' \ll 1$ and $p \gg p_c$ is shown in Fig. 9.2. In this case, $S(\omega, q)$ exhibits a threshold singularity at $x = x_p$, corresponding to the threshold frequency at the lower edge

$$\omega_q^- \equiv v_F q x_p \approx vq + \frac{\text{sgn} f_0''}{2\pi x_0} \frac{q^3}{2mq_c} = vq - \frac{1}{2\pi x_0} \frac{q^3}{2mq_c}. \tag{9.37}$$

Moreover, most of the spectral weight is smeared out over the interval $0 < x - x_p < \tilde{\gamma}_p$, or equivalently $\omega_q^- < \omega < \omega_q^- + \gamma_q$, where the energy scale γ_q is defined by

$$\gamma_q = v_F q \tilde{\gamma}_p = \frac{3}{8\pi x_0} \frac{q^3}{2mq_c} \approx \frac{3}{4} |\omega_q^- - vq|. \tag{9.38}$$

The energy γ_q can be identified with the width of the ZS resonance on the frequency axis. The crucial point is now that for $q \gg q_c$ Eq. (9.38) is much larger than the estimated broadening $w_q \propto q^2/m$ of the ZS resonance due to the terms which we have neglected by making the approximation A discussed in Sec. 7.2 (which amounts to ignoring in bosonic loop integrations nonlinear terms in the energy dispersion). Our approximation A is therefore only justified in the regime where the broadening γ_q due to the q-dependence of the interaction f_q is large compared with the broadening w_q due to the nonlinear energy dispersion in bosonic loop integrations. We thus conclude that the calculations in this chapter are only valid as long as $\gamma_q \gtrsim w_q$. A comparison of γ_q and w_q is shown in Fig. 9.3. Obviously, the condition $w_q = \gamma_q$ defines a characteristic crossover scale q_* where the q-dependence of the width of the ZS resonance changes from q^2 to q^3. Using Eqs. (8.22) and (9.38) we obtain the following estimate for the crossover momentum scale,

$$q_* = \frac{8\pi Z_w x_0}{3\sqrt{3}} q_c, \tag{9.39}$$

which has the same order of magnitude as $q_c = 1/(m|f_0''|)$. We conclude that the results for $S(\omega, q)$ presented in this chapter are only valid for $q \gtrsim q_*$, and hence
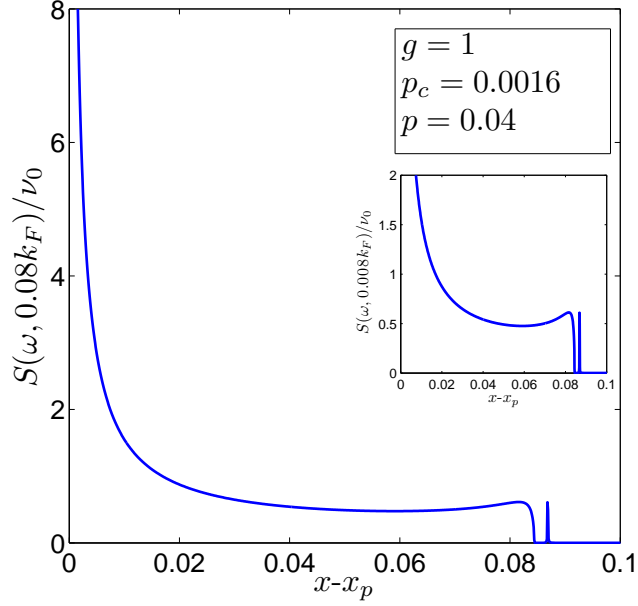
Figure 9.2: Graph of the dynamic structure factor $S(\omega, q)$ given in Eq. (9.36) as a function of $x - x_p$ for $f_0'' \ll 1$, $p = 0.04 = 25 p_c$ and $g = 1$. For simplicity we have set $Z_2 \approx 1$, which is accurate for $p_0 \ll 1$. For $p \gg p_c$ most of the spectral weight is carried by the main shoulder whose lower edge $x \to x_p$ is bounded by a threshold singularity. The width of the main shoulder on the x axis scales as $\tilde{\gamma}_p \propto p^2/p_c$. Recall that $x = \omega/(v_F q)$, so that the corresponding width on the frequency axis scales as $\gamma_q = v_F q \tilde{\gamma}_p \propto q^3/(m q_c)$. For $p \gg p_c$ the small "satellite peak" emerging above the upper edge of the main shoulder carries negligible spectral weight and is probably an artifact of our approximations.

do not describe the asymptotic $q \to 0$ regime. But the scale q_* can be quite small for some interactions. For example, if the interaction f_q can be approximated by a Lorentzian (2.36) with screening wave-vector $q_0 \ll k_F$, then $q_c = q_0^2/(2m f_0)$ is quadratic in q_0. For long-range interactions the regime $q_* \lesssim q \ll q_0$ where our calculation is valid can therefore be quite large and physically more relevant than the asymptotic long-wavelength regime $q \ll q_*$.

The small "satellite peak" slightly above the main shoulder in Fig. 9.2 is probably an artifact of our approximations, in particular of approximation A discussed in Sec. 7.2. It is easy to show that the satellite peak is located at a distance $\delta x \propto p_c^3/p^2 \ll \tilde{\gamma}_p$ above the upper edge $x_p + \tilde{\gamma}_p$ of the main shoulder and its width is proportional to $p^2 \tilde{\gamma}_p \propto p^4/p_c \ll \delta x \ll \tilde{\gamma}_p$. Note that in the regime $q \gg q_c$ where our calculation is valid the threshold singularity is located at $\omega_q^- \approx vq - 4\gamma_q/3$ (up to corrections of the order $q^2/m \ll \gamma_q$), while the energy scale of the satellite peak is $vq + O(q^2/m)$. However, as discussed after Eq. (9.19), in the regime $|(x - x_p)/\tilde{\gamma}_p - 1| \ll 1$ our approximation A is not reliable, so that the detailed line shape in the vicinity of the satellite peak is probably incorrect. Fortunately, for $p \gg p_c$ the
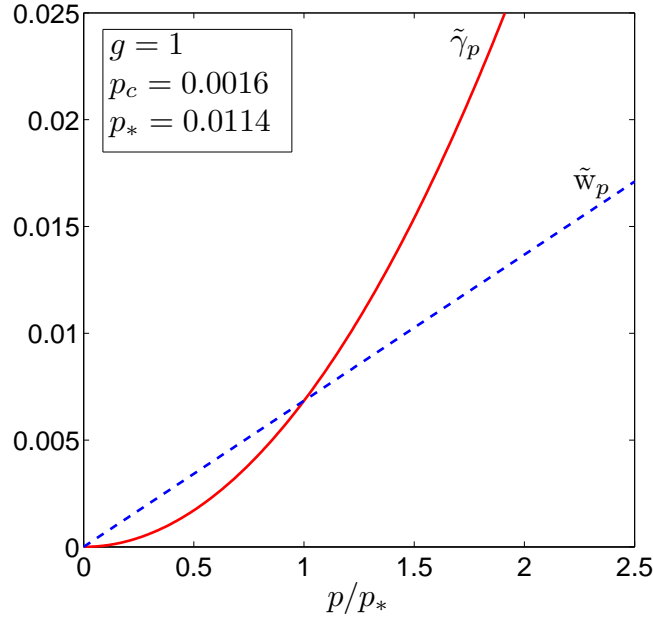
Figure 9.3: Solid line: dimensionless ZS damping $\tilde{\gamma}_p = \gamma_q/(v_F q)$ defined in Eq. (9.38) as a function of p/p_*. Dashed line: estimate of the width $\tilde{w}_p = w_q/(v_F q) = (Z_w/\sqrt{3})p$ of the ZS resonance given in Eq. (8.22).

satellite peak carries negligible weight, so that our calculation reproduces the main features of the spectral line shape. We speculate that a more accurate evaluation of our self-consistency equation for $\Pi_*(\omega, q)$ derived in Sec. 7.1, which does not rely on approximation A in Sec. 7.2, will generate additional weight in the dip between the upper edge of the main shoulder and the satellite peak, resulting in a single local maximum at the upper edge of the main shoulder. The spectral line shape looks then qualitatively similar to the line shape proposed in Refs. [3, 4].

Let us next consider the tails of the spectral function. For $x \gg x_p$ we obtain from Eqs. (9.35) and (9.36),

$$S(\omega, q) \sim \frac{\nu_0}{\pi Z_2} \frac{\Gamma(x, p)}{x^4}, \tag{9.40}$$

$$\Gamma(x, p) \sim \frac{\pi^2 p_c}{6 Z_2 x_0^4} \tilde{g}_p^2 \tilde{\gamma}_p x^2. \tag{9.41}$$

Inserting our result (9.17) for $\tilde{\gamma}_p$ we obtain

$$S(\omega, q) \sim \frac{\nu_0 \tilde{g}_p^2}{16 Z_2^2 x_0^5} \left[\frac{q^2}{2m\omega} \right]^2, \tag{9.42}$$

in agreement with Refs. [4, 6, 35, 38]. Note that the tail of $S(\omega, q)$ is determined by the first term on the right-hand side of the damping function $\Gamma(x, p)$ given in

Eq. (9.35), whereas the regime close to the ZS resonance is determined by the second term involving the complex function $C(z)$. This is the reason why the spectral line shape close to the ZS resonance cannot be simply obtained via extrapolation from the tails assuming a Lorentzian line shape.

Finally, Eqs.(9.33, 9.36) state that for $f_0'' > 0$ the threshold singularity appears at the upper edge $x = x_p$, so that the resulting spectral line shape does not resemble the line shape obtained in Refs [3,4]. On the other hand, an interaction with $f_0'' > 0$ seems to be unphysical and does not describe a stable Luttinger liquid.

9.4   Transformation of logarithmic singularity into an algebraic one

Let us consider the line shape in the vicinity of the threshold singularity $x \to x_p$. Assuming that that $f_0'' \ll 0$, for $0 < (x - x_p)/\tilde{\gamma}_p \ll 1$ we may approximate

$$\Gamma(x,p) \approx \frac{\pi^2 p_c h_1}{Z_2} \frac{x - x_p}{\tilde{\gamma}_p} = 2\pi x_0 \eta_p (x - x_p) \,, \tag{9.43}$$

$$R(x,p) \approx \frac{\pi p_c h_1}{Z_2} \frac{x - x_p}{\tilde{\gamma}_p} \ln\left[\frac{4\tilde{\gamma}_p}{x - x_p}\right] = -2 x_0 \eta_p (x - x_p) \ln\left[\frac{4\tilde{\gamma}_p}{x - x_p}\right] \,, \tag{9.44}$$

where we have defined

$$\eta_p = -\frac{\pi p_c h_1}{2 Z_2 x_0 \tilde{\gamma}_p} = \frac{4\pi^2 h_1}{3 Z_2} \frac{p_c^2}{p^2} = \frac{3 p_*^2}{4 p^2} \,. \tag{9.45}$$

In the last line we have approximated $Z_2 \approx 1$. From the above discussion it is clear that this expression can only be trusted for $p \gtrsim p_*$. A graph of η_p as a function of p/p_* is shown in Fig. 9.4. In the regime $\eta_p \ln[4\tilde{\gamma}_p/(x - x_p)] \gg 1$, which is equivalent with

$$0 < x - x_p \ll 4\tilde{\gamma}_p \exp\left[-1/\eta_p\right] \,, \tag{9.46}$$

the dynamic structure factor can thus be approximated by

$$S(\omega, q) \sim \frac{\nu_0}{2 x_0 Z_2 \eta_p} \frac{1}{(x - x_p) \ln^2\left[\frac{4\tilde{\gamma}_p}{x - x_p}\right]} \,. \tag{9.47}$$

According to Pustilnik *et al.* [3], the logarithmic singularity can be resummed to all orders, so that it is transformed into an algebraic one. Assuming that this is indeed correct, we can replace

$$x^2 - x_p^2 - R(x,p) \approx 2 x_0 (x - x_p) \left\{ 1 + \eta_p \ln\left[\frac{4\tilde{\gamma}_p}{x - x_p}\right] \right\} \to 2 x_0 (x - x_p) \left[\frac{4\tilde{\gamma}_p}{x - x_p}\right]^{\eta_p} \,. \tag{9.48}$$

For $x \to x_p$ the dynamic structure factor then diverges as

$$S(\omega, q) \sim \frac{\nu_0}{2 x_0 Z_2} \frac{\eta_p}{(4\tilde{\gamma}_p)^{2\eta_p}} \frac{1}{[x - x_p]^{\mu_p}} \,, \tag{9.49}$$
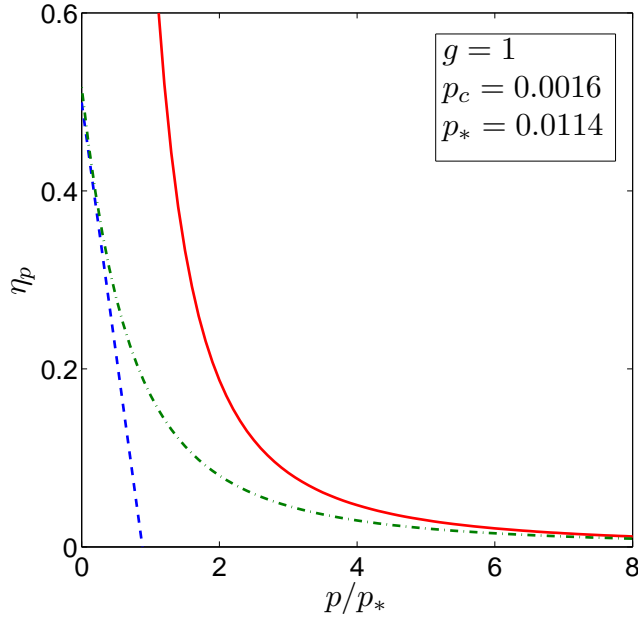
Figure 9.4: Solid line: graph of η_p defined in Eq. (9.45) as a function of p/p_* for $f_0'' < 0$. The dashed line is the weak coupling result $\eta_p \approx 1/2 - p/(4\pi p_c)$ obtained by Pustilnik *et al.* in Ref. [3]. The dashed dotted curve is a simple parabolic interpolation.

with the threshold exponent

$$\mu_p = 1 - 2\eta_p = 1 + \text{sign} f_0'' \frac{3p_*^2}{2p^2} \,. \tag{9.50}$$

Note that for $f_0'' < 0$ and $p \ll 1$ the weak coupling estimate for μ_p given by Pustilnik *et al.* [3] is in our notation

$$\mu_p \approx \frac{p}{2\pi p_c} \,, \tag{9.51}$$

implying

$$\eta_p = \frac{1}{2}[1 - \mu_p] = \frac{1}{2}\left[1 - \frac{p}{2\pi p_c}\right] \,. \tag{9.52}$$

As shown in Fig. 9.4, this is consistent with a smooth crossover to our result (9.45) at $p/p_* = O(1)$. Qualitatively, we expect that the behavior of η_p in the crossover regime resembles the dashed-dotted interpolation curve in Fig. 9.4. Note that $\eta_p \leq 1/2$ for all p, so that $\mu_p \geq 0$. For some integrable models where η_p has recently been calculated exactly [32, 33] the momentum dependence of η_p looks different from our result for the FSM. For example, in the Calogero-Sutherland model η_p is independent of p, see Ref. [32]. However, the Fourier transform f_q of the interaction in the Calogero-Sutherland model vanishes for $q = 0$, while in the integrable XXZ-chain considered in Refs. [4, 33, 35, 36] the effective interaction of the equivalent

one-dimensional fermion system involves also momentum-transfers of the order of k_F. Moreover, in the XXZ-chain there exists no crossover scale q_c satisfying $q_c = (m|f_0''|)^{-1} \ll k_F$, so that the intermediate regime $q_c \ll q \ll k_F$ where $\gamma_q \propto q^3/q_c$ simply does not exist. The existence of such an intermediate regime seems to be a special feature of the FSM considered here, where f_q involves only small momentum-transfers and has a finite limit for $q = 0$.

Within our perturbative approach we cannot justify the resummation procedure (9.48). Possibly a careful analysis of the functional renormalization group flow equation for the irreducible polarization discussed in Sec. 4.4 will shed some light onto this difficult problem. This seems to require extensive numerics, which is beyond the scope of this thesis.

Chapter 10

Summary of part I

In the first part of this thesis we have used a functional bosonization approach to calculate the dynamic structure factor $S(\omega, q)$ of a generalized Tomonaga-Luttinger model (which we have called *forward scattering model*), consisting of spinless fermions in one dimension with quadratic energy dispersion and an effective density-density interaction involving only momentum-transfers which are small compared to k_F.

In our construction we have used a Hubbard-Stratonovich transformation within the path integral formalism to build up a bosonized theory. The resulting bosonized action $S_{\text{eff}}[\Delta\phi]$ includes then interaction in the form of symmetrized fermion loops and reduces to its Gaussian part (or noninteracting part) for a linearized energy dispersion.

In Chap. 5, we have used our bosonic perturbative approach from Chap. 3 and have derived a self-consistency equation for the irreducible polarization $\Pi_*(\omega, q)$ which does not suffer from the mass-shell singularities encountered in other pertur-bative expansions. For the explicit evaluation of $S(\omega, q)$ we had to make some drastic approximations. In particular, in bosonic loop integrations we have neglected curvature corrections to the free polarization, see approximation A discussed in Sec. 7.2. In Chap. 8, it has been shown that because of the sharp-momentum transfer cutoff, our approximation exhibit a new mass-shell singularity at the renormalized energy vq. Nevertheless in Chap. 9 we have found a regime of wave-vectors $q_c \ll q \ll k_F$ where an explicit analytic calculation of the spectral line shape is possible. The crossover scale $q_c = 1/(m|f_0''|)$ is determined by the second derivative f_0'' of the Fourier transform of the interaction at $q = 0$. For interactions whose Fourier trans-form can be approximated by a Lorentzian with screening wave-vector $q_0 \ll k_F$, the crossover scale q_c is proportional to q_0^2, so that the regime $q_c \ll q \ll k_F$ is quite large and can be experimentally more relevant than the asymptotic long-wavelength regime $q \ll q_c$.

We have shown that for $q_c \ll q \ll k_F$ the width of the ZS resonance on the frequency axis scales as $\gamma_q \propto q^3/(mq_c)$. Our result is consistent with a smooth crossover at $q \approx q_c$ to the asymptotic long-wavelength result $\gamma_q \propto q^2/m$ obtained by other authors [3–5]. The spectral line shape is non-Lorentzian, with a main hump whose low-energy side for $f_0'' < 0$ is bounded by a threshold singularity at $\omega = \omega_q^- \approx vq - 4\gamma_q/3$, a small local maximum around $\omega \approx vq - \gamma_q/3$, and a high-frequency tail

which scales as q^4/ω^2. Considering $f_0'' < 0$, for $\omega \to \omega_q^- + 0$ the threshold singularity is within our approximation logarithmic, $S(\omega, q) \propto [(\omega - \omega_q^-) \ln^2 (\omega - \omega_q^-)]^{-1}$. Assuming that higher orders in perturbation theory exponentiate the logarithm, we obtain an algebraic threshold singularity with exponent $\mu_q = 1 - 2\eta_q$ and $\eta_q \propto q_c^2/q^2$ for $q \gg q_c$. This features agree also with the results of Pustilnik *et al.* [3] and Pereira *et al.* [4] who have shown independently that the dynamic structure factor exhibits a threshold singularity at the lower edge, $\omega = \omega_q^-$.

It is by now established that, at least in integrable models, $S(\omega, q)$ indeed exhibits algebraic threshold singularities [4,32,33,35,36]. However, for generic nonintegrable models there is no proof that the logarithmic singularities generated in higher orders of perturbation theory indeed conspire to transform the logarithm encountered at the first order into an algebraic singularity, as suggested by Pustilnik *et al.* [3]. This would require a thorough analysis of the higher-order terms in perturbative expansion, which so far has not been performed.

On the other hand, for the explicit evaluation of the self-consistency equation for the irreducible polarization $\Pi_*(\omega, q)$ derived in Sec. 7.1 we had to rely in this work on approximation A discussed in Sec. 7.2. We have argued that this approximation is not sufficient to calculate the dynamic structure factor for $q \lesssim q_c$, because it neglects the dominant damping mechanism in this regime. Moreover, for sharp momentum-transfer cutoff our approximation A breaks down for frequencies in the vicinity of the mass-shell singularity. It would be interesting to evaluate the self-consistency equation for the irreducible polarization $\Pi_*(\omega, q)$ derived in Sec. 7.1 without relying on approximation A. We believe that in this case our functional bosonization result for $S(\omega, q)$ does not exhibit any mass-shell singularities even for sharp cutoff.

In Chap. 4 we have presented a functional renormalization group equation [see Eq. (4.76)] for the irreducible polarization which goes beyond the self-consistent perturbation theory based on functional bosonization used here. A thorough analysis of Eq. (4.76) using numerical methods still remains to be done. Possibly, this equation will be a good starting point for addressing some of the open problems mentioned above.

Part II

Application of FRG to the Anderson impurity model

Chapter 11

Introduction

The Anderson impurity model (AIM), which was proposed by Anderson, to describe the magnetic impurities in metals is one of the basic models in the condensed matter theory [72–74]. The model Hamiltonian is characterized by free conduction electrons, which are coupled to a single interacting impurity,

$$
\begin{aligned}
\hat{H} &= \sum_{\mathbf{k}\sigma}(\epsilon_{\mathbf{k}} - \sigma h)\hat{c}_{\mathbf{k}\sigma}^{\dagger}\hat{c}_{\mathbf{k}\sigma} + \sum_{\sigma}(E_d - \sigma h)\hat{d}_{\sigma}^{\dagger}\hat{d}_{\sigma} \\
&+ U\hat{d}_{\uparrow}^{\dagger}\hat{d}_{\uparrow}\hat{d}_{\downarrow}^{\dagger}\hat{d}_{\downarrow} + \sum_{\mathbf{k}\sigma}(V_{\mathbf{k}}^{*}\hat{d}_{\sigma}^{\dagger}\hat{c}_{\mathbf{k}\sigma} + V_{\mathbf{k}}\hat{c}_{\mathbf{k}\sigma}^{\dagger}\hat{d}_{\sigma})\,.
\end{aligned}
\tag{11.1}
$$

Here $\hat{c}_{\mathbf{k}\sigma}$ and $\hat{c}_{\mathbf{k}\sigma}^{\dagger}$ denote the annihilation and the creation operators of a conduction electron with momentum $\mathbf{k}$, spin σ and energy dispersion $\epsilon_{\mathbf{k}}$ respectively. $\hat{d}_{\sigma}$ and $d_{\sigma}^{\dagger}$ annihilate and create an impurity electron in the d-orbital with spin σ and atomic energy E_d. The scattering potential $V_{\mathbf{k}}$ is the hybridization between the conduction electrons and the impurity while U is the screened Coulomb potential between two impurity electrons with different spins. Finally h represents the Zeemann energy arising from the magnetic field.

The thermodynamical and spectral properties of the AIM can be obtained with the help of the Wilson's numerical renormalization group (NRG) [74–78]. Despite this progress and the confirmation of NRG results via Bethe Ansatz [79, 80], there is no analytical method, describing the spectral properties of the AIM. In addition the investigation of the spectral function $A(\omega)$ of d-electrons for all frequencies in context of the NRG needs some computational effort while the calculation of $A(\omega)$ for arbitrary frequencies ω is desirable by means of the dynamical mean field theory describing strong correlation in a realistic three-dimensional fermion system.

11.1   Elementary theory of the AIM

Firstly we formulate the AIM in the language of functional integrals. The action S is a function of the fermionic Grassmann fields $\{c_{\mathbf{k}\sigma}, \bar{c}_{\mathbf{k}\sigma}\}$ describing the conduction electrons and $\{d_{\sigma}, \bar{d}_{\sigma}\}$ describing the impurities. Carrying out the integrations over the fields associated with the conduction electrons, the ratio of the interacting and

noninteracting partition function can be determined,

$$\frac{\mathcal{Z}}{\mathcal{Z}_0} = \frac{\int \mathcal{D}[\bar{d}, d] \, e^{-S_0[\bar{d},d] - S_U[\bar{d},d]}}{\int \mathcal{D}[\bar{d}, d] \, e^{-S_0[\bar{d},d]}} \, , \tag{11.2}$$

where the Gaussian part of the action is

$$S_0[\bar{d}, d] = -\int_\omega \sum_\sigma [i\omega - \xi_0^\sigma - \Delta^\sigma(i\omega)]\bar{d}_{\omega\sigma} d_{\omega\sigma} \, , \tag{11.3}$$

with

$$\xi_0^\sigma = E_d - \mu - \sigma h \, , \tag{11.4}$$

$$\Delta^\sigma(i\omega) = \sum_{\mathbf{k}} \frac{|V_{\mathbf{k}}|^2}{i\omega - \epsilon_{\mathbf{k}} + \mu + \sigma h} \, . \tag{11.5}$$

Δ^σ is called the hybridization function. In Eq. (11.3) $\int_\omega = \frac{1}{\beta} \sum_{i\omega}$ represents the summation over the fermionic Matsubara frequencies where β is the inverse of the temperature T. Note that we work in the grand canonical ensemble where β and the chemical potential μ are constant. Furthermore, μ can be controlled by the filling of the conduction band. The non-Gaussian part of the action is given by

$$S_U[\bar{d}, d] = U \int_{\omega_1} \int_{\omega_2} \int_{\omega_3} \int_{\omega_4} \beta \delta_{\omega_1 + \omega_3, \omega_2 + \omega_4} \, \bar{d}_{\omega_1 \uparrow} d_{\omega_2 \uparrow} \bar{d}_{\omega_3 \downarrow} d_{\omega_4 \downarrow} \, . \tag{11.6}$$

The Kronecker delta $\beta \delta_{\omega_1 + \omega_3, \omega_2 + \omega_4}$ ensures the energy conservation during the interaction. At zero temperature ($\beta \to \infty$), we use the replacement

$$\int_\omega = \frac{1}{\beta} \sum_{i\omega} \longrightarrow \int \frac{d\omega}{2\pi} \, , \tag{11.7}$$

$$\beta \delta_{\omega_1 + \omega_3, \omega_2 + \omega_4} \longrightarrow 2\pi \delta(\omega_1 + \omega_3 - \omega_2 - \omega_4) \, . \tag{11.8}$$

Considering the AIM without magnetic field, the total energy of the system is E_d if the d-level is single occupied. On the other hand, the total energy of the system for the double occupied d-states is given by $2E_d + U$. Therefore, in the case of the vanishing magnetic field we distinguish between three different regimes characterized by the relative positions of μ, E_d and $E_d + U$ (see Ref. [81]):

- *Local moment regime*: $E_d \ll \mu \ll E_d + U$.
  The d-level is located below the Fermi energy and therefore is occupied by an impurity electron. On the other hand, the double occupancy is forbidden because of the strong interactions. The d level retains thus the single occupancy. In this regime spin fluctuations play an important role.

- *Mixed valence regime*: $E_d \approx \mu \ll E_d + U$ or $E_d \ll \mu \approx E_d + U$.
  In the first case d-level can be empty or occupied by a single electron while in the second case the d-level fluctuates between the single and the double occupancy. In both cases charge fluctuations as well as spin fluctuations become important.
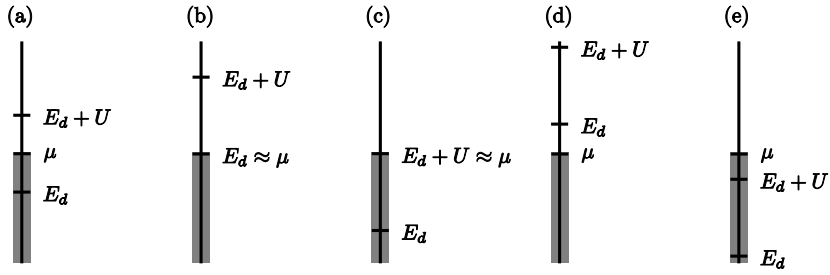
Figure 11.1: Different occupancy regimes which are described by the relative positions of μ, E_d and E_d+U. The shaded region corresponds to the number of occupied states. Graph (a) represents the local moment regime while graphs (b) and (c) correspond to the mixed valence regime. Graphs (d) and (e) represent empty orbital and double occupancy regime, respectively.

- *Empty orbital and double occupancy regime*:
  In the empty orbital regime $\mu \ll E_d \leq E_d + U$ the interaction between impurity electrons is weak so that the d-level remains empty and in the double occupancy regime $E_d \leq E_d + U \ll \mu$ the d-level becomes double occupied. Note that in both regimes neither charge nor spin fluctuations are important.

A graphical representation of these regimes is shown in Fig. 11.1. In this thesis we are interested in the local moment regime, where the occupancy of only one impurity state is allowed. In the local moment regime and at low energies the AIM is equivalent to *the Kondo model*, which contains only the spin degrees of freedom of the impurity.

In the context of the AIM and the Kondo model, one can study the effect of magnetic impurities on the resistivity of metals. In the early 1930s it was known that the magnetic impurities in metals cause a resistance decreasing by decreasing temperature at high temperatures. However, this resistance reaches a local minimum at a certain temperature and increases for $T \to 0$ [82]. Kondo showed perturbatively that there is one logarithmic part $\ln(T)$, which contributes to the resistivity and increases as $T \to 0$ [83]. Nevertheless, because of the divergence of the logarithmic function, the perturbation theory fails at low temperatures. Soon experimental works discovered the deviation from the perturbation theory in this regime and this issue became known as *the Kondo Problem*. Indeed, there is one temperature, called *the Kondo temperature* T_K, which describes the limit of the validity of the Kondos result. This means that the perturbation theory applied by Kondo is correct only at $T \gg T_K$.

11.2   Self-consistent Hartree-Fock approximation

In this section we estimate the magnetization within the mean field theory. We determine for the renormalized quasi particle energy,

$$\xi^\sigma = \xi_0^\sigma + \delta\xi^\sigma, \tag{11.9}$$

$$\delta\xi^\sigma = U \int_\omega G_0^{\bar\sigma}(i\omega) = U N_{\bar\sigma} = \frac{U}{2}[N - \sigma\mu_{\mathrm{HF}}], \tag{11.10}$$

where N_σ is the average of the occupation number of the impurity fermions with the spin σ and $N = N_\uparrow + N_\downarrow$ is the total average of the occupation number. Furthermore, $\mu_{\mathrm{HF}} = N_\uparrow - N_\downarrow$ represents the corresponding magnetization in the self-consistent Hartree-Fock approximation. The self-consistent Hartree-Fock Green function is given by

$$G_0^\sigma(i\omega) = \frac{1}{i\omega - \xi^\sigma - \Delta^\sigma(i\omega) + \sigma h}. \tag{11.11}$$

Here we focus on the wide band limit, where we may approximate

$$\Delta^\sigma(i\omega) = -i\Delta^\sigma \mathrm{sgn}(\omega). \tag{11.12}$$

According to Eq. (11.5), the hybridization function $\Delta^\sigma = \Delta$ becomes independent of the spin projection if the magnetic field vanishes. For more simplicity we also assume that this independence remains valid for $h \neq 0$. The Hartree-Fock Green function for the impurity electrons can therefore be written as

$$G_0^\sigma(i\omega) = \frac{1}{i\omega - \xi^\sigma + i\Delta\,\mathrm{sgn}(\omega) + \sigma h}, \tag{11.13}$$

and the ratio of the total partition function to the Hartree-Fock partition function will be given by

$$\frac{\mathcal{Z}}{\mathcal{Z}_{\mathrm{HF}}} = \frac{\int \mathcal{D}[\bar{d}, d]\, e^{-S_0[\bar{d},d] - S_U[\bar{d},d]}}{\int \mathcal{D}[\bar{d}, d]\, e^{-S_{\mathrm{HF}}[\bar{d},d]}}, \tag{11.14}$$

with

$$S_{\mathrm{HF}}[\bar{d}, d] = -\int_\omega \sum_\sigma \left[G_0^\sigma(i\omega)\right]^{-1} \bar{d}_{\omega\sigma} d_{\omega\sigma}. \tag{11.15}$$

11.3   Fermi liquid behavior

We take the limit $h \to 0$ and anticipate that there is no spontaneous magnetization. In the *particle-hole symmetric case*, where $E_d - \mu = U/2$ and $N = 1$, the Hartree-Fock Green function for vanishing magnetic field simplifies to

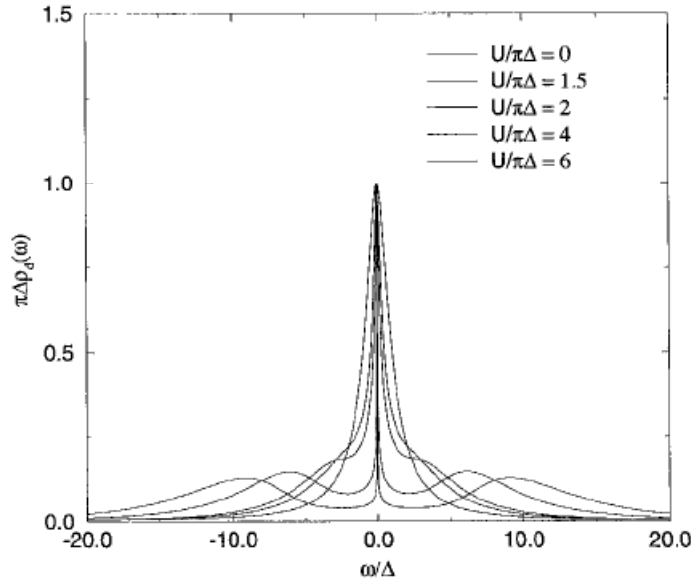$$G_0^\sigma(i\omega) = \frac{1}{i\omega + i\Delta\mathrm{sgn}(\omega)}. \tag{11.16}$$

Figure 11.2: Exact NRG results for the spectral function of d-electrons in the particle hole symmetric AIM at zero magnetic field. This graph is extracted from Ref. [85] and shows that if the interaction U increases, the weight of Kondo peak, appearing at $\omega = 0$ becomes exponentially smaller.

Note that the analytical continuation $(i\omega \rightarrow \omega + i0)$ maps $\mathrm{sgn}\omega$ to -1. The Hartree-Fock spectral function thus exhibits a quasi particle peak with the width Δ. Nozières [84] has obtained as the first one low energy features in the context of the Fermi liquid theory. Figure 11.2, extracted from a work done by Hewson [85], displays the variation of the exact spectral function by changing of the interaction U. Note that these results are based on the NRG. For $U \neq 0$ the spectral line shape involves a sharp resonance which arises at $\omega = 0$ and is called *Kondo peak* as well as two shoulders (on both sides of the Kondo peak) which correspond to the Hubbard bands [86]. Yosida and Yamada [87, 88] have built up a perturbative approach for small $U/(\pi\Delta)$ and shown that in the atomic limit, i.e., $\Delta \rightarrow 0$ these schoulders carry the entire weight of the spectrum and their position is given by $\omega = \pm U/2$. However this perturbation theory is well defined only for $U/(\pi\Delta) < 2.5$. On the other hand, the exact result via the Bethe ansatz [79,80] shows that at strong coupling $(U \rightarrow \infty)$ the weight of the Kondo peak exhibits the same exponential behavior as the Kondo temperature T_K,

$$Z_{\mathrm{KP}} \approx \sqrt{\frac{8U}{\pi^2\Delta}}\, e^{-\frac{\pi U}{8\Delta}} \,, \tag{11.17}$$

where the Kondo temperature is described in Sec. 11.1.

As we have mentioned above, we intend to develop an analytical tool, to calculate the spectral line shape of $A(\omega)$. Recently there have been many attempts to handle this problem [89–101]. This part of the thesis extends the work done by Bartosch

et al. [101], using the exact functional renormalization group (FRG) approach to the AIM (see also Refs. [96, 100]). The general theory of the exact FRG is already known from Chap. 4. The only distinction between this part and Ref. [101] is that we try to improve the FRG approach using the magnetic field as the RG cutoff. Our aim is to gain a well defined FRG expansion even in the strong coupling limit.

The rest of this part is organized as follows. In Chap. 12, we show that we encounter an unphysical instability within the self-consistent Hartree-Fock approximation. We introduce thus *the spin-singlet particle-hole channel* decoupling the interaction (11.6) via a complex Hubbard-Stratonovich field which is associated with transverse spin-flip fluctuations. We handle also the spectral properties of the system within *ladder approximation* which we obtain at the level of the Gaussian approximation. Finally we give an introduction to the general formalism of the exact FRG to the AIM with mixed boson-fermion fields. In Chap. 13 we build up the FRG flow equations in bosonic and fermionic sector, introducing an additive cutoff only in the fermionic propagator, called *magnetic field cutoff*. We adopt a proper truncation whereby the flow equation will not remain exact and use Dyson-Schwinger equations to derive the *skeleton equation* in the bosonic sector. In Chap. 14 we choose the simplest case of additive cutoff, where the cutoff is already the magnetic field itself. We show that the FRG approach in the spin-singlet particle-hole channel removes the singularity which occurs due to the Hartree-Fock approximation. On the other hand, we find that the mean field magnetic moment is not a suitable initial condition for the self-energy. To overcome this problem, we have to dilute the effect of the magnetic field. We use therefore in Chap. 15 a modified magnetic field cutoff. Finally, we show that for sufficiently weak interaction $U/(\pi\Delta) \lesssim 2$ our solution for the quasi particle weight agrees with the exact results from NRG. But we are not able to reproduce the Kondo-scaling given by Eq. (11.17). In Chap. 16 we present a conclusion and an outline of this part.

Chapter 12

Spin-singlet particle-hole channel

In this chapter we proceed with some perturbative approaches to the AIM and prove how the Hartree-Fock approximation causes a singularity known as the Stoner instability. To this end, we describe shortly the transverse particle-hole channel that couples the fermionic fields to new bosonic fields. Thereby one carries out the Hubbard-Stratonovic transformation which is known from Chap. 3. In addition, we explain the ladder approximation (LA) associated with the given channel and show that because of the arising singularity, the functional renormalization group is required for further treatments. The first two sections of this chapter follow closely Ref. [101].

12.1 Partial bosonization in the spin-singlet particle-hole channel

We have used already the Hubbard-Stratonovich transformation in Chap. 3. We will apply here a similar procedure to bosonize the AIM. According to Eq. (11.13) the integration (11.10) is performable at zero temperature and one obtains for mean field magnetization in the case of the particle-hole symmetric AIM,

$$
G_0^\sigma(i\omega) = \frac{1}{i\omega + i\Delta\mathrm{sgn}\omega + \sigma\frac{U\mu_{\mathrm{HF}}}{2} + \sigma h} \, , \tag{12.1}
$$

$$
\mu_{\mathrm{HF}} = \int_\omega \sum_\sigma \sigma G_0^\sigma(i\omega) = \frac{2}{\pi} \arctan\left[\frac{\pi u_0}{2}\mu_{\mathrm{HF}} + \frac{h}{\Delta}\right] \, , \tag{12.2}
$$

where

$$
u_0 = \frac{U}{\pi\Delta} \, . \tag{12.3}
$$

However, it turns out that by taking the limit $h \to 0$, the above equation leads to a value $\mu_{\mathrm{HF}} \neq 0$ if $u_0 > 1$. This behavior is known as the Stoner instability and is an artifact of the Hartree-Fock approximation [74]. According to Refs. [93, 95], transverse spin fluctuations will help us to remove the Stoner instability in the strong

coupling limit. In the spin-singlet particle-hole channel, we decouple the fermionic d-fields via the bosonic Hubbard-Stratonovic fields $\chi_{\bar{\omega}}$ and $\bar{\chi}_{\bar{\omega}}$ as follows,

$$\frac{\mathcal{Z}}{\mathcal{Z}_{\text{HF}}} = \frac{\int \mathcal{D}[\Phi] e^{-S_0[\Phi] - S_1[\Phi]}}{\int \mathcal{D}[\Phi] e^{-S_0[\Phi]}}, \tag{12.4}$$

where the super-field $\Phi = [d_\uparrow, \bar{d}_\uparrow, d_\downarrow, \bar{d}_\downarrow, \chi, \bar{\chi}]$ contains four fermionic and two bosonic components. The Gaussian and interacting parts of the action in this construction are given by

$$S_0[\Phi] = -\int_\omega \sum_\sigma [G_0^\sigma(i\omega)]^{-1} \bar{d}_{\omega\sigma} d_{\omega\sigma} + \int_{\bar{\omega}} U^{-1} \bar{\chi}_{\bar{\omega}} \chi_{\bar{\omega}}, \tag{12.5}$$

$$S_1[\Phi] = \int_{\bar{\omega}} [\bar{s}_{\bar{\omega}} \chi_{\bar{\omega}} + s_{\bar{\omega}} \bar{\chi}_{\bar{\omega}}] - \int_\omega \sum_\sigma \delta\xi^\sigma \bar{d}_{\omega\sigma} d_{\omega\sigma}, \tag{12.6}$$

where

$$s_{\bar{\omega}} = \int_\omega \bar{d}_{\omega\downarrow} d_{\omega+\bar{\omega}\uparrow}, \qquad \bar{s}_{\bar{\omega}} = \int_\omega \bar{d}_{\omega+\bar{\omega}\uparrow} d_{\omega\downarrow}, \tag{12.7}$$

are density fields. In this notations, ω and $\bar{\omega}$ represent the fermionic and bosonic Matsubara frequencies respectively. Note that the second term in (12.6) subtracts the renormalization part from the Hartree-Fock Green function and this subtractions gives rise to the bare noninteracting Green function of d-fermions in (12.5). The first term in (12.6) describes the coupling between the fermionic and the bosonic field in the action and can be written as

$$\int_{\bar{\omega}} [\bar{s}_{\bar{\omega}} \chi_{\bar{\omega}} + s_{\bar{\omega}} \bar{\chi}_{\bar{\omega}}] = \int_{\bar{\omega}} \int_\omega \Big[\Gamma_0^{\bar{d}_\uparrow d_\downarrow \chi}(\omega + \bar{\omega}, \omega, \bar{\omega}) \bar{d}_{\omega+\bar{\omega}\uparrow} d_{\omega\downarrow} \chi_{\bar{\omega}}$$
$$+ \Gamma_0^{\bar{d}_\downarrow d_\uparrow \bar{\chi}}(\omega - \bar{\omega}, \omega, \bar{\omega}) \bar{d}_{\omega-\bar{\omega}\downarrow} d_{\omega\uparrow} \bar{\chi}_{\bar{\omega}} \Big], \tag{12.8}$$

where the three-legged spin-flip vertices are given by

$$\Gamma_0^{\bar{d}_\uparrow d_\downarrow \chi}(\omega + \bar{\omega}, \omega, \bar{\omega}) = \Gamma_0^{\bar{d}_\downarrow d_\uparrow \bar{\chi}}(\omega - \bar{\omega}, \omega, \bar{\omega}) = 1. \tag{12.9}$$

Figure 12.1 shows the graphical representation of these vertices. In FRG approach, the flow equations give rise to a modification of these parameters from their initial value of unity.

12.2 Ladder approximation

In this section we handle the bosonized theory on the level of the Gaussian approximation. Similar to the bosonization of the Luttinger liquid, the fermions in Eq. (12.4) can be integrated out, so that we get an effective action $S_{\text{eff}}[\bar{\chi}, \chi]$, which

Figure 12.1: Graphical representation of the coupling between the fermions and bosons in the Hubbard-Stratonovich action $S_1[\Phi]$ for a) $\Gamma_0^{\bar{d}_\uparrow d_\downarrow \chi}(\omega + \bar{\omega}, \omega, \bar{\omega})$ and b) $\Gamma_0^{\bar{d}_\downarrow d_\uparrow \bar{\chi}}(\omega - \bar{\omega}, \omega, \bar{\omega})$. The ingoing solid arrows denote $d_{\omega\sigma}$ and the outgoing ones denote $\bar{d}_{\omega\sigma}$. Similarly, the ingoing and outgoing wavy arrows represent $\chi_{\bar{\omega}}$ and $\bar{\chi}_{\bar{\omega}}$ respectively.

only depend on the spin-flip fields $\chi_{\bar{\omega}}$ and $\bar{\chi}_{\bar{\omega}}$. In the Gaussian approximation, the expansion of this effective action to the quadratic order of bosonic fields leads to

$$S_{\text{eff}}[\bar{\chi}, \chi] \approx \int_{\bar{\omega}} \left[U^{-1} - \Pi_0^\perp(i\bar{\omega}) \right] \bar{\chi}_{\bar{\omega}} \chi_{\bar{\omega}} , \tag{12.10}$$

where $\Pi_0^\perp(i\bar{\omega})$ is called the noninteracting dynamic spin-flip susceptibility and is given by

$$\Pi_0^\perp(i\bar{\omega}) = - \int_\omega G_0^\uparrow(i\omega) G_0^\downarrow(i\omega - i\bar{\omega}) . \tag{12.11}$$

Here $G_0^\sigma(i\omega)$ represents as before the Hartree-Fock Green function defined in (11.13). For $h = 0$ the integration above can be carried out in the particle-hole symmetric case and we obtain

$$\lim_{h \to 0} \Pi_0^\perp(i\bar{\omega}) = \frac{1}{\pi\Delta} f_0^\perp \left(\frac{|\bar{\omega}|}{\Delta} \right) , \tag{12.12}$$

where

$$f_0^\perp(x) = \frac{\ln[1 + x]}{x(1 + x/2)} , \tag{12.13}$$

and the subscript indicates the zero magnetic field $h = 0$. In ladder approximation (LA) we resum infinite terms in perturbation series [20],

$$\begin{aligned} \Pi_{\text{LA}}^\perp(i\bar{\omega}) &= \Pi_0^\perp(i\bar{\omega}) + \Pi_0^\perp(i\bar{\omega}) U \Pi_0^\perp(i\bar{\omega}) \\ &+ \Pi_0^\perp(i\bar{\omega}) U \Pi_0^\perp(i\bar{\omega}) U \Pi_0^\perp(i\bar{\omega}) + \cdots = \frac{\Pi_0^\perp(i\bar{\omega})}{1 - U \Pi_0^\perp(i\bar{\omega})} . \end{aligned} \tag{12.14}$$

The dynamic structure factor describing here transverse spin fluctuations is defined similar to Eq. (2.11),

$$S^\perp(\omega) = \text{Im} \, \Pi^\perp(i\bar{\omega} \to \omega + i0) . \tag{12.15}$$
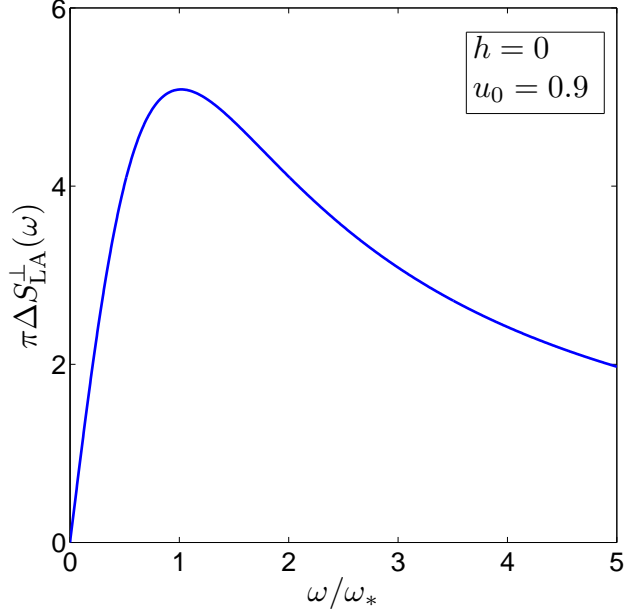
Figure 12.2: Graph of the spectral density of transverse spin fluctuations for the particle-hole symmetric AIM within ladder approximation. Here we set $h = 0$ and $u_0 = U/(\pi\Delta) = 0.9$ and the characteristic energy scale in this approximation is given by $\omega_* = \Delta(1 - u_0)$.

.

Keep in mind that the analytical continuation $\bar{\omega} \to \omega + i0$ maps the expression $|\bar{\omega}|$ to $-i\omega$. A graph of $S^\perp(\omega)$ within LA is shown in Fig. 12.2. For $\bar{\omega} \ll \Delta$ we use the expansion $f_0^\perp(x) = 1 - x + \mathcal{O}(x^2)$ and we get

$$\Pi_{\mathrm{LA}}^\perp \approx \frac{1}{\pi} \frac{1}{\omega_* + u_0|\bar{\omega}|}\,, \qquad \Leftrightarrow \qquad S_{\mathrm{LA}}^\perp(\omega) \approx \frac{1}{\pi} \frac{u_0\omega}{\omega_*^2 + u_0^2\omega^2}\,, \tag{12.16}$$

where $\omega_* = \Delta(1 - u_0)$ is the characteristic energy scale. Obviously for $u_0 \to 1$ this parameter vanishes, which is an artifact of the Stoner instability discussed in the previous section.

In order to understand the problem better, we consider the fermionic Green function within the ladder approximation. The leading diagrams contributing to the self-energy in this approach are shown in Fig. 12.3. The first diagram in this figure does not depend on frequency and has the value of $\delta\xi^\sigma$. We have

$$\Sigma^\sigma(i\omega) = \delta\xi^\sigma + U^2 \int_{\bar{\omega}} \Pi_{\mathrm{LA}}^\perp(i\bar{\omega}) G_0^{\bar{\sigma}}(i\omega - i\sigma\bar{\omega})\,. \tag{12.17}$$

We consider now the weight of the quasi particle residue which is defined by

$$Z = \frac{1}{1 - \left.\frac{\partial\Sigma^\sigma(i\omega)}{\partial(i\omega)}\right|_{\omega=0}}\,. \tag{12.18}$$
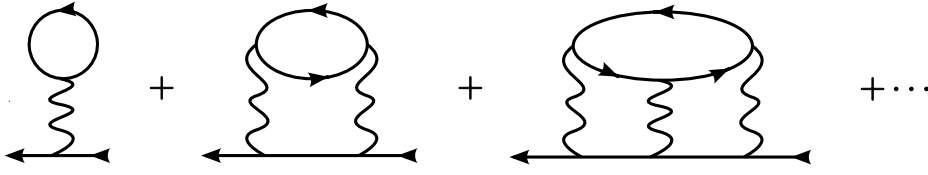
Figure 12.3: Diagrams occurred in the particle-hole ladder approximation of the fermionic self-energy. The solid lines with arrows denote the Hartree-Fock Green function and the wavy lines denote the coupling U.

.

Using $\mathrm{sgn}\,\bar{\omega} = 2\Theta(\bar{\omega}) - 1$, we get

$$
\begin{aligned}
\left.\frac{\partial \Sigma^{\sigma}(i\omega)}{\partial(i\omega)}\right|_{\omega=0} &= U^2 \lim_{\omega\to 0} \frac{\partial}{\partial(i\omega)} \int_{\bar{\omega}} \Pi_{\mathrm{LA}}^{\perp}(i\bar{\omega}) G_0^{\bar{\sigma}}(i\omega - i\sigma\bar{\omega}) \\
&= -\lim_{\xi\to 0} U^2 \int_{\bar{\omega}} \frac{\Pi_{\mathrm{LA}}^{\perp}(i\bar{\omega})[1 + 2\Delta\,\delta(\bar{\omega})]}{(i\bar{\omega} + i\Delta\,\mathrm{sgn}\bar{\omega} + \xi)^2} \\
&= -U^2 \int_{\bar{\omega}} \left[\frac{\Pi_{\mathrm{LA}}^{\perp}(i\bar{\omega})}{[i\bar{\omega} + i\Delta\,\mathrm{sgn}(\bar{\omega})^2]} - \lim_{\xi\to 0} \frac{2\Pi_{\mathrm{LA}}^{\perp}(i\omega)}{\Delta} \frac{\delta(\bar{\omega})}{[\mathrm{sgn}(\bar{\omega}) - i\frac{\xi}{\Delta}]^2} \right],
\end{aligned}
$$
(12.19)

where ξ is an additive convergence factor. Here, we have naively assumed that we can carry out the partial differentiation $\frac{\partial}{\partial(i\omega)}$ before the given frequency integration. The integration over the part with the delta function can be performed using the method which was proposed before by Morris [64] for any function $f(\Theta(x))$ of the step function multiplied with $\delta(x)$,

$$
\delta(x)\,f(\Theta(x)) = \delta(x) \int_0^1 dt\, f(t)\,.
$$
(12.20)

We find that

$$
\lim_{\xi\to 0} \frac{\delta(\bar{\omega})}{[\mathrm{sgn}(\bar{\omega}) - i\frac{\xi}{\Delta}]^2} = \lim_{\xi\to 0} \frac{\delta(\bar{\omega})}{[2\Theta(\bar{\omega}) - 1 - i\frac{\xi}{\Delta}]^2} = -\delta(\bar{\omega})\,,
$$
(12.21)

and consequently we obtain

$$
\begin{aligned}
\left.\frac{\partial \Sigma^{\sigma}(i\omega)}{\partial(i\omega)}\right|_{\omega=0} &= \frac{U^2}{2\pi} \left[\int_{-\infty}^{\infty} d\bar{\omega}\, \frac{\Pi_{\mathrm{LA}}^{\perp}(i\bar{\omega})}{[|\bar{\omega}| + \Delta]^2} - \frac{2\Pi_{\mathrm{LA}}^{\perp}(0)}{\Delta} \right] \\
&= u_0^2 \left[\int_0^{\infty} dx\, \frac{f_0^{\perp}(x)}{[1 - u_0 f_0^{\perp}(x)](1 + x)^2} - \frac{f_0^{\perp}(0)}{1 - u_0 f_0^{\perp}(0)} \right].
\end{aligned}
$$
(12.22)

The remaining integration can be carried out numerically. The result is shown in Fig. 12.4. Clearly, for $u_0 \to 1$ the weight of the quasi particle peak goes to zero. This hints at the breakdown of the LA if the interaction U increases. However, as will be discussed in detail in Chap. 14 the Stoner instability can be eliminated, if we use the functional renormalization group to go beyond the LA.
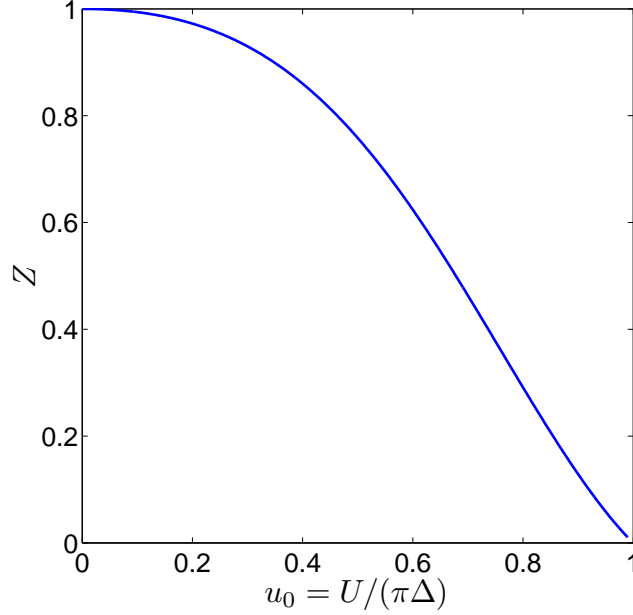
Figure 12.4: Wave function renormalization factor or the weight of the quasi particle residue of the particle-hole symmetric AIM as a function of the coupling U at $h = 0$ and in ladder approximation. Within LA, the wave function renormalization factor vanishes if $u_0 = U/(\pi\Delta)$ reaches 1. The given perturbative approach thus fails by increasing interaction.

12.3   Generating functionals for the FRG

In this section, we describe the application of the FRG to the AIM. Since the Euclidean action given by Eqs. (12.5, 12.6) does not exhibits any momentum dependence, the problem is here $0 + 1$-dimensional. Hence, we apply the cutoff Λ to the frequency label of the propagators. We use the same procedure as in Ref. [101], but we introduce the RG cutoff in the fermionic propagator instead of the bosonic one. In Chap. 4, we have described the general formalism for the functional renormalization group. In order to apply an appropriate FRG approach to the AIM, it is therefore useful to express the Gaussian part of the action given by (12.5) in form of Eq. (4.2),

$$S_0[\Phi] = -\frac{1}{2}(\Phi, [\mathbf{G}_0]^{-1}\Phi)\,, \qquad \mathbf{G}_0^{-1} = \begin{pmatrix} [\mathbf{G}_0^\uparrow]^{-1} & 0 & 0 \\ 0 & [\mathbf{G}_0^\downarrow]^{-1} & 0 \\ 0 & 0 & -\mathbf{U}^{-1} \end{pmatrix}\,, \quad (12.23)$$

where the block matrices $\mathbf{G}_0^\sigma$ and $\mathbf{U}$ are given by,

$$\mathbf{G}_0^\sigma = \begin{pmatrix} 0 & \hat{G}_0^\sigma \\ \zeta[\hat{G}_0^\sigma]^T & 0 \end{pmatrix}\,, \qquad \mathbf{U} = \begin{pmatrix} 0 & \hat{U} \\ [\hat{U}]^T & 0 \end{pmatrix}\,, \qquad (12.24)$$
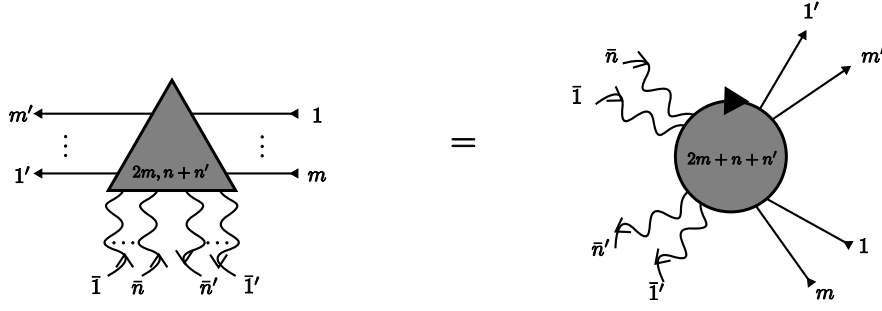
Figure 12.5: The flowing irreducible vertices are shown with shaded three angles, where the label $(2m, n + n')$ explains that the vertex has $2m$ fermionic, n incoming bosonic and n' outgoing bosonic external legs.

with $\zeta = -1$ and the label α involving the frequencies and the spins,

$$[\hat{G}_0^\sigma]_{\omega,\omega'} = \beta \delta_{\omega,\omega'} G_0^\sigma(i\omega)\,, \qquad [\hat{U}]_{\bar\omega,\bar\omega'} = \beta \delta_{\bar\omega,\bar\omega'} U\,. \qquad (12.25)$$

The generating functionals of the AIM resemble those of the bosonized one-dimensional electron system explained in Chap. 4, with an important difference that the bosonic fields are complex here. The irreducible vertices obey the frequency conservation and are symmetric with respect to the exchange of labels involving the same type of fields. Because of the particle conservation, the number of incoming and outgoing fermion legs which are associated respectively with the fields d_σ and $\bar{d}_\sigma$ must be the same. The generating functional for the irreducible vertices reads

$$\Gamma_\Lambda[\Phi] = \sum_{n',n,m=0}^{\infty} \frac{1}{(m!)^2 n! n'!} \int_{\omega'_1} \cdots \int_{\omega'_m} \int_{\omega_1} \cdots \int_{\omega_m} \int_{\bar\omega'_1} \cdots \int_{\bar\omega'_{n'}} \int_{\bar\omega_1} \cdots \int_{\bar\omega_n}$$

$$\times \beta \delta_{\omega'_1 + \cdots + \omega'_m + \bar\omega'_1 + \cdots + \bar\omega'_{n'}, \omega_1 + \cdots + \omega_m + \bar\omega_1 + \cdots + \bar\omega_n}$$

$$\times \Gamma_\Lambda^{(\bar{d}_{\sigma'_1} \cdots \bar{d}_{\sigma'_m} d_{\sigma_1} \cdots d_{\sigma_m} \bar\chi_1 \cdots \bar\chi_{n'} \chi_1 \cdots \chi_n)} (\omega'_1, \cdots, \omega'_m; \omega_1, \cdots, \omega_m; \bar\omega'_1, \cdots, \bar\omega'_{n'}; \bar\omega_1, \cdots, \bar\omega_n)$$

$$\times \bar{d}_{\omega'_1 \sigma'_1} \cdots \bar{d}_{\omega'_m \sigma'_m} d_{\omega_1 \sigma_1} \cdots d_{\omega_m \sigma_m} \bar\chi_{\bar\omega'_1} \cdots \bar\chi_{\bar\omega'_{n'}} \chi_{\bar\omega_1} \cdots \chi_{\bar\omega_n}\,. \qquad (12.26)$$

Fig. 12.5 shows a graphical representation of the irreducible vertices. For the super-field $\Phi = [d_\uparrow, \bar{d}_\uparrow, d_\downarrow, \bar{d}_\downarrow, \chi, \bar\chi]$ we define the associated source super-field $J = [\bar{j}_\uparrow, j_\uparrow, \bar{j}_\downarrow, j_\downarrow, \bar{J}, J]$, i.e.,

$$(J, \Phi) = \sum_\sigma \int_\omega [\bar{j}_{\omega\sigma} d_{\omega\sigma} + \bar{d}_{\omega\sigma} j_{\omega\sigma}] + \int_{\bar\omega} [\bar{J}_{\bar\omega} \chi_{\bar\omega} + J_{\bar\omega} \bar\chi_{\bar\omega}]\,. \qquad (12.27)$$

The generating functionals for the connected Green function can therefore be written as

$$\mathcal{G}_c^\Lambda[J] = \sum_{n',n,m=0}^{\infty} \frac{1}{(m!)^2 n! n'!} \int_{\omega'_1} \cdots \int_{\omega'_m} \int_{\omega_1} \cdots \int_{\omega_m} \int_{\bar\omega'_1} \cdots \int_{\bar\omega'_{n'}} \int_{\bar\omega_1} \cdots \int_{\bar\omega_n}$$

$$\times \beta \delta_{\omega'_1 + \cdots + \omega'_m + \bar\omega'_1 + \cdots + \bar\omega'_{n'}, \omega_1 + \cdots + \omega_m + \bar\omega_1 + \cdots + \bar\omega_n}$$

$$\times \mathcal{G}_c^{(\bar{j}_{\sigma'_1} \cdots \bar{j}_{\sigma'_m} j_{\sigma_1} \cdots j_{\sigma_m} \bar{J}_1 \cdots \bar{J}_{n'} J_1 \cdots J_n)} (\omega'_1, \cdots, \omega'_m; \omega_1, \cdots, \omega_m; \bar\omega'_1, \cdots, \bar\omega'_{n'}; \bar\omega_1, \cdots, \bar\omega_n)$$

$$\times \bar{j}_{\omega'_1 \sigma'_1} \cdots \bar{j}_{\omega'_m \sigma'_m} j_{\omega_1 \sigma_1} \cdots j_{\omega_m \sigma_m} \bar{J}_{\bar\omega'_1} \cdots \bar{J}_{\bar\omega'_{n'}} J_{\bar\omega_1} \cdots J_{\bar\omega_n}\,. \qquad (12.28)$$

Similar to the one-dimensional fermionic systems, because of the particle conservation, the matrix of the full Green function has the same block structure as the free propagator containing the fermionic and bosonic propagators,

$$
\mathbf{G}_\Lambda = -\left.\frac{\delta^{(2)}\mathcal{G}_{c,\Lambda}}{\delta J\,\delta J}\right|_{J=0} = \begin{pmatrix} \mathbf{G}_\Lambda^\uparrow & 0 & 0 \\ 0 & \mathbf{G}_\Lambda^\downarrow & 0 \\ 0 & 0 & -\mathbf{F}_\Lambda^\perp \end{pmatrix}. \tag{12.29}
$$

Likewise the self-energy $\mathbf{\Sigma}_\Lambda$ consists of one line irreducible fermionic self-energy and the irreducible spin-flip susceptibility,

$$
\mathbf{\Sigma}_\Lambda = \begin{pmatrix} \mathbf{\Sigma}_\Lambda^\uparrow & 0 & 0 \\ 0 & \mathbf{\Sigma}_\Lambda^\downarrow & 0 \\ 0 & 0 & \mathbf{\Pi}_\Lambda^\perp \end{pmatrix}, \tag{12.30}
$$

where

$$
\mathbf{\Sigma}_\Lambda^\sigma = \begin{pmatrix} 0 & \zeta[\hat{\Sigma}_\Lambda^\sigma]^T \\ \hat{\Sigma}_\Lambda^\sigma & 0 \end{pmatrix}, \qquad \mathbf{\Pi}_\Lambda^\perp = \begin{pmatrix} 0 & \hat{\Pi}_\Lambda^\perp \\ [\hat{\Pi}_\Lambda^\perp]^T & 0 \end{pmatrix}, \tag{12.31a}
$$

$$
\mathbf{G}_\Lambda^\sigma = \begin{pmatrix} 0 & \hat{G}_\Lambda^\sigma \\ \zeta[\hat{G}_\Lambda^\sigma]^T & 0 \end{pmatrix}, \qquad \mathbf{F}_\Lambda^\perp = \begin{pmatrix} 0 & \hat{F}_\Lambda^\perp \\ [\hat{F}_\Lambda^\perp]^T & 0 \end{pmatrix}, \tag{12.31b}
$$

and

$$
[\hat{\Sigma}_\Lambda^\sigma]_{\omega,\omega'} = \beta\delta_{\omega,\omega'}\Sigma_\Lambda^\sigma(i\omega), \qquad\qquad [\hat{\Pi}_\Lambda^\perp]_{\bar{\omega},\bar{\omega}'} = \beta\delta_{\bar{\omega},\bar{\omega}'}\Pi_\Lambda^\perp(i\bar{\omega}), \tag{12.32a}
$$

$$
[\hat{G}_\Lambda^\sigma]_{\omega,\omega'} = \beta\delta_{\omega,\omega'}G_\Lambda^\sigma(i\omega), \qquad\qquad [\hat{F}_\Lambda^\perp]_{\bar{\omega},\bar{\omega}'} = \beta\delta_{\bar{\omega},\bar{\omega}'}F_\Lambda^\perp(i\bar{\omega}). \tag{12.32b}
$$

The flow equations of the system are given by the general equation (4.43). In the following chapter we discuss the FRG expansion to the AIM and find a simple truncation to numerically solve the coupled flow equations of irreducible vertices.

Chapter 13

FRG approach to the AIM: frequency cutoff scheme

In this chapter, we describe the FRG approach for our mixed boson-fermion theory, which was introduced accurately in the previous chapter. We derive FRG flow equations for the two-legged vertices, using a cutoff which is included in the flowing fermionic Green function. This cutoff is different from other ones used in previous works within FRG formalism [96,100,101]. As will be discussed in detail, this cutoff represented by $h_\Lambda(i\omega)$ corresponds to the magnetic field and is called *magnetic field cutoff*.

In Sec. 13.2 we truncate the exact FRG flow equation for the self-energy of d-electrons, setting the irreducible three-legged and four-legged vertex functions equal to their initial values. Furthermore, we use Dyson-Schwinger equations to prove the *skeleton equation* for the flowing spin-flip susceptibility $\Pi_\Lambda^\perp(i\bar{\omega})$. In Sec. 13.3 we expand the fermionic self-energy to second order in the frequency to close the set of flow equations.

13.1   Cutoff in fermionic propagator

As we have pointed out, the spectral properties of the AIM is known from the numerical renormalization group method [74]. Furthermore, one can obtain the spectral function of the d-electrons for $U \ll \Delta$ analytically, using perturbation theory [87,88]. But this perturbative approach fails in strong coupling regime ($U \gg \Delta$). Because the system exhibits no momentum dependence, we cannot use the momentum cutoff, which is common for the development of the FRG flow equations. Therefore, in order to work beyond the LA, we can impose a cutoff in frequency space, which behaves as a large magnetic field. We introduce a smooth cutoff in the fermionic part of the Gaussian action $S_0[\Phi]$ given in Eq. (12.5),

$$[G_{0,\Lambda}^\sigma(i\omega)]^{-1} = [G_0^\sigma(i\omega)]^{-1} + \sigma h_\Lambda(i\omega). \tag{13.1}$$

As the simplest case if we choose $h_\Lambda(i\omega) = \Lambda$, it is obvious that this cutoff satisfies the properties of $\mathbf{R}_\Lambda$ defined in (4.39). The irreducible self-energy for particles

with spin σ and the irreducible transverse spin susceptibility $\Pi_\Lambda^\perp(i\bar\omega)$ are defined in (12.32a). We obtain for d-electron propagator,

$$[G_\Lambda^\sigma(i\omega)]^{-1} \;=\; [G_0^\sigma(i\omega)]^{-1} - \Sigma_\Lambda^\sigma(i\omega) + \sigma h_\Lambda(i\omega) \tag{13.2}$$

and for the bosonic spin-flip operator,

$$F_\Lambda^\perp(i\bar\omega) = [U^{-1} - \Pi_\Lambda^\perp(i\bar\omega)]^{-1} = \frac{U}{1 - U\Pi_\Lambda^\perp(i\bar\omega)} \,. \tag{13.3}$$

According to the general FRG formalism given by Eq. (4.43), the exact FRG flow equation for the spin-σ self-energy in the frequency cutoff scheme can be obtained easily. We have

$$\partial_\Lambda \Sigma_\Lambda^\sigma(i\omega) \;=\; \sum_{\sigma'} \int_{\omega'} \dot G_\Lambda^{\sigma'}(i\omega') \Gamma_\Lambda^{(\bar d_\sigma d_\sigma \bar d_{\sigma'} d_{\sigma'})}(\omega,\omega,\omega',\omega') + \int_{\bar\omega} F_\Lambda^\perp(i\bar\omega) \dot G_\Lambda^{\bar\sigma}(i\omega - i\sigma\bar\omega)$$

$$\times \;\; \Gamma_\Lambda^{(\bar d_\sigma d_{\bar\sigma} \chi_\sigma)}(\omega, \omega - \sigma\bar\omega, \bar\omega) \, \Gamma_\Lambda^{(\bar d_{\bar\sigma} d_\sigma \chi_{\bar\sigma})}(\omega - \sigma\bar\omega, \omega, \bar\omega) \,. \tag{13.4}$$

Where $\dot G_\Lambda^\sigma(i\omega)$ is the corresponding fermionic single scale propagator, which is defined by

$$\dot G_\Lambda^\sigma(i\omega) = [\bar\sigma \partial_\Lambda h_\Lambda(i\omega)][G_\Lambda^\sigma(i\omega)]^2 \,. \tag{13.5}$$

A graphical representation of the exact FRG flow equation of the self-energy is shown in Fig. 13.1. $\Gamma_\Lambda^{(\bar d_\sigma d_\sigma \bar d_{\sigma'} d_{\sigma'})}$, $\Gamma_\Lambda^{(\bar d_\sigma d_{\bar\sigma} \chi_\sigma)}$ and $\Gamma_\Lambda^{(\bar d_{\bar\sigma} d_\sigma \chi_{\bar\sigma})}$ are flowing irreducible vertex functions, where the first one has four fermionic external legs and the last two have two fermionic and one bosonic external legs. We have used for the three-legged vertices the short notations

$$\chi_\uparrow = \chi \,, \qquad\qquad \chi_\downarrow = \bar\chi \,, \tag{13.6}$$

that means,

$$\Gamma_\Lambda^{(\bar d_\uparrow d_\downarrow \chi_\uparrow)}(\omega, \omega - \bar\omega, \bar\omega) \;=\; \Gamma_\Lambda^{(\bar d_\uparrow d_\downarrow \chi)}(\omega, \omega - \bar\omega, \bar\omega) \,, \tag{13.7a}$$

$$\Gamma_\Lambda^{(\bar d_\downarrow d_\uparrow \chi_\downarrow)}(\omega - \bar\omega, \omega, \bar\omega) \;=\; \Gamma_\Lambda^{(\bar d_\downarrow d_\uparrow \bar\chi)}(\omega - \bar\omega, \omega, \bar\omega) \,. \tag{13.7b}$$

Note that because of the particle conservation the number of fermionic legs of any vertex function is always even (for any outgoing leg there is one incoming leg and vice versa). Due to Eqs. (12.6-12.9), inertial values of this vertices at $\Lambda = \Lambda_0$ are characterized by

$$\Gamma_{\Lambda_0}^{(\bar d_\sigma d_\sigma \bar d_{\sigma'} d_{\sigma'})}(\omega, \omega, \omega', \omega') \;=\; 0 \,, \tag{13.8a}$$

$$\Gamma_{\Lambda_0}^{(\bar d_\uparrow d_\downarrow \chi)}(\omega + \bar\omega, \omega, \bar\omega) \;=\; 1 \,, \tag{13.8b}$$

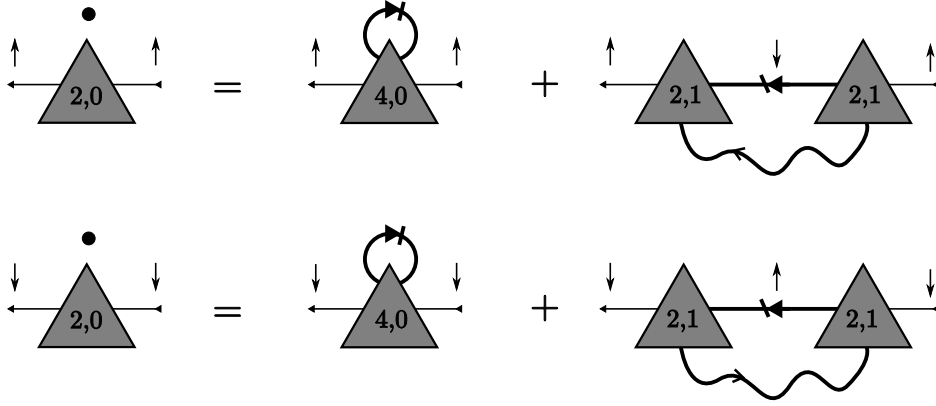$$\Gamma_{\Lambda_0}^{(\bar d_\downarrow d_\uparrow \bar\chi)}(\omega - \bar\omega, \omega, \bar\omega) \;=\; 1 \,. \tag{13.8c}$$

Figure 13.1: Exact flow equation of the fermionic self-energy $\Sigma_\Lambda^\sigma(i\omega)$ $(\sigma =\uparrow,\downarrow)$ in frequency cutoff scheme. Within our calculation, the fermionic propagator is regularized by the smooth magnetic field cutoff $h_\Lambda(\omega)$. The thick solid lines with arrow (without slash) denote the fermionic propagator given by Eq. (13.2) while the thick solid lines with arrow and slash display the fermionic single scale propagator defined in Eq. (13.5). In addition, the thick wavy lines with arrow represent the flowing bosonic propagator given by Eq. (13.3). The dot over the self-energy on the left hand side denote the derivative with respect to the RG cutoff Λ.

Since the action is hermitian, we have

$$\Gamma_\Lambda^{(\bar{d}_\uparrow d_\downarrow \chi)}(\omega, \omega - \bar{\omega}, \bar{\omega}) = \Gamma_\Lambda^{(\bar{d}_\downarrow d_\uparrow \bar{\chi})}(\omega - \bar{\omega}, \omega, \bar{\omega}). \tag{13.9}$$

Similarly the FRG flow equation of the spin-flip susceptibility is represented diagrammatically in Fig. 13.2. The analytical expression of this equation is

$$\partial_\Lambda \Pi_\Lambda^\perp(i\bar{\omega}) = \sum_{\sigma'} \int_\omega \dot{G}_\Lambda^{\sigma'}(i\omega') \Gamma_\Lambda^{(\bar{\chi}\chi\bar{d}_{\sigma'} d_{\sigma'})}(\bar{\omega}, \bar{\omega}, \omega', \omega') - \int_\omega [\dot{G}_\Lambda^\uparrow(i\omega) G_\Lambda^\downarrow(i\omega - i\bar{\omega})$$

$$+ \ G_\Lambda^\uparrow(i\omega)\dot{G}_\Lambda^\downarrow(i\omega - i\bar{\omega})]\Gamma_\Lambda^{(\bar{d}_\uparrow d_\downarrow \chi)}(\omega, \omega - \bar{\omega}, \bar{\omega})\Gamma_\Lambda^{(\bar{d}_\downarrow d_\uparrow \bar{\chi})}(\omega - \bar{\omega}, \omega, \bar{\omega}). \tag{13.10}$$

In addition, the initial value of the irreducible polarization is given by

$$\Pi_{\Lambda_0}^\perp(i\bar{\omega}) = - \int_\omega G_{\Lambda_0}^\uparrow(i\omega) G_{\Lambda_0}^\downarrow(i\omega - i\bar{\omega}). \tag{13.11}$$

As the initial value of the fermion self-energy one chooses usually $\Sigma_{\Lambda_0}(i\omega) = 0$. On the other hand, the self-consistent Hartree-Fock contribution, determined by (11.10) can be obtained from the FRG and it will be reproduced by expanding the right-hand side of Eq. (13.4) to the first order in U and setting the irreducible vertices equal to their initial values given by (13.8). It is therefore helpful to include this first-order term from the beginning into the fermionic self-energy,

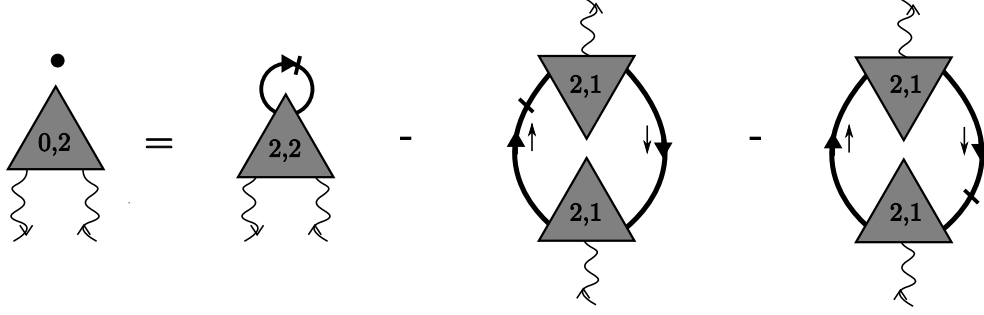$$\Sigma_{\Lambda_0}^\sigma(i\omega) = \delta\xi^\sigma = \frac{U}{2}[N - \sigma\mu_{\mathrm{HF}}] \tag{13.12}$$

Figure 13.2: Graphical representation of the exact flow equation for the spin-flip susceptibility in frequency cutoff scheme, given by Eq. (13.10).The thick solid and wavy lines with arrow have the same meaning as in Fig. 13.1. The thin wavy lines with arrow denote the external legs.

Since in the particle-hole symmetric case, $N = 1$ and $\xi_0 = E_d - \mu$ also cancels exactly $U/2$, we can write

$$G^\sigma_{\Lambda_0}(i\omega) = \frac{1}{i\omega + i\Delta \operatorname{sgn}(\omega) + \sigma\frac{U\mu_{\mathrm{HF}}}{2} + \sigma h_{\Lambda_0}(i\omega)} \,. \tag{13.13}$$

Consequently, we obtain for the flowing fermionic Green function and the single scale propagator,

$$G^\sigma_\Lambda(i\omega) \;=\; \frac{1}{i\omega + i\Delta \operatorname{sgn}(\omega) - \delta\Sigma^\sigma_\Lambda(i\omega) + \sigma h_\Lambda(i\omega)} \,, \tag{13.14}$$

$$\dot{G}^\sigma_\Lambda(i\omega) \;=\; \frac{\partial_\Lambda h_\Lambda(i\omega)\,\bar{\sigma}}{[i\omega + i\Delta \operatorname{sgn}(\omega) - \delta\Sigma^\sigma_\Lambda(i\omega) + \sigma h_\Lambda(i\omega)]^2} \,, \tag{13.15}$$

where

$$\delta\Sigma^\sigma_\Lambda(i\omega) = \Sigma^\sigma_\Lambda(i\omega) - \frac{UN}{2} \,. \tag{13.16}$$

13.2   Truncation via skeleton equation for bosonic self-energy

The FRG is given formally by exact RG flow equations. However, we know that because of the infinite number of coupled integro-differential equations, one needs a truncation to handle the problem. The flow equations of the two-legged vertex functions given in Eqs. (13.4, 13.10) are expressed via the four-legged and three-legged boson-fermion vertices. The expression for the flow equations of the three-legged and four-legged vertex functions are in turn given by the higher legged vertices like five-legged and six-legged vertices. For the cutoff in bosonic propagator flow equations of three-legged vertices are given in Ref. [102]. In our case, we can obtain equivalent flow equations using again Eq. (4.43). Fig. 13.3 shows graphically flow equations of the three-legged boson-fermion vertex functions. The vertices with a
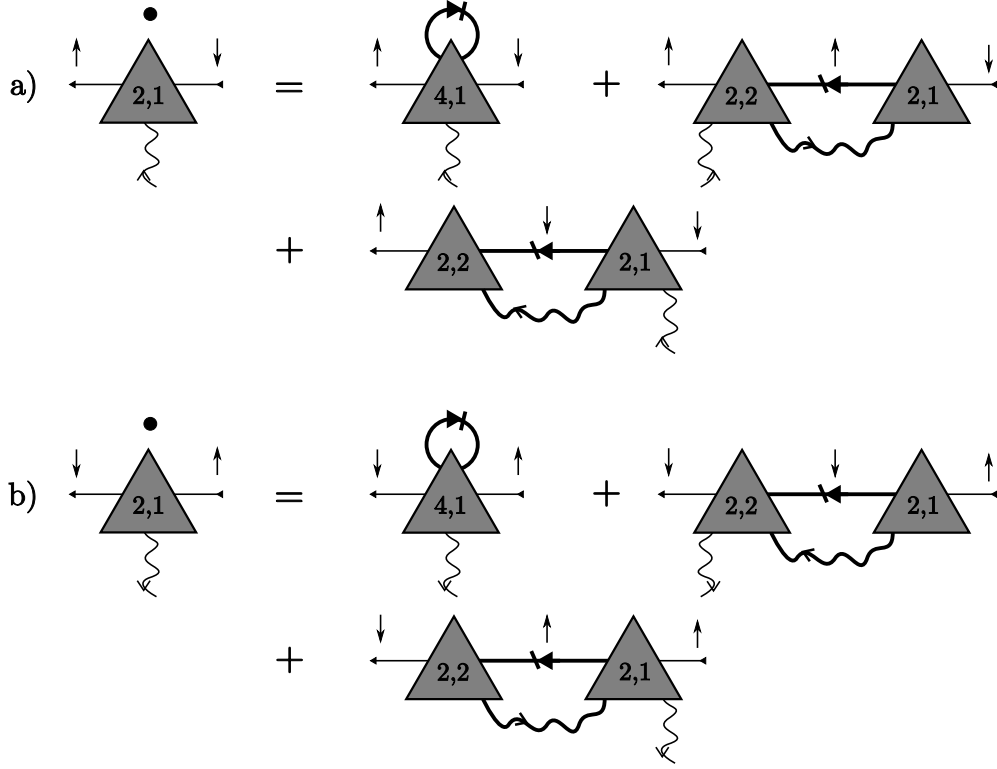
Figure 13.3: Exact FRG flow equation for the three-legged boson-fermion vertex functions a) $\Gamma_\Lambda^{(\bar{d}_\uparrow d_\downarrow \chi)}(\omega, \omega - \bar{\omega}, \bar{\omega})$ and b) $\Gamma_\Lambda^{(\bar{d}_\downarrow d_\uparrow \bar{\chi})}(\omega - \bar{\omega}, \omega, \bar{\omega})$. The solid and wavy lines with arrow have the same meaning as in Fig. 13.2.

sufficiently large number of legs at some order become also irrelevant in the RG sense. It is thus reasonable to replace the three and four-legged vertices by their initial values, which are known from (13.8),

$$\Gamma_\Lambda^{(\bar{d}_\sigma d_\sigma \bar{d}_{\sigma'} d_{\sigma'})}(\omega, \omega, \omega', \omega') \quad \approx \quad \Gamma_{\Lambda_0}^{(\bar{d}_\sigma d_\sigma \bar{d}_{\sigma'} d_{\sigma'})}(\omega, \omega, \omega', \omega') = 0\,, \qquad (13.17a)$$

$$\Gamma_\Lambda^{(\bar{d}_\uparrow d_\downarrow \chi)}(\omega, \omega - \bar{\omega}, \bar{\omega}) \quad \approx \quad \Gamma_{\Lambda_0}^{(\bar{d}_\uparrow d_\downarrow \chi)}(\omega, \omega - \bar{\omega}, \bar{\omega}) = 1\,, \qquad (13.17b)$$

$$\Gamma_\Lambda^{(\bar{d}_\downarrow d_\uparrow \bar{\chi})}(\omega - \bar{\omega}, \omega, \bar{\omega}) \quad \approx \quad \Gamma_{\Lambda_0}^{(\bar{d}_\downarrow d_\uparrow \bar{\chi})}(\omega - \bar{\omega}, \omega, \bar{\omega}) = 1\,. \qquad (13.17c)$$

Furthermore, to truncate the hierarchy of flow equations in the bosonic section, we use Dyson-Schwinger equations [57, 101] which are given by

$$\left(\zeta_\alpha J_\alpha - \frac{\delta S}{\delta \Phi_\alpha}\left[\frac{\delta}{\delta J_\alpha}\right] \right) \mathcal{G}[J_\alpha] = 0\,, \qquad (13.18)$$

to express the irreducible spin-flip susceptibility $\Pi_\Lambda^\perp(i\bar{\omega})$ in terms of fermionic Green functions. Eq. (13.18) can be proven easily, using the invariance of Eq. (4.8) with respect to the shift $\Phi + \Delta$, where $\Delta \to 0$. The expansion which is used here is called *skeleton equation* and for one-dimensional fermion systems (see Part I) is obtained in appendix B of Ref. [7]. Setting $\Phi_\alpha = \chi_{\bar{\omega}}$ or $\Phi_\alpha = \bar{\chi}_{\bar{\omega}}$ in Eq.(13.18), and considering

the action known from (12.5, 12.6) we obtain

$$\left(\bar{J}_{\bar{\omega}} - U^{-1}\frac{\delta}{\delta J_{\bar{\omega}}}\right)\mathcal{G}_\Lambda - \zeta\int_\omega \frac{\delta^2 \mathcal{G}_\Lambda}{\delta j_{\omega+\bar{\omega}\uparrow}\delta\bar{j}_{\omega\downarrow}} \;=\; 0\,, \tag{13.19a}$$

$$\left(J_{\bar{\omega}} - U^{-1}\frac{\delta}{\delta \bar{J}_{\bar{\omega}}}\right)\mathcal{G}_\Lambda - \zeta\int_\omega \frac{\delta^2 \mathcal{G}_\Lambda}{\delta j_{\omega\downarrow}\delta\bar{j}_{\omega+\bar{\omega}\uparrow}} \;=\; 0\,. \tag{13.19b}$$

$\mathcal{G}_\Lambda$ can be expressed in terms of the generating functionals of the connected Green functions $\mathcal{G}_{c,\Lambda}$ via the definition (4.15). Using Eqs. (4.25) and (4.28), the Dyson-Schwinger equations can be written in the following form,

$$\frac{\delta\Gamma}{\delta\chi_{\bar{\omega}}} - \int_\omega\left[\bar{d}_{\omega+\bar{\omega}\uparrow}d_{\omega\downarrow} + \frac{\delta^2 \mathcal{G}_{c,\Lambda}}{\delta\bar{j}_{\omega\downarrow}\delta j_{\omega+\bar{\omega}\uparrow}}\right] \;=\; 0\,, \tag{13.20a}$$

$$\frac{\delta\Gamma}{\delta\bar{\chi}_{\bar{\omega}}} - \int_\omega\left[\bar{d}_{\omega\downarrow}d_{\omega+\bar{\omega}\uparrow} + \frac{\delta^2 \mathcal{G}_{c,\Lambda}}{\delta\bar{j}_{\omega+\bar{\omega}\uparrow}\delta j_{\omega\downarrow}}\right] \;=\; 0\,. \tag{13.20b}$$

The dynamic spin susceptibility can be obtained by taking the first functional derivatives of Eq. (13.20a) with respect to $\bar{\chi}_{\bar{\omega}}$ and setting the fields equal to zero,

$$\Pi_\Lambda^\perp(i\bar{\omega}) = \left.\frac{\delta^2\Gamma}{\delta\chi_{\bar{\omega}}\,\delta\bar{\chi}_{\bar{\omega}}}\right|_{\Phi=0} = \int_\omega \left.\frac{\delta^2 \mathcal{G}_{c,\Lambda}}{\delta\bar{\chi}_{\bar{\omega}}\,\delta\bar{j}_{\omega\downarrow}\,\delta j_{\omega+\bar{\omega}\uparrow}}\right|_{\Phi=J=0}. \tag{13.21}$$

In addition, one can express $\mathcal{G}_{c,\Lambda}$ in terms of the irreducible vertices, using the tree expansion which is given by Eq. (4.32). Considering the $l=1$ term in the tree expansion, it is easy to see that

$$\left.\frac{\delta^2 \mathcal{G}_{c,\Lambda}}{\delta\bar{\chi}_{\bar{\omega}}\,\delta\bar{j}_{\omega\downarrow}\,\delta j_{\omega+\bar{\omega}\uparrow}}\right|_{\Phi=J=0} = -\int_\omega G_\Lambda^\uparrow(i\omega)G_\Lambda^\downarrow(i\omega-i\bar{\omega})\Gamma_\Lambda^{(\bar{d}_\downarrow d_\uparrow \bar{\chi})}(\omega-\bar{\omega},\omega,\bar{\omega})\,. \tag{13.22}$$

so that we get

$$\Pi_\Lambda^\perp(i\bar{\omega}) = -\int_\omega G_\Lambda^\uparrow(i\omega)G_\Lambda^\downarrow(i\omega-i\bar{\omega})\Gamma_\Lambda^{(\bar{d}_\downarrow d_\uparrow \bar{\chi})}(\omega-\bar{\omega},\omega,\bar{\omega}) \tag{13.23}$$

Likewise, we can obtain another skeleton expansion for the spin susceptibility, applying the first functional derivatives of Eq. (13.20b) with respect to $\chi_{\bar{\omega}}$ and setting the fields equal to zero,

$$\Pi_\Lambda^\perp(i\bar{\omega}) = -\int_\omega G_\Lambda^\uparrow(i\omega)G_\Lambda^\downarrow(i\omega-i\bar{\omega})\Gamma_\Lambda^{(\bar{d}_\uparrow d_\downarrow \chi)}(\omega,\omega-\bar{\omega},\bar{\omega})\,. \tag{13.24}$$

Graphical representations of the skeleton expansions for $\Pi_\Lambda^\perp(i\bar{\omega})$ are shown in Fig. 13.4, where the minus signs are omitted. Note that the skeleton equation can be derived for every irreducible vertex (in particular for the fermionic self-energy), following the same scheme as in the above derivation of Eqs. (13.23) and (13.24).
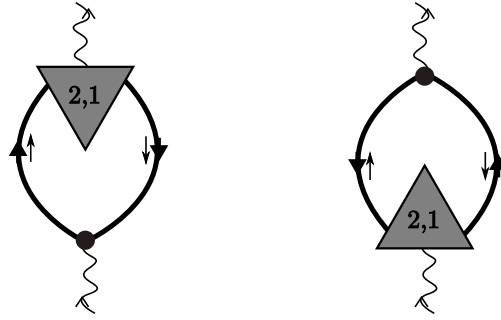
Figure 13.4: Two equivalent graphical representations of the skeleton equation for spin-flip susceptibility (without minus signs). The fat dots are the bare vertex functions shown in Fig. 12.1. The left diagram represents Eq. (13.23) and the right diagram represents Eq. (13.24).

Combining this equations with the approximations given in (13.17a-13.17c), we obtain

$$\Pi_\Lambda^\perp(i\bar\omega) = -\int_\omega G_\Lambda^\uparrow(i\omega)G_\Lambda^\downarrow(i\omega - i\bar\omega)\,. \tag{13.25}$$

The flow equation of the fermionic self-energy given by (13.4) simplifies after above truncations to

$$\partial_\Lambda\Sigma_\Lambda^\sigma(i\omega) = \int_{\bar\omega} F_\Lambda^\perp(i\bar\omega)\dot{G}_\Lambda^{\bar\sigma}(i\omega - i\sigma\bar\omega)\,. \tag{13.26}$$

13.3   Low energy approximation

Obviously, Eqs. (13.3, 13.14, 13.15, 13.25, 13.26) generate a closed system of integro-differential equations. To complete the truncations given in the previous section, we approximate the fermionic Green function by its low energy behavior. The following expansion is therefore reliable,

$$\delta\Sigma_\Lambda(i\omega) = -\sigma M_l + (1 - \frac{1}{Z_l})i\omega + \mathcal{O}(\omega^2)\,. \tag{13.27}$$

The index l denotes the flow parameter

$$l = -\ln\left(\frac{\Lambda}{\Lambda_0}\right) \qquad \Leftrightarrow \qquad \Lambda = \Lambda_0 e^{-l}\,, \tag{13.28}$$

The initial conditions therefore are given at $l = 0$ and in the limit $l \to \infty$ ($\Lambda \to 0$), we obtain the solution of the underlying model. M_l is here the flowing magnetization and Z_l is called the wave function renormalization factor which is related to the weight of the quasi particle residue. According to Eq. (13.12), the initial conditions are given by

$$M_{l=0} \;\;=\;\; \frac{U\mu_{\mathrm{HF}}}{2} = \frac{\pi\Delta u_0}{2}\mu_{\mathrm{HF}}\,, \tag{13.29}$$

$$Z_{l=0} \;\;=\;\; 1, \tag{13.30}$$

where as we know μ_{HF} is the mean field contribution to the magnetization. The flowing d-electron propagator and the corresponding single scale propagator can therefore be written as

$$G_\Lambda^\sigma(i\omega) \;\; = \;\; \frac{Z_l}{i\omega + i\Delta_l \operatorname{sgn}(\omega) + \sigma Z_l(h_\Lambda(i\omega) + M_l)}\,, \tag{13.31}$$

$$\dot{G}_\Lambda^\sigma(i\omega) \;\; = \;\; \frac{\partial_\Lambda h_\Lambda(i\omega)\,\bar\sigma\, Z_l^2}{[i\omega + i\Delta_l \operatorname{sgn}(\omega) + \sigma Z_l(h_\Lambda(i\omega) + M_l)]^2}\,, \tag{13.32}$$

where

$$\Delta_l = Z_l \Delta \tag{13.33}$$

is the renormalized flowing hybridization. Introducing now the flowing anomalous dimension,

$$\eta_l = -\partial_l \ln(Z_l)\,, \tag{13.34}$$

we obtain from Eqs. (13.26, 13.27),

$$\partial_l M_l = \sigma \Lambda \partial_\Lambda \Sigma_\Lambda^\sigma(0) = \sigma \Lambda \int_{\bar\omega} F_\Lambda^\perp(i\bar\omega) \dot{G}_\Lambda^{\bar\sigma}(i\bar\sigma\omega)\,, \tag{13.35}$$

where we used $\partial_l = -\Lambda \partial_\Lambda$. Similarly, we find

$$\begin{aligned}
\eta_l \;\; &= \;\; -\frac{\partial Z_l}{Z_l} = Z_l \Lambda \lim_{\omega \to 0} \frac{\partial}{\partial(i\omega)} \partial_\Lambda \Sigma_\Lambda^\sigma(i\omega) \\
&= \;\; Z_l \Lambda \lim_{\omega \to 0} \frac{\partial}{\partial(i\omega)} \int_{\bar\omega} F_\Lambda^\perp(i\bar\omega) \dot{G}_\Lambda^{\bar\sigma}(i\omega - i\sigma\bar\omega)\,.
\end{aligned} \tag{13.36}$$

The Eqs. (13.3, 13.25, 13.31, 13.32, 13.35, 13.36) build up a coupled system of differential equations, whose solution will be discussed in the next chapter.

Chapter 14

Magnetic field cutoff

The flow equations of different parts of the fermionic self-energy are given by Eqs. (13.35) and (13.36). To calculate the spectral properties of the AIM, we use in this chapter the magnetic field as a cutoff, i.e.,

$$h_\Lambda(i\omega) = \Lambda \,. \tag{14.1}$$

We shall show how to remove the Stoner instability known from Chap. 12 using the functional RG. In contrast to Ref. [101] we will not linearize the irreducible transverse spin-flip susceptibility given in (13.25), because for $U \gg \Delta$ the value of the full polarization in Eq. (13.3) becomes more important than the value of the inverse interaction. Since at the end $\Lambda \to 0$ and the spin-rotational invariance is not spontaneously broken, we expect that the magnetization along with the magnetic field vanishes. However it turns out that, the mean field contribution as initial condition (that means $M_{l=0} = U\mu_{HF}/2$) will not satisfy this condition. The initial condition of the magnetization will thus be altered by hand.

14.1 Fermionic and bosonic propagators

Introducing the magnetic field cutoff as defined by (14.1), we determine for the flowing fermionic Green function and the single scale propagator according to Eqs. (13.31, 13.32),

$$G_\Lambda^\sigma(i\omega) = \frac{Z_l}{i\omega + i\Delta_l \operatorname{sgn}(\omega) + \sigma Z_l(\Lambda + M_l)} \,, \tag{14.2}$$

$$\dot{G}_\Lambda^\sigma(i\omega) = \frac{\bar{\sigma} \, Z_l^2}{[i\omega + i\Delta_l \operatorname{sgn}(\omega) + \sigma Z_l(\Lambda + M_l)]^2} \,. \tag{14.3}$$

Inserting Eq. (14.2) into the skeleton equation for the spin susceptibility (13.25), and performing an elementary integration we obtain

$$\Pi_\Lambda^\perp(i\bar{\omega}) = \frac{Z_l}{\pi\Delta} \, f_\Lambda^\perp \left(\frac{|\bar{\omega}|}{\Delta_l}, \left[\frac{\Lambda + M_l}{\Delta} \right] \operatorname{sgn}\bar{\omega} \right) \,, \tag{14.4}$$

with

$$f_\Lambda^\perp(x, M) = \frac{\ln\left[1 + \frac{x}{1+iM}\right]}{(x - 2iM)(1 + x/2 - iM)} - \frac{2i \arctan M}{x - 2iM}. \tag{14.5}$$

It is clear that for $M \to 0$ (vanishing magnetic field and magnetization) $f_\Lambda^\perp(x, M)$ reduces to $f_0^\perp(x)$, given by Eq. (12.13). In order to perform the given integrations analytically, the first attempt is the expansion of the function $f_\Lambda^\perp(x, M)$ to linear order in x, which can be identified with the expansion of the dynamic spin-flip susceptibility for small frequencies $\bar\omega/\Delta$,

$$f_\Lambda^\perp(x, M) = \frac{\arctan M}{M} + \frac{ix}{2M}\left[\frac{1}{(1 - iM)^2} - \frac{\arctan M}{M}\right] + \mathcal{O}(x^2). \tag{14.6}$$

Nevertheless we can estimate the integro-differential equations numerically without this approximation.

14.2   Flow equations

Now, we consider the approximated Eqs. (13.35, 13.36) obtained in the previous chapter. Using the expression (14.3), the flow equation of the magnetization reads

$$
\begin{aligned}
\partial_l M_l &= Z_l^2 \Lambda \int_{\bar\omega} \frac{F_\Lambda^\perp(i\bar\omega)}{[i\bar\sigma\bar\omega + i\bar\sigma\Delta_l \operatorname{sgn}(\bar\omega) + \bar\sigma Z_l(\Lambda + M_l)]^2} \\
&= -2Z_l^2 \Lambda \operatorname{Re} \int_0^\infty \frac{d\bar\omega}{2\pi} \frac{F_\Lambda^\perp(i\bar\omega)}{[\bar\omega + \Delta_l - iZ_l(\Lambda + M_l)]^2}.
\end{aligned}
\tag{14.7}
$$

The calculation of the anomalous dimension is more complicated. According to (13.36) we obtain

$$
\begin{aligned}
\eta_l &= -2Z_l^3 \Lambda \lim_{\omega \to 0} \int_{\bar\omega} \frac{\sigma F_\Lambda^\perp(i\bar\omega)[1 + 2\Delta_l\,\delta(\omega + \bar\sigma\omega)]}{[i(\omega + \bar\sigma\bar\omega) + i\Delta_l \operatorname{sgn}(\omega + \bar\sigma\bar\omega) + \bar\sigma Z_l(\Lambda + M_l)]^3} \\
&= 2Z_l^3 \Lambda \int_{\bar\omega} \left[\frac{F_\Lambda^\perp(i\bar\omega)}{[i\bar\omega + i\Delta_l \operatorname{sgn}(\bar\omega) + Z_l(\Lambda + M_l)]^3}\right. \\
&\quad + \left.\frac{2\Delta_l F_\Lambda^\perp(0)\,\delta(\bar\omega)}{\left[i\Delta_l \operatorname{sgn}(\bar\omega) + Z_l(\Lambda + M_l)\right]^3}\right].
\end{aligned}
\tag{14.8}
$$

Where we have used again $\operatorname{sgn}(x) = 2\Theta(x) - 1$. The second part of the above expression can be obtained through the relation (12.20) and we derive after some algebra,

$$
\begin{aligned}
\eta_l &= -4Z_l^3 \Lambda \left[\operatorname{Im} \int_0^\infty \frac{d\bar\omega}{2\pi} \frac{F_\Lambda^\perp(i\bar\omega)}{[\bar\omega + \Delta_l - iZ_l(\Lambda + M_l)]^2}\right. \\
&\quad - \left.\frac{F_\Lambda^\perp(0)}{2\pi} \frac{\Delta_l Z_l(\Lambda + M_l)}{[\Delta_l^2 + Z_l^2(\Lambda + M_l)^2]^2}\right].
\end{aligned}
\tag{14.9}
$$

Using now the relation (13.3), we get

$$F_\Lambda^\perp(i\bar\omega) = U + \Pi_{\text{LA},\Lambda}^\perp(i\bar\omega) \,, \tag{14.10}$$

where

$$\Pi_{\text{LA},\Lambda}^\perp(i\bar\omega) = \frac{\Pi_\Lambda^\perp(i\bar\omega)}{1 - U\Pi_\Lambda^\perp(i\bar\omega)} \,, \tag{14.11}$$

We find that the terms linear in the coupling U cancel in Eq. (14.9) and η_l assumes the same form as Eq. (12.22),

$$
\begin{aligned}
\eta_l \;=\; & -4Z_l^3\Lambda\frac{U^2}{2\pi}\left[\text{Im}\int_0^\infty d\bar\omega\,\frac{\Pi_{\text{LA},\Lambda}^\perp(i\bar\omega)}{[\bar\omega + \Delta_l - iZ_l(\Lambda + M_l)]^3}\right. \\
& \left. -\;\Pi_{\text{LA},\Lambda}^\perp(0)\frac{\Delta_l Z_l(\Lambda + M_l)}{[\Delta_l^2 + Z_l^2(\Lambda + M_l)^2]^2}\right] .
\end{aligned}
\tag{14.12}
$$

14.3   Numerical estimate

In this section we examine the coupled differential equations (13.34, 14.7, 14.12) numerically. We compare our results with the exact result (11.17) for the wave function renormalization factor, obtained via the Bethe ansatz. For the numerical calculation, it is convenient to express the flow equations (14.7, 14.12) in form of the following dimensionless parameters,

$$\lambda_l = \frac{\Lambda}{\Delta_l} = \frac{\Lambda_0}{Z_l\Delta}e^{-l}\,, \qquad m_l = \frac{M_l}{\Delta}\,, \qquad u_l = \frac{U}{\pi\Delta_l} = \frac{u_0}{Z_l}\,. \tag{14.13}$$

We obtain

$$
\partial_l m_l \;=\; -Z_l\lambda_l u_l\,\text{Re}\int_0^\infty \frac{dx}{[1 - u_l f_\Lambda^\perp(x, Z_l\lambda_l + m_l)][1 + x - i(Z_l\lambda_l + m_l)]^2}\,, \tag{14.14}
$$

$$
\begin{aligned}
\eta_l \;=\; & -2Z_l\lambda_l u_l^2\left[\text{Im}\int_0^\infty dx\,\frac{f_\Lambda^\perp(x, Z_l\lambda_l + m_l)}{[1 - u_l f_\Lambda^\perp(x, Z_l\lambda_l + m_l)][1 + x - i(Z_l\lambda_l + m_l)]^3}\right. \\
& \left. -\;\frac{f_\Lambda^\perp(0, Z_l\lambda_l + m_l)\,(Z_l\lambda_l + m_l)}{[1 - u_l f_\Lambda^\perp(0, Z_l\lambda_l + m_l)][1 + (Z_l\lambda_l + m_l)^2]^2}\right] ,
\end{aligned}
\tag{14.15}
$$

where the function $f_\Lambda^\perp(x, M)$ is defined in Eq. (14.5). The initial values of $m_l = M_l/\Delta$ and Z_l are given by Eqs. (13.29, 13.30) where the Hartree-Fock magnetic moment is known from Chap. 12 [see Eq. (12.2)],

$$\mu_{\text{HF}} \;=\; \int_\omega\sum_\sigma \sigma G_{\Lambda_0}^\sigma(i\omega) = \frac{2}{\pi}\arctan\left[\frac{\pi u_0}{2}\mu_{\text{HF}} + \frac{\Lambda_0}{\Delta}\right] . \tag{14.16}$$
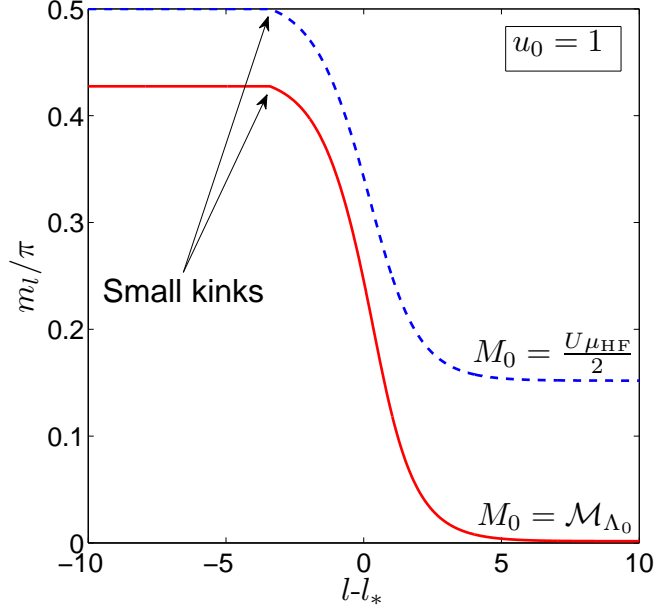
Figure 14.1: Typical flow of the magnetization in the magnetic field cutoff scheme for $u_0 = U/(\pi\Delta) = 1$ and different initial values, where $m_l = M_l/\Delta$ and we set here $\mu_{\mathrm{HF}} = 1$. The magnetization remains finite, if we choose $M_{l=0} = U\mu_{\mathrm{HF}}/2$ (dashed line) but for the modified initial value $M_{l=0} = \mathcal{M}_{\Lambda_0}$ the magnetization flows to zero (solid line). Note that for $u_0 = 1$ we obtain $\mathcal{M}_{\Lambda_0}/(\Delta\pi) \approx 0.428$. At the scale l_* the running cutoff Λ becomes equal to the hybridization, i.e., $\Lambda_0 e^{l_*} = \Delta$. Because for $l < 0$ we set $m_l = m_0$, there are small nonanalytical kinks shown by arrows.

In the ultraviolet limit we have

$$\lim_{\Lambda_0 \to \infty} \mu_{\mathrm{HF}} = 1 \,. \tag{14.17}$$

This value implies that according to the mean field approximation, for high magnetic fields in the ground state all spins point in the same direction. However by using $\partial_l Z_l = -\eta_l Z_l$ our numerical results show that the magnetization approaches a finite limit for $l \to \infty$ $(\Lambda \to 0)$ and this disagrees with the fact that there is no spontaneous magnetization. To remove this problem, we choose a suitable initial value

$$M_{l=0} = \mathcal{M}_{\Lambda_0} \,. \tag{14.18}$$

of the magnetization such that at the end $M_{l\to\infty}$ vanishes. Requiring that $m_{l\to\infty} = 0$, the value of $\mathcal{M}_{\Lambda_0}$ can differ from the mean field result $U\mu_{\mathrm{HF}}/2$. For example, the flowing magnetization for $u_0 = 1$ and two different initial conditions is shown in Fig. 14.1. The ratio of $\mathcal{M}_{\Lambda_0}$ to $U\mu_{\mathrm{HF}}/2$ as a function of the bare coupling u_0 is shown in Fig. 14.2. It is obvious that the renormalized initial value $\mathcal{M}_{\Lambda_0}$ is always smaller than the expected initial value or rather the Hartree-Fock contribution to the magnetization. In addition these two initial conditions deviate significantly for
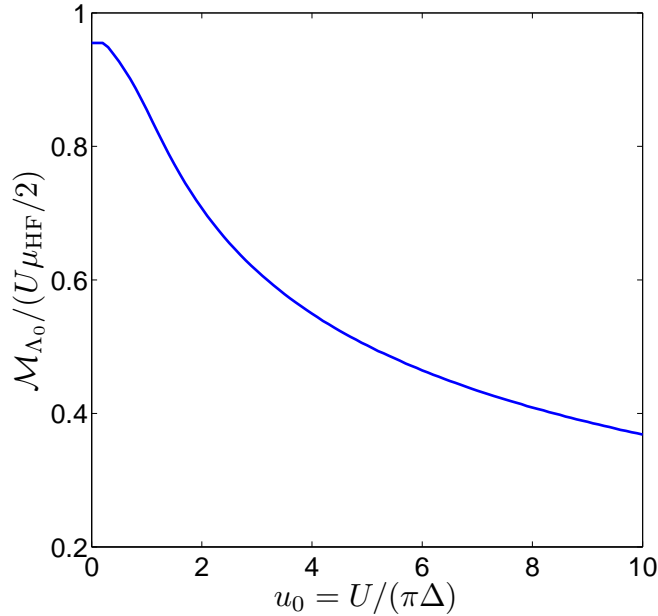
Figure 14.2: The ratio between the different initial values given by (13.29) and (14.18), where we set again $\mu_{\mathrm{HF}} = 1$. For $u_0 \ll 1$ these two coefficients are very close to each other but by increasing U the difference becomes bigger. The value of $\mathcal{M}_{\Lambda_0}$ is choosen such that $m_{l\to\infty}$ vanishes, if $m_{l=0} = \mathcal{M}_{\Lambda_0}/\Delta$.

$u_0 \gg 1$. In Chap. 15 we will show how to regularize the smooth cutoff such that the difference between $\mathcal{M}_{\Lambda_0}$ and $U\mu_{\mathrm{HF}}/2$ becomes smaller.

Next, we choose as the initial values $M_{l=0} = \mathcal{M}_{\Lambda_0}$ and $Z_{l=0} = 1$. The flowing wave function renormalization factor can be obtained numerically and the solution for different values of the bare coupling U is shown in Fig. 14.3. It is clear that in the limit $l \to \infty$ the wave function renormalization factor remains finite for all values of u_0 and in contrast to the ladder approximation discussed in Chap. 12 we can obtain $Z = \lim_{l\to\infty} Z_l$ in the strong coupling regime. The unphysical Stoner instability is therefore removed by the FRG approach including spin-singlet fluctuations. The results which we have obtained via FRG for $Z = \lim_{l\to\infty} Z_l$ as a function of the bare coupling u_0 are shown in Fig. 14.4. For comparison we show also the prediction of the ladder approximation as well as the precise results within Wilson's numerical renormalization Group obtained by Karrash *et al.* [100]. It is clear that for $u_0 = U/(\pi\Delta) \lesssim 2$ our results agree with a good approximation with the exact results in the context of NRG. On the other hand, in the strong coupling regime the numerical solution for Z does not exhibit the same exponential manner, which we expect because of Eq. (11.17). According to our numerical solution from the FRG with the magnetic field cutoff, the weight of the quasi particle residue in strong coupling regime varies linearly in $1/U$, where we estimate

$$Z = \lim_{l\to\infty} Z_l \approx \frac{0.71}{u_0} , \qquad u_0 \gg 1 . \qquad (14.19)$$
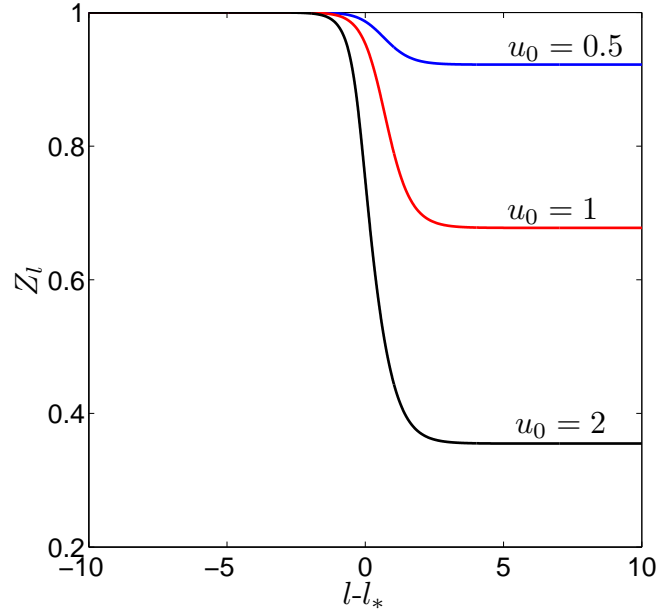
Figure 14.3: Numerical solution of the coupled differential equations (14.14-14.15) for $m_0 = \mathcal{M}_{\Lambda_0}/\Delta$ and different values of the bare coupling $u_0 = U/(\pi\Delta)$. The scale l_* is defined by $\Lambda_0 e^{l_*} = \Delta$.
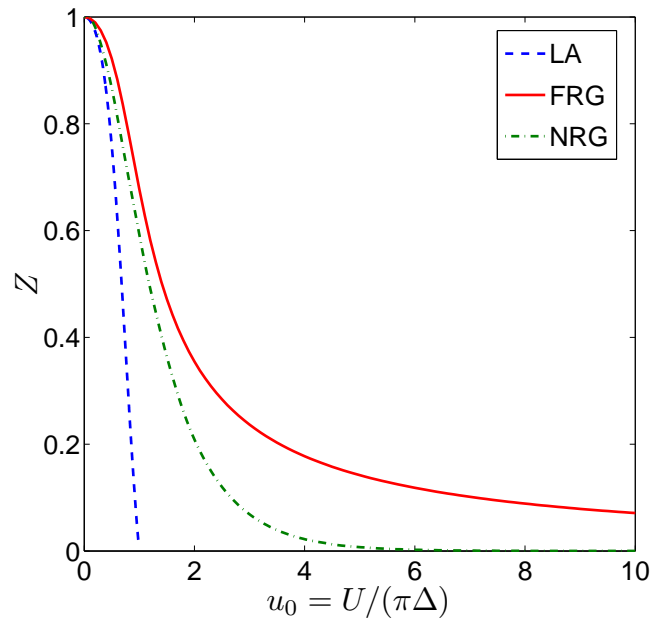

Figure 14.4: FRG solution for the wave function renormalization factor which is compared with the results obtained within ladder approximation and with the exact NRG results.

Chapter 15

Modified magnetic field cutoff

Because the frequency independent magnetic field cutoff $h_\Lambda(i\omega) = h_\Lambda(0) = \Lambda$ does not guarantee that the flowing magnetization with the initial condition $M_{l=0} = U\mu_{\mathrm{HF}}/2$ vanishes for $l \to \infty$, we need another magnetic field cutoff which suppress the former tendency due to the magnetic field. To this end we introduce a cutoff which prohibits that the magnetic field affects the frequencies exceeding the RG parameter Λ,

$$h_\Lambda(i\omega) = (\Lambda - |\omega|)\Theta(\Lambda - |\omega|)\,. \tag{15.1}$$

We obtain thus for the flowing fermion Green function and the single scale propagator,

$$G_\Lambda^\sigma(i\omega) = \frac{Z_l}{i\omega + i\Delta_l \operatorname{sgn}(\omega) + \sigma Z_l[(\Lambda - |\omega|)\Theta(\Lambda - |\omega|) + M_l]}\,, \tag{15.2}$$

$$\dot{G}_\Lambda^\sigma(i\omega) = \frac{\bar{\sigma}\,\Theta(\Lambda - |\omega|)Z_l^2}{[i\omega + i\Delta_l \operatorname{sgn}(\omega) + \sigma Z_l(\Lambda - |\omega| + M_l)]^2}\,. \tag{15.3}$$

Let us first derive the irreducible polarization within the approximation given by the skeleton equation (13.25). According to Eq. (15.2) the calculation of the spin susceptibility in this case is much more cumbersome than for the constant magnetic field [see Eq. (14.4)]. Because of the cutoff defined by (15.1), we are interested in the frequencies which are smaller than Λ. After a tedious algebra we find that,

$$\Theta(\Lambda - |\bar{\omega}|)\,\Pi_\Lambda^\perp(i\bar{\omega}) = \frac{Z_l}{\pi\Delta}\,f_{h_\Lambda}^\perp\left(\frac{|\bar{\omega}|}{\Delta_l}, \frac{\Lambda}{\Delta_l}, \frac{M_l}{\Delta_l}, Z_l\operatorname{sgn}\bar{\omega}\right)\,, \tag{15.4}$$

where the complicated function $f_{h_\Lambda}^\perp$ is given by

$$
f_{h_\Lambda}^\perp(x, \lambda, M, z) = \frac{[izx + iz(1 + \lambda - izM)]\ln\left[1 + \frac{x}{1+\lambda-izM}\right]}{(x - 2izM)[(iz - 1)x + iz(1 + \lambda + 2M - izM)]}
$$

$$
+ \frac{[iz(iz - 1)x + iz(1 + \lambda + izM)]\ln\left[1 + \frac{(iz-1)x}{1+\lambda+izM}\right]}{[2iz(1 + \lambda + M) - (1 + z^2)x][(iz - 1)x + iz(1 + \lambda + 2M - izM]}
$$

$$
- \frac{2[iz(iz + 1)x + 1 + 2iz + z^2(\lambda + M)]\ln\left[1 + \frac{(iz+1)x}{1-iz(\lambda+M)}\right]}{(iz + 1)[2 - 2iz(\lambda + M) + (1 + iz)x][2iz(1 + \lambda + M) - (1 + z^2)x]}
$$

$$
- \frac{2i[2iz(1 + \lambda) - z^2 x]\arctan\left[\frac{zM}{1+\lambda}\right]}{(x - 2izM)[2iz(1 + \lambda + M) - (1 + z^2)x]} + \frac{2i\arctan[z(\lambda + M)]}{2iz(1 + \lambda + M) - (1 + z^2)x}. \quad (15.5)
$$

Taking the limit $x \to 0$, which is equivalent to $\bar{\omega} \to 0$, we obtain

$$
f_{h_\Lambda}^\perp(0, \lambda, M, z) = \frac{(1 + \lambda)\arctan\left[\frac{zM}{1+\lambda}\right] + M\arctan[z(\lambda + M)]}{zM(1 + \lambda + M)}. \quad (15.6)
$$

Next, we consider the Hartree-Fock contribution to the magnetization and show how it changes in the modified magnetic field cutoff scheme.

15.1 Self-consistent Hartree-Fock approximation

By definition, the Hartree-Fock self-consistency equation for the magnetic moment is given by

$$
\begin{aligned}
\mu_{\text{HF}} &= \int_\omega \sum_\sigma \sigma G_{\Lambda_0}^\sigma(i\omega) \\
&= \int_\omega \sum_\sigma \frac{\sigma}{i\omega + i\Delta_l \operatorname{sgn}(\omega) + \sigma[(\Lambda_0 - |\omega|)\Theta(\Lambda_0 - |\omega|) + \frac{U\mu_{\text{HF}}}{2}]} \\
&= \int_\omega \sum_\sigma \left[\frac{\sigma\Theta(\Lambda_0 - |\omega|)}{i\omega + i\Delta_l \operatorname{sgn}(\omega) + \sigma\left[\Lambda_0 - |\omega| + \frac{U\mu_{\text{HF}}}{2}\right]} \right. \\
&\quad \left. + \frac{\sigma\Theta(|\omega| - \Lambda_0)}{i\omega + i\Delta_l \operatorname{sgn}(\omega) + \sigma\frac{U\mu_{\text{HF}}}{2}}\right]. \quad (15.7)
\end{aligned}
$$

Carrying out the integrations, after some algebra we obtain

$$
\begin{aligned}
\mu_{\text{HF}} &= \frac{1}{\pi}\arctan\left[\frac{\pi u_0}{2}\mu_{\text{HF}} + \frac{\Lambda_0}{\Delta}\right] + \frac{1}{\pi}\arctan\left[\frac{\frac{\pi u_0}{2}\mu_{\text{HF}}}{1 + \frac{\Lambda_0}{\Delta}}\right] \\
&+ \frac{1}{2\pi}\ln\left[\frac{1 + \left(\frac{\pi u_0}{2}\mu_{\text{HF}} + \frac{\Lambda_0}{\Delta}\right)^2}{\left(1 + \frac{\Lambda_0}{\Delta}\right)^2 + \left(\frac{\pi u_0}{2}\mu_{\text{HF}}\right)^2}\right]. \quad (15.8)
\end{aligned}
$$

Finally, if we take the limit $\Lambda_0 \to \infty$, we estimate

$$\lim_{\Lambda_0 \to \infty} \mu_{\text{HF}} = \frac{1}{2} \, . \tag{15.9}$$

This value arising due to the diluted magnetic field is the half of the magnetic moment which is obtained in (14.17). This expression yields for the initial value of the magnetization $M_{l=0} \approx U/4$.

15.2   FRG flow equations

The flow equation for the magnetic moment can again be obtained analytically, inserting the expression (15.3) in Eq. (13.35). We have

$$
\begin{aligned}
\partial_l M_l &= Z_l^2 \Lambda \int_{\bar{\omega}} \frac{F_\Lambda^\perp(i\bar{\omega}) \, \Theta(\Lambda - |\bar{\omega}|)}{[i\bar{\sigma}\bar{\omega} + i\bar{\sigma}\Delta_l \, \text{sgn}(\bar{\omega}) + \bar{\sigma} Z_l(\Lambda - |\bar{\omega}| + M_l)]^2} \\
&= -2Z_l^2 \Lambda \, \text{Re} \int_0^\Lambda \frac{d\bar{\omega}}{2\pi} \frac{F_\Lambda^\perp(i\bar{\omega})}{[\bar{\omega} + \Delta_l - iZ_l(\Lambda - \bar{\omega} + M_l)]^2} \, .
\end{aligned}
\tag{15.10}
$$

Now, we consider the anomalous dimension η_l. Similar to Eq. (14.8) we obtain according to Eqs. (15.3) and (13.36),

$$
\eta_l = 2Z_l^3 \Lambda \int_{\bar{\omega}} \left[\frac{F_\Lambda^\perp(i\bar{\omega}) \left[1 + i\text{sgn}(\bar{\omega})Z_l \right] \Theta(\Lambda - |\bar{\omega}|)}{[i\bar{\omega} + i\Delta_l \, \text{sgn}(\bar{\omega}) + Z_l(\Lambda - |\bar{\omega}| + M_l)]^3} \right.
$$
$$
\left. + \frac{2\Delta_l F_\Lambda^\perp(0) \, \delta(\bar{\omega})}{\left[i\Delta_l \, \text{sgn}(\bar{\omega}) + Z_l(\Lambda + M_l) \right]^3} - \frac{F_\Lambda^\perp(i\bar{\omega}) \, \delta(\Lambda - |\bar{\omega}|)}{[i\bar{\omega} + i\Delta_l \, \text{sgn}(\bar{\omega}) + Z_l(\Lambda - |\bar{\omega}| + M_l)]^2} \right], \tag{15.11}
$$

where we have again used $\text{sgn}(x) = 2\Theta(x) - 1$. Applying the relations (12.20, 14.10), we find that the linear terms in U cancel each other out and we obtain after some algebra,

$$
\begin{aligned}
\eta_l &= -4Z_l^3 \Lambda \frac{U^2}{2\pi} \left[\text{Im} \int_0^\Lambda d\bar{\omega} \, \frac{\Pi_{\text{LA},\Lambda}^\perp(i\bar{\omega}) \, (1 + iZ_l)}{[\bar{\omega} + \Delta_l - iZ_l(\Lambda - \bar{\omega} + M_l)]^3} \right. \\
&\quad + \left. \text{Im} \frac{\Pi_{\text{LA},\Lambda}^\perp(i\Lambda)}{2[\Lambda + \Delta_l - iZ_l M_l]^2} - \Pi_{\text{LA},\Lambda}^\perp(0) \frac{\Delta_l Z_l(\Lambda + M_l)}{[\Delta_l^2 + Z_l^2(\Lambda + M_l)^2]^2} \right] . \tag{15.12}
\end{aligned}
$$

Finally, if we introduce the dimensionless coefficients defined by (14.13), the differential equations can be written in the following form,

$$
\partial_l m_l = -Z_l \lambda_l u_l \, \mathrm{Re} \int_0^{\lambda_l} \frac{dx}{[1 - u_l f_{h_\Lambda}^\perp(x, \lambda_l, m_l/Z_l, Z_l)][1 + x - i(Z_l\lambda_l - Z_l x + m_l)]^2} ,
\tag{15.13}
$$

$$
\eta_l = -2Z_l \lambda_l u_l^2 \left[\mathrm{Im} \int_0^{\lambda_l} dx \, \frac{f_{h_\Lambda}^\perp(x, \lambda_l, m_l/Z_l, Z_l)}{1 - u_l f_{h_\Lambda}^\perp(x, \lambda_l, m_l/Z_l, Z_l)} \frac{1 + iZ_l}{[1 + x - i(Z_l\lambda_l - Z_l x + m_l)]^3} \right.
$$

$$
+ \mathrm{Im} \frac{f_{h_\Lambda}^\perp(\lambda_l, \lambda_l, m_l/Z_l, Z_l)}{1 - u_l f_{h_\Lambda}^\perp(\lambda_l, \lambda_l, m_l/Z_l, Z_l)} \frac{1}{2[1 + \lambda_l - im_l]^2}
$$

$$
\left. - \frac{f_{h_\Lambda}^\perp(0, \lambda_l, m_l/Z_l, Z_l)}{1 - u_l f_{h_\Lambda}^\perp(0, \lambda_l, m_l/Z_l, Z_l)} \frac{Z_l\lambda_l + m_l}{[1 + (Z_l\lambda_l + m_l)^2]^2} \right] ,
\tag{15.14}
$$

15.3   Numerical results

We demand again that, by the initial condition $M_{l=0} = \mathcal{M}_{\Lambda_0}$, the magnetic moment M_l in the limit $l \to \infty$ flows to zero. A graph of the ratio between the estimated value $\mathcal{M}_{\Lambda_0}$ and $U\mu_{\mathrm{HF}}/2$ as a function of $u_0 = U/(\pi\Delta)$ is shown in Fig. 15.1. For comparison we depict also the results obtained in the previous chapter, using frequency independent magnetic field cutoff. It is obvious that the value $\mathcal{M}_{\Lambda_0}$ for the modified magnetic field cutoff is closer to $U\mu_{\mathrm{HF}}/2$ than for the usual magnetic field cutoff. Note that in the case of $h_\Lambda(i\omega) = \Lambda$ the magnetic moment could not become larger than $U\mu_{\mathrm{HF}}/2$ (where $\mu_{\mathrm{HF}} = 1$), otherwise *the physical magnetization* would be bigger than unity where the whole spins point in the same direction.

Setting now $M_{l=0} = \mathcal{M}_{\Lambda_0}$ and $Z_{l=0} = 1$, the numerical evaluation of the wave function renormalization factor yields again $Z = \lim_{l\to\infty} Z_l$ is finite for the whole values of the bare coupling $u_0 = U/(\pi\Delta)$. The determined numerical solution of Z for the modified magnetic field cutoff is shown in Fig. 15.2. This results are compared with the prediction of the ladder approximation, the result for the frequency independent magnetic field cutoff from Chap. 14 and the exact results obtained via NRG in Ref. [100]. Obviously, our new results for Z do not deviate essentially from the results obtained for the frequency independent cutoff $h_\Lambda(i\omega) = \Lambda$. In Fig. 15.3, we show that our results for $u_0 \lesssim 2$ are improved, because the difference between FRG and NRG results decreases slightly.

However, in the limit $u_0 \to \infty$, we cannot again recover the exponential suppression given by Eq. (11.17). Furthermore, in Fig. 15.4 we show the data in Fig. 15.2 by plotting $1/Z$ on a logarithmic scale. Note that at strong coupling the exact results obtained by NRG behave as a linear function on the logarithmic scale. In Fig. 15.5 we compare on the same scale our final results with the results obtained by Bartosch *et al.* [101], who studied the same problem using FRG in two channels, transverse and longitudinal spin channels and introduced the RG cutoff in bosonic propagators. Obviously for $u_0 \lesssim 2$ our results coincide better with the exact re-
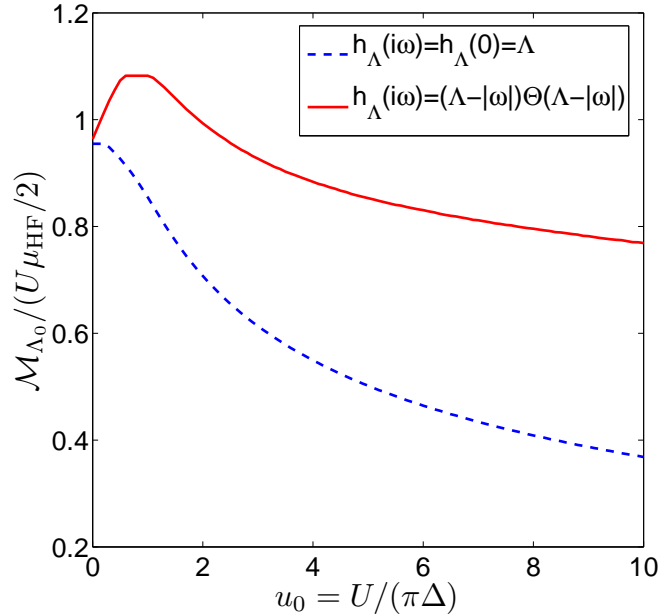
Figure 15.1: The ratio of $\mathcal{M}_{\Lambda_0}$ to $U\mu_{\mathrm{HF}}/2$ for the magnetic field cutoff (dashed line) and for the modified magnetic field cutoff (solid line). For $h_\Lambda(i\omega) = h_\Lambda(0) = \Lambda$, we set as before $\mu_{\mathrm{HF}} = 1$ while for $h_\Lambda(i\omega) = (\Lambda - |\omega|)\Theta(\Lambda - |\omega|)$ we set $\mu_{\mathrm{HF}} = 1/2$ [see Eq. (15.9)]. It is obvious that for the modified magnetic field cutoff the determined value of $\mathcal{M}_{\Lambda_0}$ is closer to $U\mu_{\mathrm{HF}}/2$ than for the usual magnetic field cutoff.

sults. On the other hand, in the strong coupling regime, the cutoff in the bosonic propagator and calculation in two channels lead to a more suitable approach than the modified magnetic field cutoff, because the wave function renormalization factor becomes smaller.

Eventually it is instructive to treat the spectral density of d-electrons, defined by

$$A(\omega) = -\frac{1}{\pi}\,\mathrm{Im}G^\sigma(i\omega \to \omega + i0)\,, \tag{15.15}$$

where $G^\sigma(i\omega)$ is approximated by $G^\sigma_{\Lambda=0}(i\omega)$. We obtain thus,

$$\pi\Delta A(\omega) = \frac{1}{1 + (\frac{\omega}{Z\Delta})}\,, \tag{15.16}$$

where $Z = \lim_{l\to\infty} Z_l$ is obtained within FRG using modified magnetic field cutoff. A graph of the spectral density for different values of the coupling $u_0 = U/(\pi\Delta)$ is shown in Fig. 15.6.

Within our low energy approximation (13.27), we can obtain the behavior of the quasi particle peak (here the Kondo resonance) in the context of the Fermi liquid theory. But, we cannot recover the line shape for $\omega > \Delta$, in particular the
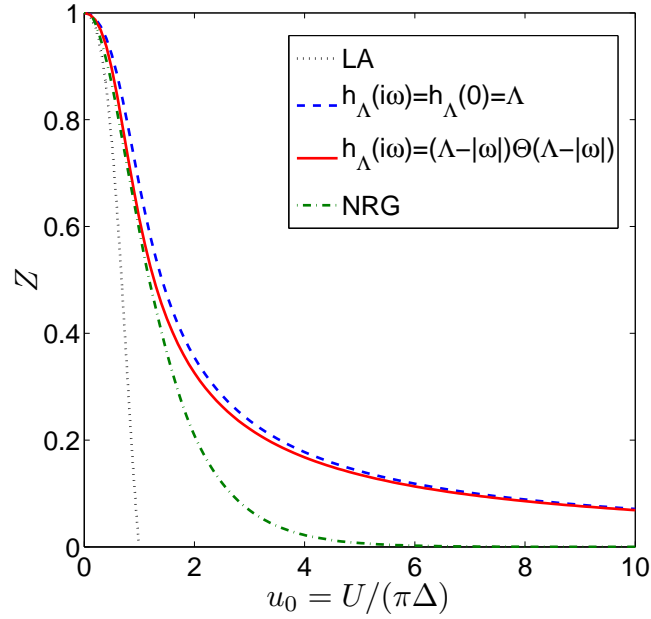
Figure 15.2: Numerical solution for $Z = \lim_{l \to \infty} Z_l$ as a function of the bare coupling $u_0 = U/(\pi\Delta)$ for the modified magnetic field cutoff, which is shown by solid line. The new results resemble the results from the previous chapter which are obtained within the frequency independent magnetic field cutoff scheme and are shown by dashed line.

broadened Hubbard peaks. For further investigation, it is therefore necessary to take into account that in the limit $u_0 \to \infty$, the weight of the Kondo peak becomes negligibly small and therefore the spectral function is not more characterized by the Kondo resonance but rather by the Hubbard-band peaks. On the other hand, the study of the AIM considering transverse as well longitudinal spin fluctuations is described in Refs. [103–107]. The authors of Ref. [101] have also applied FRG in both the transverse and the longitudinal channel. It is thus useful to work with two types of channels to obtain better results.
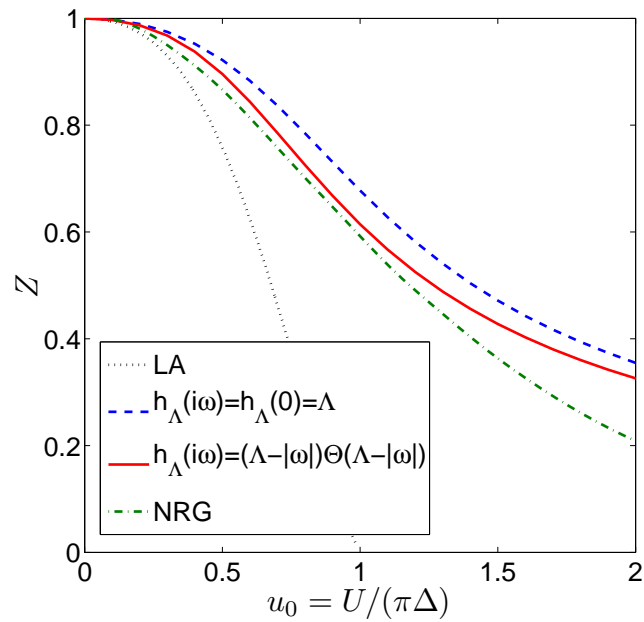
Figure 15.3: Comparison of the FRG results within different cutoff schemes with the accurate NRG solution at regime $u_0 = U/(\pi\Delta) < 2$. The results for the modified magnetic field cutoff are closer to the exact NRG results than for $h_\Lambda(i\omega) = \Lambda$.
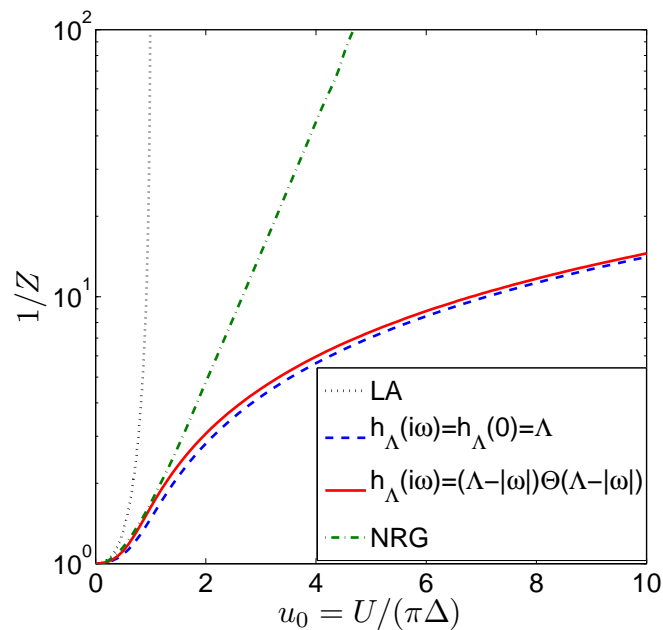

Figure 15.4: Redrawing of Fig. 15.2 by plotting the inverse wave function renormalization factor $1/Z$ on a logarithmic scale
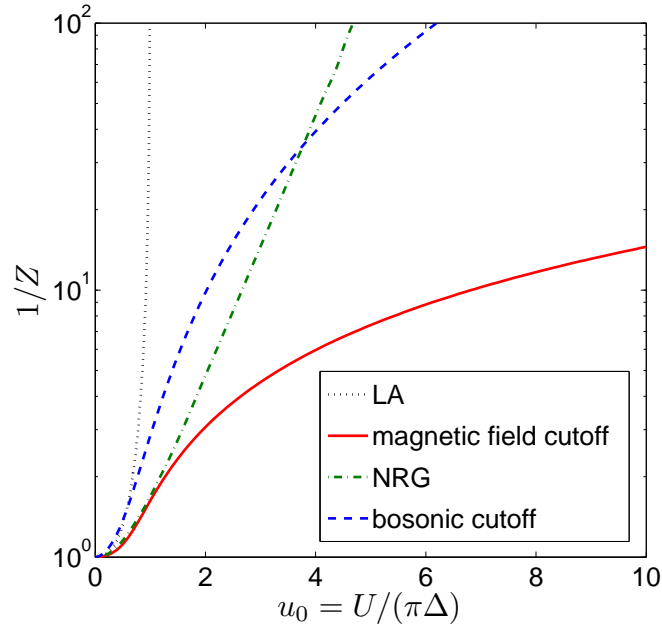
Figure 15.5: Comparison of our results with the exact NRG results from Ref. [100] and the FRG results from Ref. [101] which are obtained in longitudinal and transverse spin channels, using the cutoff in bosonic propagators. The magnetic field cutoff represents in this graph the "modified" magnetic field cutoff i.e., $h_\Lambda(i\omega) = (\Lambda - |\omega|)\Theta(\Lambda - |\omega|)$.
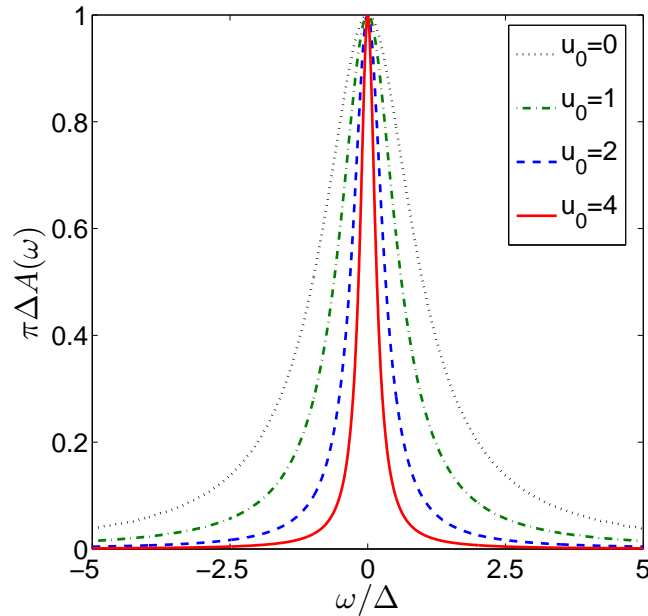

Figure 15.6: Spectral function of d-electrons for low energies and different values of $u_0 = U/(\pi\Delta)$.

Chapter 16

Summary of part II

In the second part of this thesis, we applied the exact FRG approach to the particle-hole symmetric Anderson impurity model at zero temperature. We have worked out the spectral properties of the Anderson impurity model and mapped the fermionic problem onto a mixed Bose-Fermi theory to handle the challenge in the transverse spin-flip channel. This strategy was proposed before in Ref. [101] and is based on the partial bosonization within FRG [7, 57, 58, 60–63]. In the transverse spin channel one can thus remove the unphysical Stoner instability which is an artifact of the Hartree-Fock approximation.

For our FRG approach we have employed the magnetic field cutoff as a cutoff in the fermionic propagator. We have developed the flow equation for the self-energy and used the skeleton equation following from the Dyson-Schwinger equations to express the irreducible spin-flip susceptibility in terms of the fermionic Green functions. For more simplicity we have also approximated the irreducible three- and four-legged vertices by their initial values. Because the four-legged vertices vanish at the beginning, we have neglected these parameters throughout this work. This truncations are reasonable because the vertices with higher number of legs becomes irrelevant in the RG sense. Furthermore we have expanded the self-energy in powers of the frequency so that we have obtained two separated terms, where the first one denotes the flowing magnetization and the second one describes the wave function renormalization factor. Note that this expansion is only good for $\omega < \Delta$. If we use the modified magnetic field cutoff, the initial condition of the self-energy is given with a good approximation by the Hartree-Fock approximation. According to our results, the evaluated wave function renormalization factor Z agrees very well in the regime $u_0 = U/(\pi\Delta) \lesssim 2$ with the exact results obtained via the NRG method. However, in the strong coupling regime $U \to \infty$ we could not reproduce the exponential suppression for the weight of the Kondo peak given by Eq. (11.17).

Finally, we point out that in order to improve these results in the strong coupling regime, we should solve the coupled differential equations (13.25, 13.26), by taking into account that the Fermi liquid approximations given by Eqs. (13.31, 13.32) are not more reliable, as the weight of the Kondo peak becomes exponentially small. Indeed, in the strong coupling regime, two high energy Hubbard band peaks (see Fig. 11.2) become important. We expect thus, due to the agreement of our results

with the accurate NRG results for the small value of U, in the strong coupling regime the problem becomes treatable without linearizing the fermionic self-energy.

Bibliography

[1] A. A. Abrikosov, L. P. Gorkov, and I. E. Dzyaloshinski, *Methods of Quantum Field Theory in Statistical Physics*, Dover Publications, New York, 1975.

[2] D. Pines and P. Nozières, *The Theory of Quantum Liquids*, Addison-Wesley, New York, 1988.

[3] M. Pustilnik, M. Khodas, A. Kamenev, and L. I. Glazman, Phys. Rev. Lett. **96**, 196405 (2006).

[4] R. G. Pereira, J. Sirker, J.-S. Caux, R. Hagemans, J. M. Maillet, S. R. White, and I. Affleck, Phys. Rev. Lett. **96**, 257202 (2006).

[5] K. V. Samokhin, J. Phys.: Cond. Mat. **10**, L533 (1998).

[6] S. Teber, Eur. Phys. J. B **52**, 233 (2006).

[7] F. Schütz, L. Bartosch, and P. Kopietz, Phys. Rev. B **72**, 035107 (2005).

[8] T. Giamarchi, *Quantum Physics in One Dimension*, Clarendon Press, Oxford, 2004.

[9] T. Giamarchi, cond-mat/0702565.

[10] F. D. M. Haldane, J. Phys. C **14**, 2585 (1981).

[11] B. Dardel, D. Malterre, M. Grioni, P. Weibel, Y. Bear, and F. Lévi, Phys. Rev. Lett. **67**, 3144 (1991).

[12] B. Dardel, D. Malterre, M. Grioni, P. Weibel, Y. Bear, and F. Lévi, Europhys. Lett. **24**, 687 (1993).

[13] G.-H. Gweon, J. W. Allen, R. Claessen, J. A. Clack, D. M. Poirier, P. J. Benning, C. G. Olson, W. P. Ellis , Y-X Zhang, and L F Schneemeyer, J. Phys.: Cond. Mat. **8**, 9923 (1996).

[14] J. D. Denlinger, G.-H. Gweon, J.W. Allen, C.G. Olson, J. Marcus, C. Schlenker, and L.-S. Hsu, Phys. Rev. Lett. **82**, 2540 (1999).

[15] S. Tomonaga, Prog. Theor. Phys. **5**, 544 (1950).

[16] J. M. Luttinger, J. Math. Phys. **4**, 1154 (1963).

[17] D. C. Mattis and E. L. Lieb, J. Math. Phys. **6**, 304 (1965).

[18] A. Luther and I. Peschel, Phys. Rev. B **9**, 2911 (1974).

[19] J. Sólyom, Adv. Phys. **28**, 201 (1979).

[20] A. L. Fetter and J. D. Walecka, *Quantum Theory of Many-Particle Systems*, McGraw-Hill, New York, 1971.

[21] I. E. Dzyaloshinskii and A. I. Larkin, Zh. Eksp. Teor. Fiz. **65**, 411 (1973).

[22] I. E. Dzyaloshinskii and A. I. Larkin, Sov. Phys. JETP **38**, 202 (1974).

[23] V. Meden and K. Schönhammer, Phys. Rev. B **46**, 15753 (1992).

[24] K. Schönhammer, cond-mat/9710330.

[25] K. Schönhammer in:, *Interacting Electrons in Low Dimensions*, Kluwer, Dordrecht, 2005.

[26] A. V. Chubukov, D. L. Maslov, and R. Saha, Phys. Rev. B **77**, 085109 (2008).

[27] A. V. Chubukov, D. L. Maslov, and F. H. L. Essler, Phys. Rev. B **77**, 161102 (2008).

[28] J. W. Negele and H. Orland, *Quantum many-particle systems*, Addison-Wesley, Redwood City, 1988.

[29] P. Pirooznia and P. Kopietz, Eur. Phys. J. B **58**, 291 (2007).

[30] F. Capurro, M. Polini, and M. P. Tosi, Physica B **325**, 287 (2003).

[31] M. Pustilnik, E. G. Mishchenko, L. I. Glazman, and A. V. Andreev, Phys. Rev. Lett. **91**, 126805 (2003).

[32] M. Pustilnik, Phys. Rev. Lett. **97**, 036404 (2006).

[33] V. V. Cheianov and M. Pustilnik, Phys. Rev. Lett. **100**, 126403 (2008).

[34] S. Teber, Phys. Rev. B **76**, 045309 (2007).

[35] R. G. Pereira, J. Sirker, J.-S. Caux, R. Hagemans, J. M. Maillet, S. R. White, and I. Affleck, J. Stat. Mech. P08022 .

[36] R. G. Pereira, S. R. White, and I. Affleck, Phys. Rev. Lett. **100**, 027206 (2008).

[37] K. Schönhammer, Phys. Rev. B **75**, 205103 (2007).

[38] D. N. Aristov, Phys. Rev. B **76**, 085327 (2007).

[39] Plötz, page arXiv:0708.1424 (unpublished) (2007).

[40] A. V. Rozhkov, Phys. Rev. B **77**, 125109 (2008).

[41] G. Mahan, *Many Particle Physics*, Plenum, New York, 1990.

[42] P. Pirooznia, F. Schütz, and P. Kopietz, Phys. Rev. B **78**, 075111 (2008).

[43] H. C. Fogedby, J. Phys. C **9**, 3757 (1976).

[44] D. K. K. Lee and Y. Chen, J. Phys. A **21**, 4155 (1988).

[45] P. Kopietz, J. Hermisson, and K. Schönhammer, Phys. Rev. **52**, 10877 (1995).

[46] P. Kopietz and K. Schönhammer, Z. Phys. B **100**, 259 (1996).

[47] P. Kopietz and G. E. Castilla, Phys. Rev. Lett. **76**, 4777 (1996).

[48] T. Busche and P. Kopietz, Int. J. Mod. Phys. B **14**, 1481 (2000).

[49] P. Kopietz, *Bosonization of interacting fermions in arbitrary dimensions*, Springer, Berlin, 1997; (cond-mat/0605402).

[50] R. L. Stratonovich, Sov. Phys. Doklady **2**, 416 (1958).

[51] J. Hubbard, Phys. Rev. Lett. **3**, 77 (1959).

[52] V. N. Popov, *Functional Integrals and Collective Excitations*, Cambridge University Press, Cambridge, 1983.

[53] C. C. W. Metzner and C. D. Castro, Adv. Phys. **47**, 3 (1998).

[54] A. Neumayr and W. Metzner, Phys. Rev. B **58**, 15449 (1998).

[55] A. Neumayr and W. Metzner, J. Stat. Phys. **96**, 613 (1999).

[56] C. Kopper and J. Magnen, Ann. Henri Poincaré **2**, 513 (2001).

[57] P. Kopietz, L. Bartosch, and F. Schütz, *Lectures on the Renormalization Group*, Springer, Heidelberg, 2010.

[58] F. Schütz and P. Kopietz, J. Phys. A.: Math. Gen. **39**, 8205 (2006).

[59] A. Sinner, N. Hasselmann, and P. Kopietz, J. Phys.: Condens. Matter **20**, 075208 (2008).

[60] C. W. Tobias Baier, Eike Bick, Phys. Rev. B **70**, 125111 (2004).

[61] C. W. Tobias Baier, Eike Bick, Phys. Lett. B **605**, 144 (2005).

[62] C. Wetterich, Phys. Rev. B **75**, 085102 (2007).

[63] W. M. P. Strack, R. Gersch, Phys. Rev. B **78**, 014522 (2008).

[64] T. R. Morris, Int. J. Mod. Phys. A **9**, 2411 (1994).

[65] C. Wetterich, Phys. Lett. B **301**, 90 (1993).

[66] J. Berges, N. Tetradis, , and C. Wetterich, Phys. Rep. **363**, 223 (2002).

[67] D. Litim, Phys. Rev. D **64**, 105007 (2001).

[68] L. G. Aslamasov and A. I. Larkin, Phys. Lett. **26A**, 238 (1968).

[69] L. G. Aslamasov and A. I. Larkin, Sov. Phys.—Solid State **10**, 875 (1968).

[70] A. Neumayr and W. Metzner, Phys. Rev. B **67**, 035112 (2003).

[71] S. Ledowski and P. Kopietz, J. Phys.: Condens. Matter **15**, 4779 (2003).

[72] P. W. Anderson, Phys. Rev. **124**, 41 (1961).

[73] P. W. Anderson, Rev. Mod. Phys. **50**, 191 (1978).

[74] A. C. Hewson, *The Kondo Problem To Heavy Fermions*, Cambridge University Press, Cambridge, 1993.

[75] H. R. Krishna-murthy, J. Wilkins, and K. Wilson, Phys. Rev. B **21**, 1003 (1980).

[76] T. A. Costi, A. C. Hewson, and V. Zlatić, J. Phys.: Condens. Matter **6**, 2519 (1994).

[77] W. Hofstetter, Phys. Rev. Lett. **85**, 1508 (2000).

[78] R. Bulla, T. A. Costi, and T. Pruschke, Rev. Mod. Phys. **80**, 395 (2008).

[79] A. M. Tsvelick and P. B. Weigmann, Adv. Phys. **32**, 453 (1983).

[80] P. B. Wiegmann, Sov. Phys. JETP Lett. **31**, 392 (1980).

[81] P. Coleman, cond-mat/0206003.

[82] A. H. Wilson, *The Theory of Metals*, Cambridge University Press, Cambridge, 1953.

[83] J. Kondo, Prog. Theor. Phys. **32**, 37 (1964).

[84] P. Nozières, J. Low Temp. Phys. **17**, 31 (1974).

[85] A. C. Hewson, Adv. Phys. **43**, 543 (1994).

[86] F. Gebhard, *The Mott Metal-Insulator Transition*, Springer, Berlin, 1997.

[87] K. Yosida and K. Yamada, Prog. Theor. Phys. **53**, 1286 (1975).

[88] K. Yamada, Prog. Theor. Phys. **53**, 970 (1975).

[89] D. M. Newns and J. Read, J. Phys. C **16**, 3273 (1983).

[90] D. M. Newns and J. Read, Adv. Phys. **36**, 799 (1988).

[91] P. Coleman, Phys. Rev. B **29**, 2 (1984).

[92] E. Müller-Hartmann, Z. Phys. B **57**, 281 (1984).

[93] D. E. Logan, M. P. Eastwood, and M. A. Tusch, J. Phys.: Condens. Matter **10**, 2673 (1998).

[94] A. C. Hewson, J. Phys.: Condens. Matter **13**, 110011 (2001).

[95] N. L. Dickens and D. E. Logan, J. Phys.: Condens. Matter **13**, 4505 (2001).

[96] R. Hedden, V. Meden, T. Pruschke, and K. Schönhammer, J. Phys.: Condens. Matter **16**, 5279 (2001).

[97] J. Kroha and P. Wölfe, *Theoretical Methods for Strongly Correlated Electrons*, edited by, D. Sénéchal, A. M. Tremblay, and C. Bourbonnais, Springer, Berlin, 2004.

[98] V. Janiš and P. Augustinský, Phys. Rev. B **75**, 165108 (2007).

[99] V. Janiš and P. Augustinský, Phys. Rev. B **77**, 85106 (2008).

[100] C. Karrasch, R. Hedden, R. Peters, T. Pruschke, K. Schönhammer, and V. Meden, J. Phys.: Condens. Matter **20**, 345205 (2008).

[101] L. Bartosch, H. Freire, J. J. R. Cardenas, and P. Kopietz, J. Phys.: Condens. Matter **21**, 305602 (2009).

[102] S. Ledowski and P. Kopietz, Phys. Rev. B **75**, 045134 (2007).

[103] S. Q. Wang, W. E. Evenson, and J. R. Schrieffer, Phys. Rev. Lett. **23**, 92 (1969).

[104] D. R. Hamann, Phys. Rev. Lett. **23**, 95 (1969).

[105] C. Castellani and C. D. Castro, Phys. Rev. Lett. **70A**, 37 (1979).

[106] H. J. Schulz, Phys. Rev. Lett. **65**, 2462 (1990).

[107] C. A. Macêdo and M. D. Coutinho-Filho, Phys. Rev. B **43**, 13515 (1991).

Deutsche Zusammenfassung

In dieser Arbeit untersuchen wir niedrigenergetische Anregungen in niedrigdimensionalen Fermi-Systemen. Diese Dissertation besteht aus zwei Teilen. In dem ersten Teil studieren wir die Eigenschaften der bosonischen Anregung *nullter Schall* in eindimensionalen Fermigasen während wir im zweiten Teil Einteilchen-Anregungen der Störelektronen im Anderson-Störstellen-Modell betrachten.

I. Dynamischer Strukturfaktor von Luttingerflüssigkeiten

Das Verhalten der eindimensionalen Elektronensystemen zeigt einige exotische Eigenschaften, die von der Fermi-Flüssigkeitstheorie nach Landau [2] abweichen. Diese Eigenschaften die auch experimentell nachgewiesen worden sind [11–14], fasst man unter Luttinger-Flüssigkeitstheorie zusammen [8,10]. Eines der wichtigen Modelle, welches solche Systeme beschreibt ist das Tomonaga-Luttinger-Modell (TLM) [15, 16]. Da die Fermi-Fläche in eindimensionalen Fermigasen nur aus zwei Punkten k_F und $-k_F$ besteht, linearisiert man in diesem Modell die Energiedispersion um diese beiden Fermi-Punkte.

Im ersten Teil der Dissertation interessieren wir uns für die bosonische Anregung, die der nullte Schall heißt und durch Dichte-Fluktuationen erzeugt wird. Da das TLM exakt lösbar ist, ist die Dichte-Dichte-Korrelationsfunktion $\Pi(Q)$, durch die RPA-Näherung gegeben. Der dynamische Strukturfaktor besitzt deshalb einen Delta-Peak $S_{\mathrm{TLM}}(\omega, q) = Z_q \delta(\omega - \omega_q)$, wobei $\omega_q = v_0 |q|$ der Energie des nullten Schalls entspricht.

Die Frage ist es nun, wie sich der dynamische Strukturfaktor ändert wenn wir die quadratische Energiedispersionen auch in die Rechnung einbeziehen. Bis jetzt, hat es mehrere Versuche gegeben um diese Frage zu beantworten. Die erfolgreichsten Arbeiten stammen von Pereira *et al.* [4,35,36], die ein exakt lösbares Modell betrachtet haben, sowie Pustilnik *et al.* [3,32], die eine Störungstheorie ohne Bosonisierung durchgeführt haben. In den beiden Arbeiten wurde gezeigt, dass der dynamische Strukturfaktor sich für $q \to 0$ wie q^2/m verbreitet und die Linienform eine sogenannte Schwelle-Singularität an der unteren Grenze aufweist.

Im Teil I haben wir den Effekt der quadratischen Korrekturen zu der Energiedispersion betrachtet. Ferner haben wir mit einer Wechselwirkung gearbeitet, die durch die Vorwärtsstreuung $g_2 = g_4 = f_q$ gegeben ist, wobei f_q von kleinen Im-

pulsüberträge $q < q_0$ dominiert ist. Der Hamilton-Operator hat also folgende Form

$$
\begin{aligned}
\hat{H} &= \hat{H}_0 + \hat{H}_{\text{int}}\,, \\
\hat{H}_0 &= \sum_k \epsilon_k \hat{c}_k^\dagger \hat{c}_k\,, \\
\hat{H}_{\text{int}} &= \frac{1}{2} \sum_q f_q \hat{\rho}_{-q} \hat{\rho}_q\,,
\end{aligned}
$$

wobei $\epsilon_k = k^2/2m$ und $\hat{\rho}_q = \sum_k \hat{c}_k^\dagger \hat{c}_{k+q}$ ist die Dichte-Operator. Das so konstruierte Modell nennen wir dann *Vorwärts-Streuung-Modell* (FSM). Das exakt lösbare Modell, das von Pereira *et al.* studiert wurde, beschreibt in Wirklichkeit die Heisenberg XXZ Spin-Kette, die äquivalent zu einem eindimensionalen fermionischen System ist. Dieses Modell besitzt jedoch neben Vorwärtsstreuung, Rückwärtsstreuung und auch Wechselwirkungen mit großen Impulsüberträgen. Das von Pereira *et al.* betrachtete Modell ist deshalb verschieden von unserem FSM. Anderseits haben Pustilnik *et al.* nicht die Renormierung der Geschwindigkeit des nullten Schalls berücksichtigt. Außerdem, haben Pustilnik *et al.* nicht die höhere Störungsreihe analysiert sowie angenommen dass durch eine Resummation die logarithmische Divergenz in erster Ordnung der Störungsreihe in einer algebraischen Divergenz umwandelbar ist. Trotz dieser Fortschritte, ist deshalb eine genaue Angabe der Linienform des dynamischen Strukturfaktors für nicht exakt lösbare Modelle noch nicht bekannt.

In dieser Arbeit benutzen wir die funktionale Bosonisierung um die Dichte-Dichte Wechselwirkung mittels eines bosonischen Hubbard-Stratonovich Feldes ϕ_Q zu entkoppeln. Integrieren wir über die fermionischen Felder $\{c_K, \bar{c}_K\}$, erhalten wir ein rein bosonisches Modell, wobei die bosonisierte effektive Wirkung $S_{\text{eff}}[\Delta\phi]$ für die linearisierte Energiedispersion quadratisch ist. Die Wechselwirkungsterme werden deshalb von der Band-Krümmung erzeugt und sie werden durch die symmetrisierten Fermion-Schleifen $L_S^{(n)}(Q_1, \ldots, Q_n)$ mit $n > 2$ beschrieben. Hier $\Delta\phi_Q = \phi_Q + i\delta_{Q,0}\bar{\phi}$, mit $Q = (i\bar{\omega}, q)$, $\delta_{Q,0} = \beta V \delta_{\bar{\omega},0}\delta_{q,0}$ und $\bar{\phi}$ ist der Erwartungswert des Feldes ϕ für $Q = 0$. Im Kapitel 4, leiten wir die funktionale Renormierungsgruppe für das FSM her, indem wir gemischte Bose-Fermi-Felder einführen. Damit erhalten wir die Flussgleichung für die irreduzibele Polarisierung. In Kapitel 6 kommen wir jedoch wieder auf die funktionale Bosonisierung zurück. Für eine Störungsreihe müssen wir nämlich auch die symmetrisierten Fermion-Schleifen bestimmen. Zur führenden Ordnung in $1/m$ zeigen wir

$$
L_S^{(n)}(Q_1, \ldots, Q_n) \propto (1/m)^{n-2}\,,
$$

so dass für die linearisierte Energiedispersion (d.h. $1/m \to 0$) der Wechselwirkunganteil von $S_{\text{eff}}[\Delta\phi]$ verschwindet. Im Rahmen der bosonisierten Störungstheorie erhalten wir eine selbst konsistente Gleichung für die irreduzibele Polarisierung $\Pi_*(Q)$.

In unserer Störungsreihe entwickeln wir $\Pi_*(Q)$ nach der zweiten Potenz von $q_0 \propto 1/m$. Deshalb tauchen nur $L_S^{(3)}$ und $L_S^{(4)}$ in unserer Rechnung auf. Um jedoch $S(\omega, q)$ zu bestimmen, müssen wir einige weitere Näherungen machen: Wir ersetzen die nicht-wechselwirkende Polarisierungen $\Pi_0(Q)$ in den Fermion-Schleifen

$L_S^{(3)}$ und $L_S^{(4)}$ durch ihre Beiträge für $1/m \to 0$. Ein wichtiges Zwischenergebnis unserer Rechnung ist, dass die von uns entwickelte Methode im Gegensatz zu anderen störungstheoretischen Methoden keine Mass-Shell-Singularität erzeugt. Diese unphysikalischen Singularitäten tauchten in den anderen Arbeiten in Zusammenhang mit der konventionellen Bosonisierung auf.

Unsere Rechnung ist jedoch für den Bereich $q_c \ll q \ll k_F$ gültig, wobei der Übergangsparameter $q_c = 1/(mf_0'')$ durch die zweite Ableitung f_0'' der Fourier-Transformation der Wechselwirkung an der Stelle $q = 0$ gegeben ist. Wenn die Fourier-Transformation der Wechselwirkung durch eine Lorentz-Kurve mit der Breite q_0 approximiert werden kann, erhalten wir $q_c \propto q_0^2$, so dass der Bereich $q_c \ll q \ll k_F$ breit genug ist um experimentelle Untersuchungen durchzuführen. Das wichtigste Ergebnis unserer Rechnung zeigt, dass die Breite des nullten Schalls sich für $q_c \ll q \ll k_F$ wie $\gamma_q \propto q^3/(mq_c)$ verhält. Im Übergangbereich $q \approx q_c$ ist unser Ergebnis konsistent mit dem asymptotischen Verhalten für lange Wellenlängen $\gamma_q \propto q^2/m$, das bereits von den anderen Autoren gezeigt worden ist [3–5]. Für $f_0'' < 0$, ist die spektralen Linienform nicht Lorentz-förmig und sie besitzt eine Schwelle-Singularität an der Stelle $\omega = \omega_q^- \approx vq - 4\gamma_q/3$, ein kleines lokales Maximum um $\omega \approx vq - \gamma_q/3$, und einen Schwanz bei den hohen Frequenzen, der wie q^4/ω^2 skaliert. Hier ist v die renormierte Geschwindigkeit des nullten Schalls. Für $f_0'' < 0$ und für $\omega \to \omega_q^- + 0$ verhält sich die Schwelle-Singularität innerhalb unserer Näherung logarithmisch, d.h.,

$$S(\omega, q) \propto \frac{1}{\eta_q(\omega - \omega_q^-) \ln^2(\omega - \omega_q^-)} \, .$$

Nehmen wir an, dass die höheren Ordnungen in der Störungsreihe den Logarithmus potenzieren, dann bekommen wir eine algebraische Singularität mit dem Exponent $\mu_q = 1 - 2\eta_q$, wobei $\eta_q \propto q_c^2/q^2$ für $q \gg q_c$.

Von anderen Autoren ist es schon nachgewiesen worden dass $S(\omega, q)$ für die exakt lösbare Modelle algebraische Schwelle-Singularitäten besitzt [4,32,33,35,36]. Jedoch gibt es immernoch keinen Beweis dafür, dass die logarithmischen Divergenzen bei der Summation in der höheren Ordnung der Störungtheorie in die algebraischen Singularitäten übergehen (Dies wurde zuerst in Ref. [3] vorgeschlagen und in unserer Rechnung angenommen). Dieser Beweis benötigt einige analytische Rechnungen bei der Entwicklung der Störungsreihe, die wir nicht durchgeführt haben.

Anderseits haben wir für die explizite Bestimmung der Selbtskonsistenz-Gleichung der irreduziblen Polarisierung $\Pi_*(\omega, q)$, die wir im Abschnitt 7.1 hergeleitet haben, die Approximation A vom Abschnitt 7.2 benutzt. Wir haben aber gezeigt, dass die Approximation A nicht ausreicht, um den dynamischen Strukturfaktor für $q \lesssim q_c$ zu bestimmen, da die Dämpfung in diesem Bereich von anderen Termen dominiert ist. Außerdem versagt unsere Approximation A, für Wechselwirkungen mit scharfem Impuls-Cutoff d.h. $f_q = f_0\Theta(q_0 - |q|)$. Es wäre deshalb interessant die Selbtskonsistenz-Gleichung für die irreduzible Polarisierung $\Pi_*(\omega, q)$ in Abschnitt 7.1 ohne die Approximation A zu betrachten. Wir erwarten dass in diesem Fall unser Ergebnis für $S(\omega, q)$ keine Mass-Shell-Singularität besitzt, sogar wenn der

Impuls-Cutoff der Wechselwirkung scharf ist.

In Kapitel 4 haben wir im Zusammenhang der FRG eine Flussgleichung für die irreduzibele Polarisierung hergeleitet. Vielleicht kann die FRG ein guter Startpunkt sein, um noch offene Probleme in diesem Teil der Arbeit zu klären.

II. Anwendung der FRG auf das Anderson-Störstellen-Modell

Das Anderson-Störstellen-Modell (AIM) wurde von Anderson vorgeschlagen um magnetische Störstellen in Metallen zu beschreiben. Der Hamiltonoperator besteht hier aus nicht wechselwirkenden Leitungselektronen, die an eine einzige wechselwirkende magnetische Störstelle im d-Orbital gekoppelt sind,

$$
\begin{aligned}
\hat{H} &= \sum_{\mathbf{k}\sigma}(\epsilon_{\mathbf{k}} - \sigma h)\hat{c}_{\mathbf{k}\sigma}^{\dagger}\hat{c}_{\mathbf{k}\sigma} + \sum_{\sigma}(E_d - \sigma h)\hat{d}_{\sigma}^{\dagger}\hat{d}_{\sigma} \\
&+ U\hat{d}_{\uparrow}^{\dagger}\hat{d}_{\uparrow}\hat{d}_{\downarrow}^{\dagger}\hat{d}_{\downarrow} + \sum_{\mathbf{k}\sigma}(V_{\mathbf{k}}^{*}\hat{d}_{\sigma}^{\dagger}\hat{c}_{\mathbf{k}\sigma} + V_{\mathbf{k}}\hat{c}_{\mathbf{k}\sigma}^{\dagger}\hat{d}_{\sigma})\,,
\end{aligned}
$$

wobei $\epsilon_{\mathbf{k}}$ die Energiedispersion der Leitungselektonen mit Impuls $\mathbf{k}$ darstellt und E_d der atomaren Energie der d-Elektronen entspricht. Die örtliche Abstoßung zwischen den Störelektronen bezeichnen wir hier mit U und die Hybridisierungsenergie zwischen den Leitungselektronen und den d-Elektronen mit $V_{\mathbf{k}}$.

Wir interessieren uns für den *Bereich der lokalen Impulse*, wo der Grundzustand durch die einfache Besatzung gegeben ist. Weiterhin setzen wir die Teilchen-Loch-Symmetrie voraus, die durch $N = 1$ und $E_d - \mu = -U/2$ charakterisiert ist. Dabei bezeichnen wir die durchschnittliche Besetzungszahl mit N und μ ist das chemische Potential. Wir erhalten die effektive Wirkung für die d-Elektronen indem wir die Leitungselektronen integrieren. Die Kopplung an die Leitungselektronen führt dann zu einer effektiven Selbstenergie für die d-Elektronen,

$$
\Delta^{\sigma}(i\omega) = \sum_{\mathbf{k}} \frac{|V_{\mathbf{k}}|^2}{i\omega - \epsilon_{\mathbf{k}} + \mu + \sigma h}\,.
$$

Für ein verschwindendes Magnetfeld und im Grenzwert breiter Bänder, können wir außerdem einsetzen: $\Delta^{\sigma}(i\omega) = \Delta$.

Im Teil II haben wir mit Hilfe der FRG die Spektralfunktion $A(\omega)$ von d-Elektronen im Teilchen-Loch-symmetrischen AIM bei verschwindender Temperatur bestimmt. Wir bemerken, dass die Spektralfunktion der d-Elektronen bereits aus der numerischen Renormierungsgruppe bekannt ist [74, 85]. Man weiß, dass das Spektrum eine scharfe Resonanz bei verschwindender Frequenz besitzt, die man als Kondo-Peak bezeichnet. Ferner gibt es zwei Schultern auf beiden Seiten des Kondo-Peaks die den Hubbard-Bändern entsprechen [86]. Wenn die Hybridisierungsenergie $V_{\mathbf{k}}$ zwischen den Leitungselektronen und den d-Elektronen verschwindet, dann tragen die beiden Hubbard-Band-Peaks das Gewicht des ganzen Spektrums, wobei die

Positionen der Hubbard-Band-Peaks durch $\pm U/2$ gegeben sind [88]. Mit Hilfe des Bethe-Ansatzes ist es außerdem gezeigt worden, dass für $U/\Delta \gg 1$ das Gewicht des Kondo-Peaks exponentiell abfällt [79, 80],

$$Z_{\mathrm{KP}} \approx \sqrt{\frac{8U}{\pi^2 \Delta}}\, e^{-\frac{\pi U}{8\Delta}}\,.$$

Eine "analytische Bestimmung" der Spektralfunktion $A(\omega)$ für jede beliebige Frequenz ω fehlt jedoch. Für weitere Untersuchungen der reellen dreidimensionalen fermionischen Systeme im Zusammenhang der dynamischen Molekularfeldtheorie ist außerdem die genaue Kenntnis über das Verhalten von $A(\omega)$ erforderlich.

An dieser Stelle benutzen wir wieder Hubbard-Stratonovich Transformation um das fermionische System auf ein gemischtes Bose-Fermi-System abzubilden und das Problem in einem transversalen Spin-Flip-Kanal zu behandeln. Diese Strategie ist in Ref. [101] vorgeschlagen worden und basiert auf der partiellen Bosonisierung innerhalb der FRG [7, 57, 58, 60–63]. Es ist bekannt, dass es durch die Bosonisierung im transversalen Spin-Kanal möglich ist, die unphysikalische Stoner-Instabilität zu eliminieren, die man durch die Hartree-Fock Näherung erhält.

In unserer FRG-Rechnung, benutzen wir das Magnetfeld als ein Cutoff im fermionischen Propagator. Zur Lösung der FRG Flussgleichungen verwenden wir die Dyson-Schwinger Gleichungen um die irreduzible Polarisierung mit Hilfe der fermionischen Greenfuntionen darzustellen. Die entstehende Gleichung nennt man die *Skelett-Gleichung* im bosonischen Sektor. Zur weiteren Vereinfachung, vernachlässigen wir außerdem den Fluss der irreduziblen Vertices mit drei Beinchen. Da die irreduziblen Vertex-Funktionen mit vier Beinchen am Anfang verschwinden, können wir sie ganz vernachlässigen. Diese Trunkierungen sind deshalb plausibel, weil die Vertex-Funktionen mit einer höheren Anzahl von Beinchen irrelevant in RG-Sinn sind. Wir entwickeln auch die Selbstenergie bis zur ersten Potenz der Frequenz, wobei die nullte Potenz der fließenden Magnetisierung M_l entspricht. Aus der ersten Potenz erhalten wir den Wellenfunktions-Renormierungsfaktor Z_l, der äquivalent zu dem Gewicht des Kondo-Peaks ist. Der Parameter $l = -\ln(\Lambda/\Lambda_0)$ ist durch den RG-Koeffizienten Λ gegeben, so dass die Anfangsbedingung an der Stelle $l = 0$ ($\Lambda = \Lambda_0$) definiert ist. In dieser Näherung, vernachlässigen wir das Gewicht der Hubbard-Bänder und es ist klar, dass diese Entwicklung nur für $\omega \lesssim \Delta$ gültig sein kann. Es zeigt sich, dass die Anfangsbedingung so gewählt sein muss, dass die Magnetisierung $M_{l\to\infty}$ am Ende gegen Null fließt da der RG-Cutoff verschwindet. Wenn wir einen veränderten Magnetfeld-Cutoff einführen, der es nicht erlaubt, dass die höheren Frequenzen von dem Magnetfeld beeinflusst werden, sehen wir, dass der Anfangswert für die fließende Selbstenergie mit sehr guter Näherung durch den Hartree-Fock-Wert gegeben ist.

Unsere Ergebnisse zeigen, dass die berechneten Werte für die Wellenfunktions-Renormierungsfaktor $Z = Z_{l\to\infty}$ im Bereich $u_0 = U/(\pi\Delta) < 2$ sehr gut mit den exakten Werten, die man aus NRG kennt übereinstimmen. Trotzdem konnten wir im Bereich der starken Kopplung $U \to \infty$ die exponentielle Unterdrückung vom Kondo-Peak nicht reproduzieren.

Um unsere Ergebnisse bei der starken Kopplung zu verbessern, sollten wir die gekoppelte Flussgleichungen auswerten ohne die gegebene Entwicklung für die fließende Selbstenergie durchzuführen. In der Tat, wenn die Wechselwirkung U wächst, fällt das Gewicht des Kondo-Peaks exponentiell ab. Deshalb benötigen wir für weitere Untersuchungen eine andere Approximation die auch das Gewicht der Hubbard-Bänder berücksichtigt.

Veröffentlichungen

1. Peyman Pirooznia and Peter Kopietz
   Damping of zero sound in Luttinger liquids,
   Eur. Phys. J. B **58**, 291 (2007).

2. Peyman Pirooznia, Florian Schütz, and Peter Kopietz
   Dynamic structure factor of Luttinger liquids with quadratic energy dispersion and long-range interactions,
   Phys. Rev. B **78**, 075111 (2008).

Lebenslauf

Persönliche Daten

Name:	Peyman Pirooznia
Geburtsdatum:	10. September 1981
Geburtsort:	Shemiran, Iran
Staatsangehörigkeit:	Deutsch

Ausbildung und Studium

2005-2010	Doktorand am Institut für theoretische Physik in der Goethe-Universität Frankfurt Betreuer: Prof. Dr. Peter Kopietz
November 2005	Diplom in Physik Note: Sehr gut
2003-2005	Diplomarbeit am Institut für Theoretische Physik in Frankfurt Betreuer: Prof. Dr. Peter Kopietz Thema: "Berechnung der Dichte-Dichte Korrelationsfunktion in eindimensionalen Fermigasen"
2000-2005	Physikstudium an der J. W. Goethe-Universität Frankfurt
1999-2000	Besuch des Studienkollegs Johann Wolfgang Goethe-Universität Frankfurt
1999	Abitur am iranischen Gymnasium in Frankfurt am Main
1994	Einreise in die Bundesrepublik Deutschland

Danksagung